STRUCTURAL AND ELECTRICAL PROPERTIES OF THICK FILM OF V_2O_5 DOPED RuO_2

NATIONAL CHEMICAL LABORATORY
TH-359
Date
LIBRARY

A Thesis submitted to
THE UNIVERSITY OF POONA
for the degree of
MASTER OF SCIENCE
[partly by papers and partly by research]
in
C H E M I S T R Y

621·382:661·888·45(043)
SHI

By
R. P. S H I N D E

National Chemical Laboratory,
Pune 411 008.

1981

ACKNOWLEDGEMENT

COMPUTERISED

I wish to express my sincere gratitude to Dr. A. P. B. Sinha for his invaluable guidance and constant encouragement throughout the course of this work.

I am thankful to Mr. M. S. Setty for designing the experimental set-ups and for his guidance in carrying out the experimental measurements.

I am grateful to the Director, National Chemical Laboratory, Pune, for permitting me to submit this work in the form of thesis.

R P Shinde

R. P. Shinde

CONTENTS

		Page
	GENERAL INTRODUCTION	1
CHAPTER - I -	HISTRORICAL SURVEY	4
CHAPTER - II -	E X P E R I M E N T A L	33
CHAPTER - III -	R E S U L T S	49
CHAPTER - IV -	D I S C U S S I O N	58
	R E F E R E N C E S	74

---000---

GENERAL INTRODUCTION

Thick film technology is the latest innovation in the microelectronics circuitry. In the past decade or so this has been gaining importance by virtue of the reliability and performance of the circuit elements. Thick film materials generally consist of electrically active solids, low softening glass frits, organic fillers and solvents. Each of these has a definite role to play in getting the passive components such as conductors, resistors, capacitors, etc. The thick film components are obtained by screen printing the formulations/pastes and firing according to a time-temperature schedule.

In recent years, ruthenium dioxide has been widely used as a functional material for thick film resistors. It is stable at sufficiently high temperatures and has metallic conductivity at room temperature. It is reported that ruthenium dioxide exhibits non-stoichiometry and is partially deficient in oxygen with a corresponding amount of Ru^{3+} in place of Ru^{4+}. This deviating valency affects the stability of the ruthenium dioxide-based thick film resistors[9].

The properties of fired ruthenium dioxide-based thick film resistors have been controlled by various additives such as Sb_2O_5, CeO_2, Ta_2O_5, Sb_2O_3, Bi_2O_3, Al_2O_3 and CaF_2 as TCR modifiers[45-50]. These additives are added along with ruthenium dioxide while formulating the paste. Solid solutions of RuO_2 with the additives, when used as conductor components of thick film resistors, have improved the stability

of RuO_2-based thick film resistors[7,8]. The solid solutions of RuO_2 with oxides such as Nb_2O_5[9], Ta_2O_5, PbO and Bi_2O_3 have been tried for conductive phase in thick film resistors[45,46]. The addition of pentavalent dopant was based on 'Control Valency Process'[9].

Work on the control of valency in semiconducting oxide was first reported by E. J. Verwey and coworkers[8]. It was shown that the introduction of suitable ions into the lattice structure of a variable valence oxide could, without deforming it, balance the ions of deviating valency already within the lattice and still maintain overall charge neutrality. Verwey obtained a composition $Li^{+}_{\delta}Ni^{2+}_{(1-2\delta)}Ni^{3+}_{\delta}O$ by calcining nickel oxide with lithium carbonate at 1200°C under oxidising conditions. The product had the same structure as nickel oxide but with a smaller unit cell and Ni^{3+} content was broadly equivalent to the amount of lithium oxide added.

G. S. Iles[9] suggested that valency variation in RuO_2 might be controlled by similar doping technique leading to a better stability and reproducibility of RuO_2 based thick film resistors together with a measure of control over both sheet resistivity and temperature coefficient of resistance (TCR). He introduced a pentavalent ion, Nb^{5+}, into the lattice structure of RuO_2 to balance the already established Ru^{3+} ions and maintained overall charge neutrality. He used niobium pentoxide as dopant for this purpose.

For this type of ionic substitution to take place, the diffusing ion must have an ionic radius similar to that of ruthenium which is 0.67Å. However, the system RuO_2-V_2O_5 has not been studied in detail as conductive phase in thick film resistors. Vanadium in its pentavalent state has a radius of 0.59Å and therefore is well suited as a doping element.

This lead us to study the structural properties of RuO_2-V_2O_5 system and the electrical properties of the thick film resistors of RuO_2-V_2O_5 compositions.

Various amounts of V_2O_5 were successfully introduced into the RuO_2 lattice. The resultant oxide system was found to obey Vegard's law which states that the extent of the change in the lattice parameter of the host oxide is proportional to the molecular percentage of the added dopant.

We have presented the results of this study in the following pages. The first part forms the historical survey of the subject. The second part deals with material preparation and methods of measurements. The results and discussion form the last part of the thesis.

CHAPTER - I

HISTORICAL SURVEY

1.1. CRYSTAL STRUCTURE OF RUTHENIUM OXIDE

F. A. Cotton and J. T. Mague[1] proposed that ruthenium dioxide has the tetragonal rutile crystal structure (Figure 1.1) with two formula unit per unit cell. They showed that regular ruthenium atoms are in body-centred arrangement. The absence of metal-atom clusters was also reported. Ruthenium dioxide belongs to the space group $P4_2/mnm$ of the tetragonal system. This was also confirmed by Bowman[6]. C. E. Bowman studied the structural properties of single crystals of ruthenium dioxide. He used $CuK\alpha$ radiation for the purpose. He reported that ruthenium is octahedrally coordinated by oxygen, four of the six Ru-O distances are $1.984 \pm 0.006 Å$ and the other two $1.942 \pm 0.010 Å$.

Krishna Rao and Leela Iyengar[4] carried out a precise X-ray determination of the lattice constant of ruthenium dioxide in the temperature range 30-702°C. The values of coefficient of expansion (α) in the directions parallel and perpendicular to c axis are presented. The results indicated that a parameter increases and 'c' parameter decreases continuously with increasing temperature that is ruthenium dioxide has a negative coefficient of linear thermal expansion and increases with increasing temperature.

J. M. Fletcher and coworkers[2] also studied the variation of lattice parameters from room temperature to 795°C and found that ruthenium dioxide expands in the 'a' direction and contracts in the 'c' direction. The authors suggested that the contraction

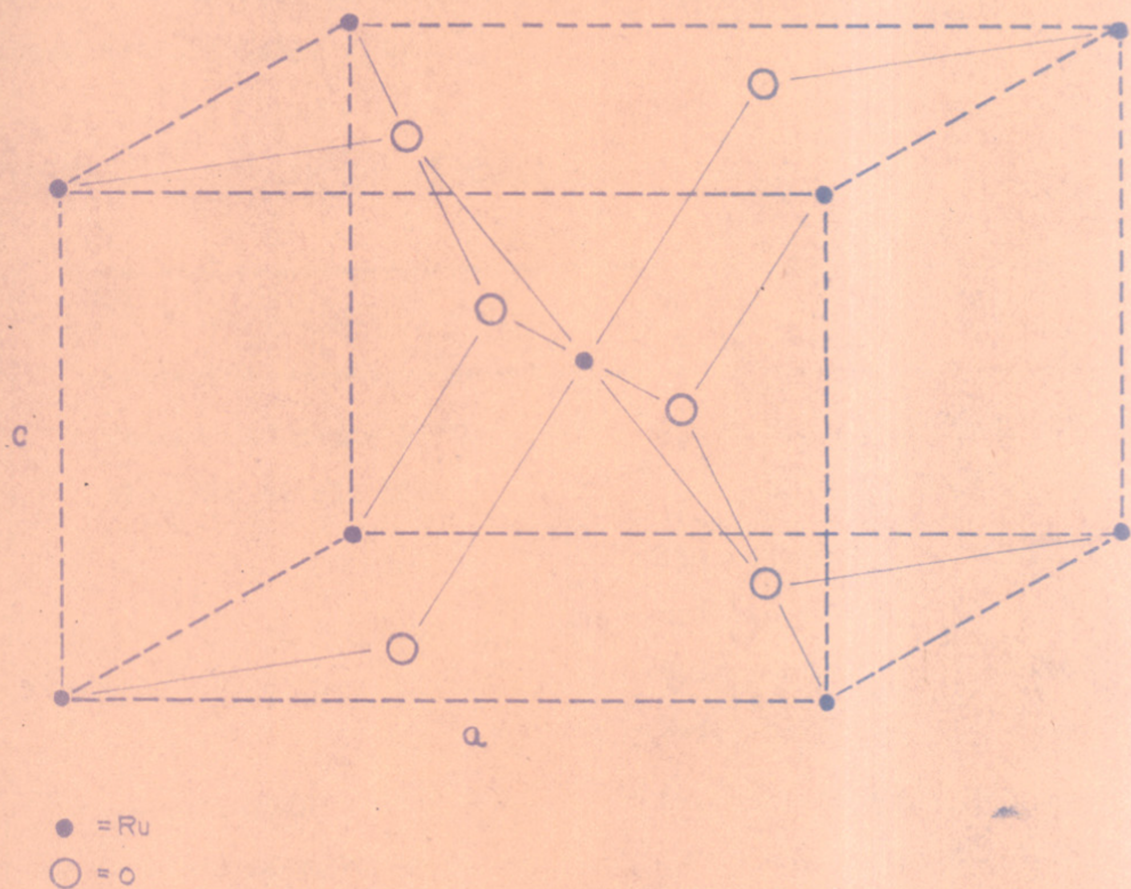

FIGURE 1.1 : CRYSTAL STRUCTURE OF RuO_2

in the 'c' direction is due to strong bonding of the dioxide bridge within the chains which exists in the 'c' direction

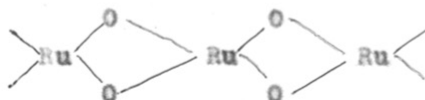

The cell dimensions reported by several authors are summarised in Table 1.1.

TABLE - 1.1[61]

	Temp. °C	Lattice parameters(Å) a	
Cotton and Mague 1966	RT	4.491±0.007	3.107±0.005
Fletcher et al. 1968	RT	4.4904±0.0001	3.1064±0.0001
	190	4.4971	3.1055
	400	4.5071	3.1031
	605	4.5204	3.1002
	795	4.5342	3.0963
Shannon 1968	RT	4.4906±0.0002	3.1064±0.000
Rao and Iyengar 1969	30	4.4909±0.0003	3.1064±0.000
	165	4.4958	3.1062
	267	4.5003	3.1051
	361	4.5053	3.1037
	461	4.5109	3.1033
	563	4.5173	3.1012
	608	4.5198	3.1008
	702	4.5258	3.0995
Bowman 1970	RT	4.4919±0.0008	3.1066±0.000

1.2. THERMODYNAMIC PROPERTIES OF RUTHENIUM DIOXIDE

E. Bell and M. Tagami[7] have studied the high temperature chemistry of the $Ru-O_2$ system over the temperature range 800-1500°C and over the oxygen pressure range 0.01 to 1.0 atm. It is reported that ruthenium dioxide is the stable solid oxide under the condition of study ΔH^{o}_{298} and S^{o}_{298} for $RuO_2(s)$ have been reported as -72.2 ± 2.0 kcal/mole and 12.5 ± 2.0 e.u. respectively. They have also showed that if temperature was kept constant at 1540°C, the dissociation pressure of the ruthenium dioxide reached one atmosphere.

C. L. McDaniel and S. J. Schneider[12] found that in air ruthenium oxidised at moderate temperatures to form ruthenium dioxide which in turn dissociated at 1405°C.

Komatsu Wazo, Moriyoshi Yosuke and Kawana Hidejiro[13] studied the sintering of ruthenium dioxide. It was reported that decomposition pressure of ruthenium dioxide was several torr at 1000° and sublimation occurred at temperature greater than 1000°C in a stream of oxygen. They have showed that the sintering of ruthenium dioxide occurred by an evaporation condensation process in an oxygen atmosphere.

V. K. Tarigrov and coworkers[14] have reported that the thermal dissociation of ruthenium dioxide occurred at 985-1190°K and proceeded as follows

$$RuO_2(s) \longrightarrow Ru(s) + O_2(g)$$

Whereas transpiration measurements performed by H. Schafer and coworkers[15] with solid ruthenium dioxide at 800°C in oxygen, showed that gaseous RuO_4 was formed according to the equation

$$RuO_2(s) + O_2(g) \rightleftharpoons RuO_4(g).$$

When the temperature was increased, the formation of gaseous RuO_3 became perceptible. Gaseous RuO was formed predominantly as a final product at high temperatures and low oxygen pressure.

G. Bayer and H. G. Widermann[16,17,18] reported a strong anisotropy of thermal expansion behaviour of ruthenium dioxide. They have studied the DTA, TG and X-ray diffraction of the oxidation of ruthenium to ruthenium dioxide.

1.3. ELECTRICAL PROPERTIES OF RUTHENIUM DIOXIDE

H. Schaefer, G. Schneidereit and W. Gerhardt[21] studied the electrical properties of single crystal of ruthenium dioxide and have remarked that the low room temperature resistivity (50 μ ohms. cm. in the c direction) of ruthenium dioxide. They observed a positive temperature coefficient of resistance between 195°K and room temperature.

J. M. Fletcher and coworkers[2] reported the electrical resistivity values of RuO_2, 48.4 ± 1.9 and 67.9 ± 1.2 μ ohms.cm. in the a and c directions respectively, indicating the anisotropic

nature of it. They further proposed that the average oxidation state of ruthenium in ruthenium dioxide was greater than + 4, which in turn supported the presence of electrons in the conduction band which were required to explain the low electrical resistivity. They also observed positive temperature coefficient of resistance at high temperature for a pellet. The apparent resistivity of the pellet increased from 216 μ ohm cm. at room temperature to 790 μ ohm cm. at $1184^{o}K$.

D.B. Rogers and coworkers[2] studied the temperature dependence of resistivity for ruthenium dioxide. The electrical resistivity measurements were made by four probe method using indium contacts. They obtained this data for single crystals and in undetermined crystallographic directions. They proposed a modified Goodenough model which rationalized all the observed electrical and crystallographic properties. A qualitative band structure for ruthenium dioxide (Figure 1.2) in which the t_{2g}^{π} orbital is assumed to be filled and consequently non-bonding has been put forward. The metallic conductivity is consistent with partially filling of the Ru-O π^{*} band.

W. D. Ryden, A.W. Lawson and C. C. Sartain[19,20] studied the temperature dependence and magnitude of resistivities and Hall constant for ruthenium dioxide. They found that ruthenium dioxide and several other oxides of 4th and 5th transition series exhibited metallic conductivities in the range 0.01-1 times the conductivity of the parent metals themselves. They measured the

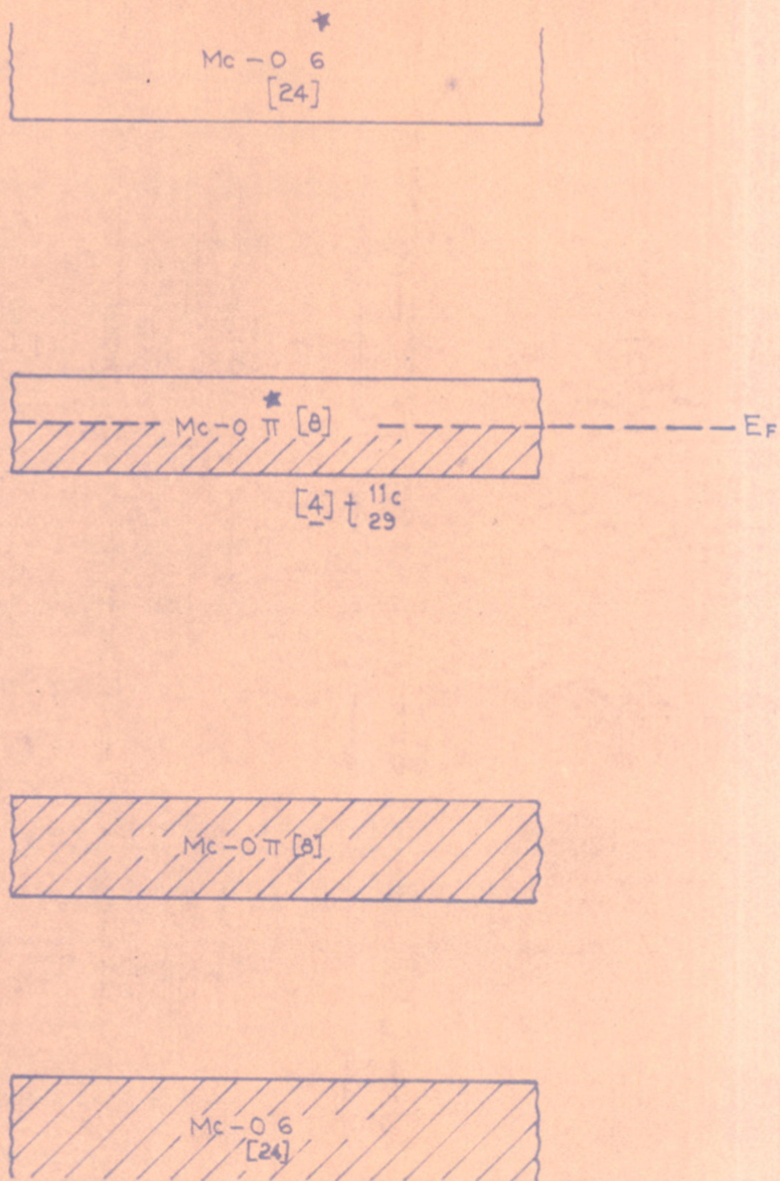

FIGURE 1.2 QUALITATIVE BAND STRUCTURE OF RUTHENIUM DIOXIDE[3]

resistivity of the single crystals of ruthenium dioxide from $4.2^{\circ}K$ to $1000^{\circ}K$ and showed that ruthenium dioxide was isotropic and does not obey Matheissen's rule. They were able to fit the resistivity of ruthenium dioxide to the relation

$$\rho = \rho_0 + \rho_2 T^2 + \rho_3 T^3 \left[J_3\left(\frac{\theta_D}{T}\right) - J_3\left(\frac{\theta_E}{T}\right) \right]$$

The electrical resistivities reported by various investigators are listed in Table 1.2.

TABLE - 1.2

Electrical resistivity of single crystal of ruthenium dioxide

S.No.	Investigators	Ref.	($300^{\circ}K$) ohm - cm	($4.2^{\circ}K$) ohm - cm	Remarks
1	Schafer and Schneidereit	21	5×10^{-5}		Mettalic
2	Rogers, et al	3	4×10^{-5}	2.2×10^{-7}	
3	Ryden, Lawson and Sartain	19, 20	$3.52 \pm 1.2 \times 10^{-5}$		Iso-tropic
4	Fletcher, et al	2	$4.84 \pm 1.9 \times 10^{-5}$		in a directio
			$6.79 \pm 1.2 \times 10^{-5}$		in c directio
5	Marcus and Butler	22	4×10^{-5}	$2. \times 10^{-9}$ at 1.1k	

*anisotropy

1.4. MIXED VALENCE OXIDES

Transition metal oxides are generally insulators in their pure state. The oxides show considerable electrical conductivity when they deviate from stoichiometry because of excess of cations or deficiency of oxygen ions.

C. Wagner and coworkers[23-26] first studied the correlation between the electrical conductivity of transition metal oxides and their deparlure from stoichiometry. They studied several oxides, typical amongst them was p-type NiO. When oxygen pressure over NiO was increased, it deviated from stoichiometry and an oxygen excess material NiO_{1+x} was obtained which was electrically conductive. This could also be viewed, more appropriate as Ni deficit material $Ni_{(1-x)}O$. In $Ni_{(1-x)}O$, Ni^{+3} ions were produced by nickel vacancies. The nickel vacancies were represented as Ni^{+3} ions or "electron hole". C. Wagner applied the law of mass action to this type of system, at sufficiently high temperature (800-1000°C), the following equilibrium condition was reported in such a state

NiO crystal + one molecule of O_2 $\rightleftharpoons$

NiO crystals containing $2Ni\square$ + $4Ni^{+3}$,

where $Ni\square$ represent a Ni vacancy in the NiO lattice. Associated with each vacancy of Ni there were $2Ni^{+3}$ ions in order to maintain charge neutrality. The equilibrium constant for reaction was given by

$$k = \frac{[Ni\Box]^2 [Ni^{+3}]^4}{pO_2}$$

but since $2[Ni\Box] = [Ni^{+3}]$

$$k = \frac{[Ni^{+3}]^6}{4\,pO_2}$$

The electrical conductivity was taken as proportional to the number of Ni^{+3} ions in the lattice and increased as $1/6^{th}$ power of the oxygen pressure. Wagner found a $1/4^{th}$ power dependence only based on certain assumptions.

Similar equilibrium relationship was applied to n-type semiconductors such as ZnO where there was an excess of Zn in the crystal lattice leading to conduction by electrons. Here the electrical conductivity was shown to be invariably proportional to oxygen pressure. The relationship between electrical conductivity and non-stoichiometry of the oxide system was established subsequently.

W. D. Johnston[27] discussed the practical limitations to the applications of such semiconductors. These were as follows:

1. It was very difficult to stretch the deviations from stoichiometry beyond a certain limit.

2. The extent of deviation from stoichiometry was observed to change with increase in temperature.

3. Further the degree of non-stoichiometry at any temperature was dependent on the oxygen partial pressure. Thus the limited range of composition, the lack of thermal stability and the problems involved in preparing reproducible samples sharply limited the utility of this type of materials.

E. J. W. Vervey[8] and coworkers were able to surmount the above deficiencies by introducing the technique of controlling valencies in semiconductors through doping. Using this technique one could control the concentration of the conducting species. This semiconducting behaviour and chemical stability became compatible. The "controlled valence" principle has been illustrated by the system $Li_xNi_{(1-x)}O$. Verwey has interpreted the conduction mechanism in the above system as follows:

Some of the Ni^{+2} ions are replaced by Li^{+1} ions ($r_{Li} = 0.70 Å$, $r_{Ni} = 0.74 Å$). In order to maintain charge neutrality, Ni^{3+} ions are formed. The hole transfer takes place from Ni^{3+} ions to Ni^{2+} ions and thus contributing to electrical conductivity. The concentration of Ni^{+3} ions and in turn Li^{+1} ions control the conductivity of the $Li_xN_{(1-x)}O$ system.

W. D. Johnston[27] studied lithium substituted transition metal oxides such as $Li_xCo_{(1-x)}O$ and $Li_xNi_{(1-x)}O$. A double exchange mechanism for conduction was proposed to explain the conduction process in the lithium-transition

metal oxides and pervoskites. He argued that at about 10% lithium, all sites would have at least one lithium ion nearest neighbour and if Verwey's contentions were correct, the activation energy at 10% Li would have been equal to zero. However, he observed still a large value for activation energy at this lithium concentration ($\sim$ 14 K Cal in $Li_xM_{1-x}O$). W.D. Johnston opined that the activation energy was associated with the ion carrying the charge and not with the lattice as a whole. The conduction process was explained by visualising a hole or trivalent metal, Ni^{+3}, being surrounded by a distorted lattice. The movement of the hole required the reorganisation of the lattice to an unstrained position. The hole was then free to move since all sites were equal. The work done to move the lattice to this unstrained position was reported to be the activation energy for conduction. The lattice distortion was found to be highly localised and was a function of the transition ion involved.

J. M. Honig[28] in his review article explained the conduction mechanisms in oxide systems by considering (i) deviation from stoichiometry and (ii) impurity incorporation in the host lattice. Examples of Li^+ substitution for Ni^{2+} in NiO and Ga^{3+} substitution for Zn^{2+} in ZnO have been given.

The first example was represented by quasi-chemical reaction as

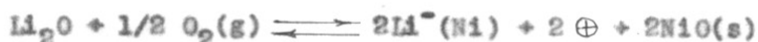

$$Li_2O + 1/2\ O_2(g) \rightleftharpoons 2Li^-(Ni) + 2 \oplus + 2NiO(s)$$

Here, (a) the oxide Li_2O had entred the host lattice and (b) an atom O was abstracted from the gas phase. The following sequence of events were depicted: (i) The two Li^+ ions in Li_2O had taken the place of two Ni^{2+} ions at their normal lattice position and gave rise to the presence of a net negative charge at each of these locations ($2Li^-(Ni)$]. (ii) The O atom originally being derived from the gas phase required two electrons to form O^{2-} ion and deficiency of two electrons (holes) (+), in the lattice was left. (iii) The O^{2-} thus generated and the O^{2-} originally present in Li_2O combined with the two displaced Ni^{2+} ions mentioned in (i) to form two additional $Ni^{2+}\ O^{2-}$ units ($2NiO(s)$). Two holes associated with two Ni^{2+} ions were formed Ni^{3+} units (not shown in equation).

In the second example, a trivalent impurity cation (Ga^{3+}) was incorporated into a divalent host lattice (ZnO). This was represented by the quasichemical reaction

$$Ga_2O_3 \rightleftharpoons 2Ga^+(Zn) + 2 \ominus + 2ZnO(s) + 1/2\ O_2(g)$$

Here, the sequence of events were explained as : (i) The two oxides Ga_2O_3 ana ZnO reacted, (ii) the gallium ion displaced two Zn^{2+} ions from their normal position and gave rise to an excess positive charge at those locations. (iii) Two of the

three O^{2-} ions originally derived from Ga_2O_3 and the two displaced Zn^{2+} ions formed additional $Zn^{2+}O^{2-}$ units (ZnO(s)), (iv) The third O^{2-} ion originally associated with Ga_2O_3 was ejected into the gas phase as 1/2 O_2(g). Two electrons left behind from (iv) were shown as $\ominus$. These carriers were responsible for the conductivity of the mixed Ga_2O_3-ZnO oxide system. These electrons converted two Zn^{2+} ions in the lattice to the Zn^{+} form. The mixed oxide was therefore designated as $Ga^{3+}_{x}Zn^{2+}_{1-x}Zn^{+}_{x}O^{2-}_{1+x}$ which indicated that Zn was encountered in two valence states.

He further mentioned that for the above type of materials, the plot of ln σ versus 1/T yielded slopes that were proportional to the free energy of activation $\Delta G^{\ddagger}$ and not proportional to the energy gaps as in the case of standard semiconductors. He obtained expressions for conductivity and Seebeck coefficient α, as

$$\sigma \sim s(1-s)$$
$$\alpha \sim \ln (1-s)/_{s}$$

where s the probability that a given site would contain an extra charge carrier was given by him as

$$s = \frac{M^{(n)}}{[M^{(n)} + M^{(n+1)}]}$$

Here, $M^{(n)}$ and $M^{(n+1)}$ are the numbers of cation in valence state n and n + 1 respectively.

1.5. RuO_2 BASED THICK FILM RESISTORS

W. M. Faber and coworkers[36] first produced RuO_2-based thick film resistors. The glass-RuO_2 mixture was suspended in an organic vehicle using ethyl cellulose dissolved in a mixture of acetone and toluene. They could vary the film thickness between 5 and 75 μ by varying the amount of organic part. The resistive paste was screen printed on the surface of a non-conducting material and fired to give resistance element having resistance value of 60-181000 $ohms/cm^2$ and with thermal coefficient of resistivity less than 100 $ppm/^oC$.

G. S. Iles[9,10] and T. H. Lemon[11] developed RuO_2-based thick film resistors incorporating Nb_2O_5 as a dopant. Iles used Nb_2O_5 upto 20 wt. % and calcined with RuO_2 to control the deviating valency of Ru within narrow limits and to the control of thermal coefficient of resistance. RuO_2 formed a solid solution with Nb_2O_5 and on adding 20 wt. % Nb_2O_5 the lattice parameter 'a' changed from 4.49Å to 4.57Å and the 'c' parameter from 3.11Å to 3.07Å. Zn and Cd borosilicate glasses were found to be preferable to Pb borosilicate glass in that they could modify the TCRs of resistor composition by ± 250. They also studied drift, power dissipation and thermal stability of the glaze resistors.

Taketa Y. and coworkers[29] used RuO_2 doped with Bi to prepare thick film resistors. They observed improved electrical properties such as low temperature dependence of resistance,

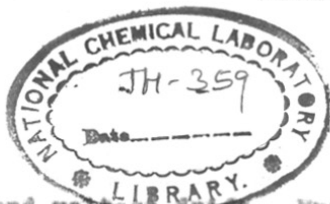
NATIONAL CHEMICAL LABORATORY
JH-359
Date
LIBRARY.

current noise and voltage drift. Mutual diffusion between conductive and glass phases was thought to be responsible for such improvements.

Y. Taketa and M. Haradome[30] developed RuO_2-based thick film resistors by using conductive and glass components and additives to improve wettability. The conductive component consisted of $Bi_2Ru_2O_7$ containing 5-20 wt. % of a dopant which had a composition similar to glass component. For example, one dopant was SiO_2 16, PbO 66, B_2O_3 10, ZnO 5 and ZrO_2 3 wt. %. They claimed to have achieved a lower drift voltage value for their resistors.

V. Taketa, M. Nita, K. Ebara and M. Haradome[31,32] investigated the resistance change of RuO_2-based thick film resistors in relation to humidity and oxidising-reducing atmospheres. The resistance change increasd with time at high humidity and with increasing RuO_2 concentration. The resistance was found to be stable in oxidising atmosphere but changed in the reducing atmosphere. They suggested use of systems such as $Bi_2Ru_2O_7$ to improve the stability of the RuO_2-based thick film resistors.

L. J. Brady[33] studied the effect of particle size of RuO_2 on the electrical properties of fired resistors. He found that alteration in the elemental resistor structure could be used to explain the changes observed.

621.382:661.888.45(043)
SHI

H. Seyama, C. Tanuma and K. Kitahara[34] studied the reliabilities of RuO_2-Bi, RuO_2-Ag and RuO_2 thick film resistors at 40° and 70°C with respect to relative humidity 91 ± 3 %. They showed that when RuO_2 based resistors were coated with a protective layer the change in resistivity was reduced compared to those without coatings.

Y. Taketa[35] studied the relation between electrical properties and RuO_2 concentration. The properties studied were TCR, current noise and specific surface resistivity. Various processing conditions for optimising the film properties were discussed. The mixture of 15-55 wt. % RuO_2, 15-25 % Ag , 20-60 % glass frit and 35-55 % organic vehicle was used to obtain the films. He used the DTA, TG, SEM, EMPA and XRD techniques to examine the chemical and structural changes with heat treatment.

There is good amount of patent literature covering the various aspects of thick film resistors. The patent literature dealing with RuO_2-based thick film resistors can be classified into five categories, according to the conductive phase used.

(1) Compositions where conductive phase is RuO_2

In this type of compositions the RuO_2 powder and glass frit powder are mixed and blended with organic vehicle to give the resistive paste. Table 1.3 summarizes the various compositions.

TABLE 1.3

Compositions containing RuO_2 as conductive phase

Composition of paste wt. % of			Composition of glass wt. % of				Sheet resistivity k Ω/sq.	TCR ppm/°C	Ref.
RuO_2	Glass	Organic vehicle	PbO	B_2O_3	SiO_2	Al_2O_3			
12.86	58.57	28.57	-	-	-	-	4.38-5.86	86	37
20	60	20	85	2	8	5	1	-	38
20	60	20	85	2	8	5	-	-	39
10	90	-	71.7	5	21	2.3	0.5	80	40

(ii) Composition where conductive phase is glass containing RuO_2

Instead of separately taking the physical mixture of RuO_2 and glass and dispersing it in organic vehicle, the glass obtained by melting and quenching the ingredients and RuO_2 together is dispersed in organic medium to give resistive paste. The resistors obtained with this resistive paste have higher sheet resistivity values (Table 1.4).

TABLE - 1.4

Compositions where conductive phase is glass containing RuO_2

Composition of conductive phase wt. % of						Organic vehicle	Sheet resistivity Ω/sq.	Ref.
PbO	B_2O_3	SiO_2	Al_2O_3	RuO_2	Other oxides			
80	3	8.1	7	1.9	-	Solution of ethyl cellulose in α terpineol	4.5×10^5	41
80	3	6.5	7	3.5	-	-do-	1.7×10^5	42
50	-	37.5	-	12.5	-	Oile spike 2, lavende oile 3, camphor oil 33, oile of potent grain 33 parts.	90	43
40-85	-	10-30	1-5	1-40	0-5			44

(iii) Compositions where a mixture of RuO_2 with other additive form conductive phase

The additives improve certain properties of thick film resistors. They are variously known as TCR modifiers or viscosity controlling agents according to their function. To obtain the resistive paste a mixture of RuO_2, additives and glass frit powder is dispersed in an organic vehicle. Table 1.5 gives different types of additives.

TABLE - 1.5

Composition where mixture of RuO_2 with additives form conductive phase

Amt.of RuO_2 wt. %	Additives	Amt.of additives wt. %	Amt.of glass wt. %	Sheet resistivity Ω/sq.	TCR ppm/deg.	Ref.
1-30	V_2O_5	1-10	-	-	< ± 20	45, 46
7-11	Ta_2O_5	4				
	Sb_2O_3 or					47
	Bi_2O_3		20			
	Ag	20				
	Modified glass	43-47				
10	Al_2O_3	23	67	5-100000	-100	48
40-60	Sb_2O_3	4	60	52	+52	49
20	CaF_2	2	46.5	31	-	50
	Nb_2O_5	0.4				

(iv) Compositions where RuO_2 forms solid solution with other oxide to provide conductive phase

The stability of thick film resistors is improved when this type of conductive phase is used. Two solid solution compositions are listed in Table 1.6.

TABLE - 1.6

Compositions where RuO_2 forms solid solutions with other oxides to provide the conductive phase

Composition of solid solns. mole %	Glass compositions wt. % of			Amt. of glass mole %	Sheet resistivity Ω/sq.	TCR ppm/deg.	Ref.
	PbO	B_2O_3	SiO_2				
Bi_2O_3 1, RuO_2 0.9 Nb_2O_5 0.5, Ta_2O_5 0.5	30	45	25	0.25	234080	-79 to -83	51
PbO 1, RuO_2 0.9 Nb_2O_5 0.5	30	45	25	0.10	85340	-115 to -103	52

(v) Compositions where ruthenates are used as conductive phase

The ruthenates listed in Table 1.7 have been evaluated as the conductive phase in thick film resistors.

TABLE - 1.7

Compositions where ruthenates are used as conductive phase

Ruthenates used	Amount of ruthenates wt. %	Glass composition wt. %					Amt. of glass wt. %	Organic vehicles used	Amt. of organic vehicle	Ref.
		PbO	B_2O_3	SiO_2	CaO	Al_2O_3				
$Tl_2Ru_2O_7$	35-45	65	10	26	-	-	45	β terpi -neol	20-30	53
$Bi_2Ru_2O_7$	10	65	10	25	-	-	50	-do-	-	54
$BaRuO_3$	30	50	8	34	5	3	70	Terpineol	-	55
$Ca_{0.5}Ba_{1.5}Ru_2O_{65}$	57.4	43.5	4.9	37.5	9.8	4.3	17	-do-	23	56

1.6. BEHAVIOUR OF RuO_2 IN GLASS

J. Mukherji[57,58] studied the RuO_2-glass systems. He determined the solubility of RuO_2 and oxidation state of Ru in silicate and phosphate glasses as a function of Na_2O and P_2O_5 content.

The results showed that the solubility of RuO_2 was almost constant at 125 ppm for compositions containing less than 25 mole % of Na_2O. The solubility increased sharply, above 25 mole % of Na_2O to nearly 2500 ppm at 40 mole % of Na_2O. The solubility of RuO_2 in phosphate glasses was nearly 200 times greater and again showed a sharp increase when P_2O_5 content was above 50 mole %.

Two of the available oxidation states of Ru were found to be in equilibrium in silicate glasses, whereas only one oxidation state of Ru was evident in phosphate glass. Ru(IV) was present along with the Ru(III) and Ru(VI) in silicate glasses having Na_2O content less than 25 mole % and greater than 25 mole % respectively. In phosphate glasses Ru(VI) and Ru(VII) were the species thought to be present when P_2O_5 was above and below 50 mole %.

Absorption spectra[59] of Ru in borosilicate and borophosphate glasses showed that Ru was present as Ru^{4+} and Ru^{7+} in borophosphate glasses and as Ru^{3+} and Ru^{4+} in borosilicate glasses. Ru^{5+} was not detected in any of the glasses studied.

R. W. Vest[61] selected for his work the lead borosilicate glasses which were more covalent than those containing

Na_2O. Hence it was difficult to apply the results discussed above to the lead borosilicate glass other than to extrapolate to low Na_2O content. This would imply that the solubility of ruthenium should be very low, perhaps only a few ppm, that the evaporation of ruthenium from the surface of a thick film resistor would be very low and that some dissolved ruthenium might be hexavalent instead of tetravalent as normally assumed.

A. Prabhu, G. L. Fuller and R. W. Vest[60] studied the solubility of RuO_2 in lead borosilicate glass. The solubility of a mixture of 10% RuO_2 powder in glass having the composition PbO 63, B_2O_3 25 and SiO_2 12 wt. % was measured. The mixture was heated from 15 minutes to 12 hours. The amount of Ru detected was plotted as a function of temperature. The results showed that the average concentration of Ru in the glass fired for 15 minutes at 800°C was approximately 4 ppm and at 1000°C, the solubility was less than 35 ppm. The effect of small particle size on solubility was used to explain why the concentration of Ru in glass fired at 1000°C was greater after 15 minutes than after 12 hours. During the initial heating, the smallest particles dissolved rapidly and created a supersaturated solution around them. The Ru then diffused through the glass and precipitated as RuO_2 on the surface of larger particles, eventually this decreased the total Ru to the equilibrium value in the glass. The increase in RuO_2 particle size by the annihilation of the smaller particles, reduced the

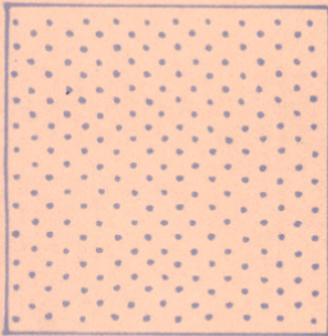

(a) UNIFORM

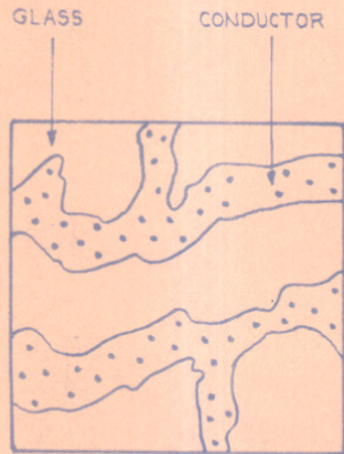

(b) UNIFORM CHANNEL

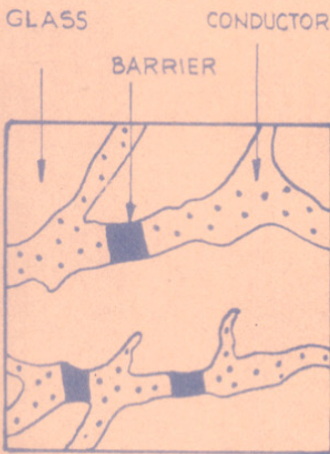

(c) NON TUNNELING BARRIER

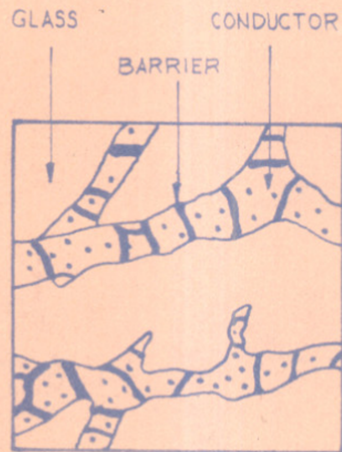

(d) TUNNELING BARRIER

FIGURE 1·3 : FOUR GENERAL CATEGORIES OF CONDUCTION MECHANISM MODEL

total surface area. It was concluded that this was a destructive force in the development of thick film microstructure.

1.7. CONDUCTION MECHANISM OF RuO_2 BASED THICK FILM RESISTORS

Many conduction mechanism models have been proposed to explain the electrical properties of thick film resistors. G. E. Pike and C. H. Seager[62] have classified them into four general categories to facilitate comparison to their data.

Figure1.3(a) illustrates the first model called the uniform model. In this model, the metallic constituents were presumed to dope the glass and provide a type of impurity conduction. Sartain[63,64] is reported to have explained his results on this model. He observed that the curves of the resistance vs temperature of thick film resistors made with RuO_2 and for glass were similar to the corresponding curves of heavily doped silicon. He concluded that RuO_2 had produced a semiconducting glass that was degenerate at high level of doping.

Figure 1.3(b) represents the uniform channel model. In this model it was reported that electric current flowed along the connected paths of conductive constituents only. These were paths supposed to have formed either by random contact or by actual particle to particle sintering. L. J. Brady[65] had proposed this model. He had assumed that conductance in thick film

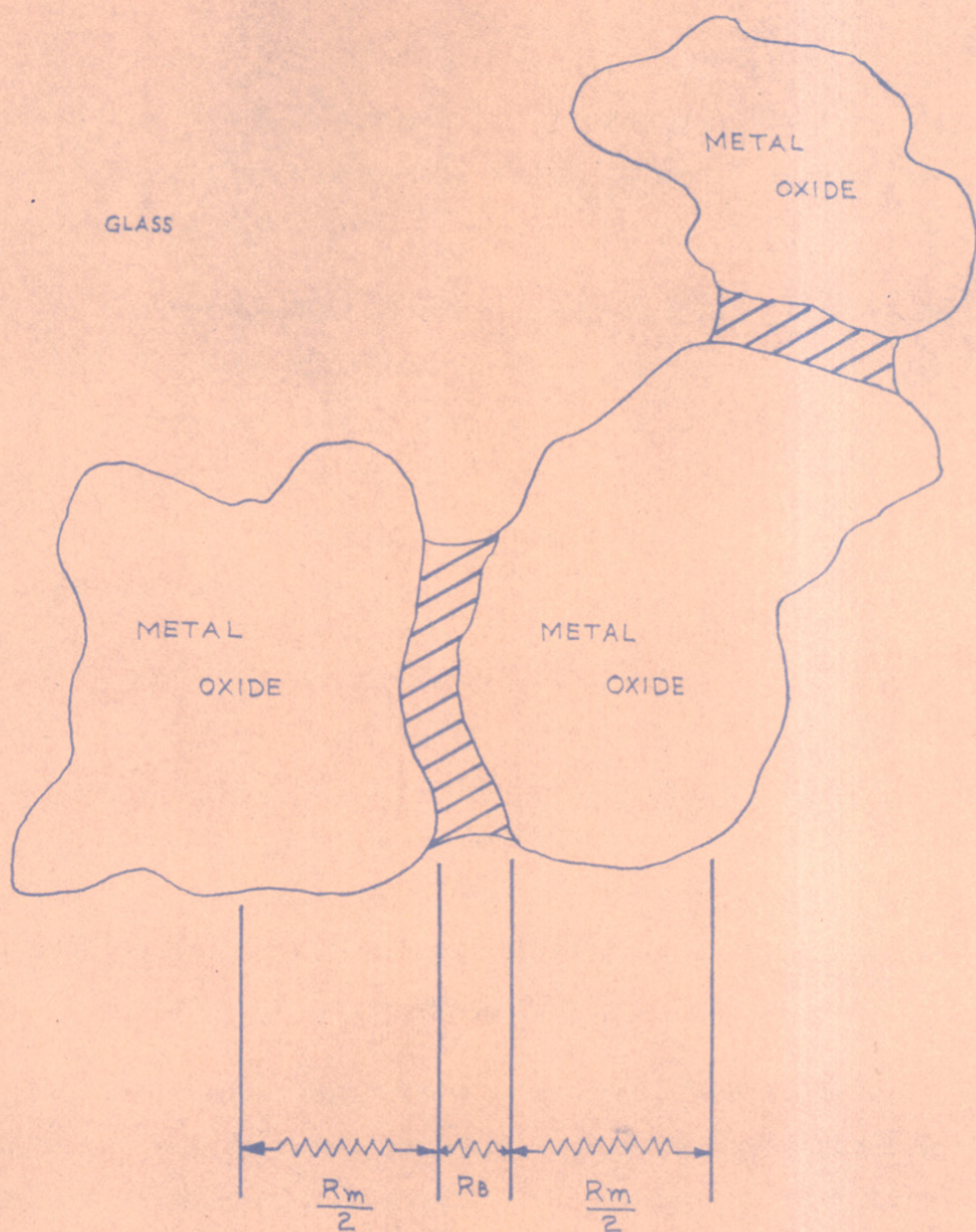

FIGURE 1·4 : THE BASIC UNIT OF TUNNEL BARRIER MODEL

resistor was due to a network of conductors in the form of overlapping cylinder or needle shaped elements arranged in a 'Jack-Straw' fashion.

A third model termed as channel model is shown in Fig. 1.3(c). Here the channels of conductive particles were interrupted by barriers of semiconducting or poorly insulating glass phase. Pike and Seager[62] placed this model in the non-tunneling barrier category because the electron transfer through the barriers was by a non-tunneling mechenism.

The last type of model, i.e. the tunnel barriers model, is illustrated in Figure 1.3(d). Here, the current channels were reported to consist of metallic particles separated by barriers. These barriers were supposed to be thinner and conduction was by tunnelling processes. These included direct particle to particle tunnelling and tunnelling through one or more intermediate states in the barrier.

Pike and Seager further proposed that in thick film resistors, the electrical conduction was through a network of interconnected chains of metal oxide particles. The metal oxide particles did not actually touch, but rather they were separated from their neighbours on the chain by the glassy layer as illustrated in Figure 1.4. Much of the resistance was supposed to be offered by these tunnel barriers. Their etching and resistering experiments supported the presence of thin glass layer in between two metal oxide particles.

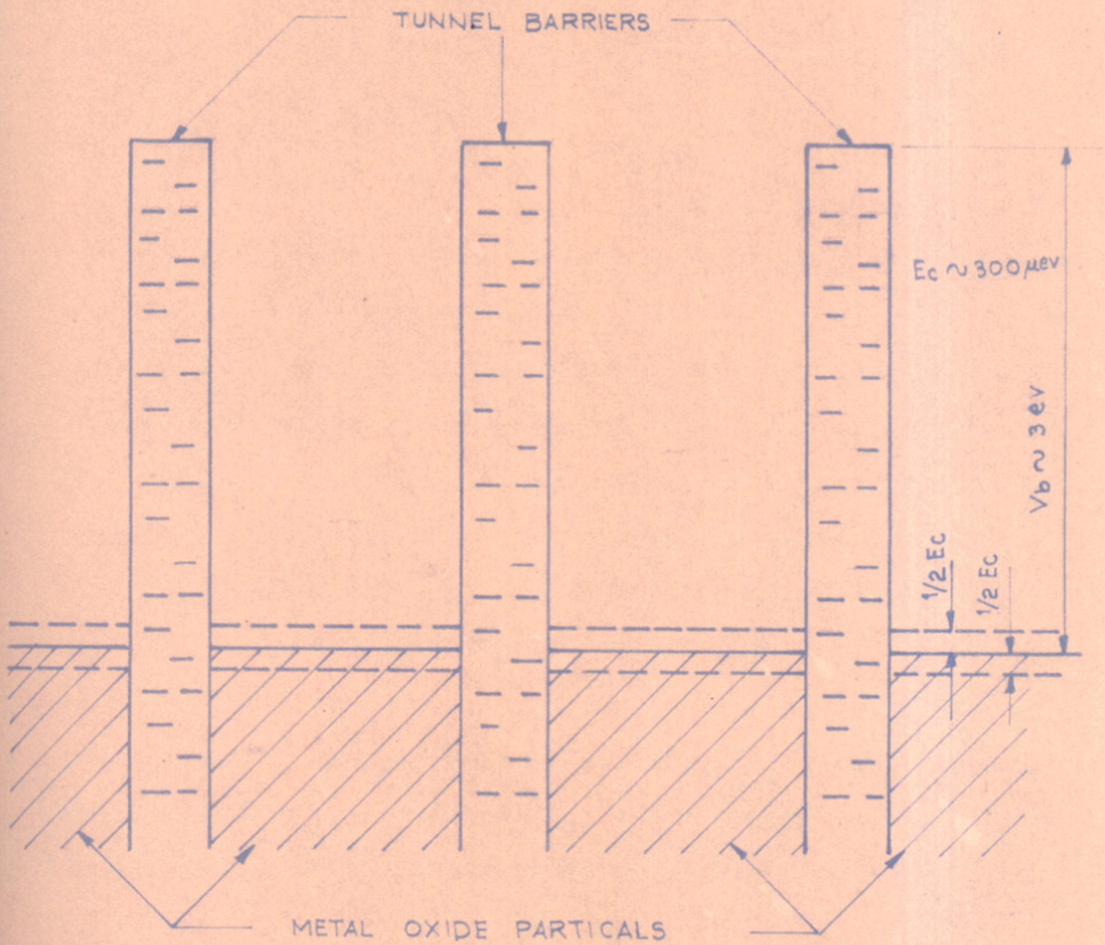

FIGURE 1·5 : ENERGY LEVEL DIAGRAM FOR TUNNEL BARRIER MODEL

For two uncharged metal spheres of radius r separated by a surface spacing s in a medium of dielectric constant, , the energy needed to transfer one electron charge from one sphere to the other is given by[66,67]

$$E_C = \frac{1}{2} Q^2/C$$
$$= e^2/[4\pi\epsilon\epsilon_0 \, r \, k\,(r,s)]$$

where k is a function which depends weakly on r and s. Pike and Seager, using parameters for thick film resistors, $r \sim 0.2$ μm, $\epsilon \sim 7$[79] and $k \sim 3$; found the charging energy $E_C \sim 340$ μeV. They showed that activation energy should be $\frac{1}{2} E_C \sim 170$ μeV. This value was in good agreement with their experimental results. They have given a energy level diagram (Figure 1.5) for a chain of particles separated by tunnel barrier of thickness s. The neutral, the first positive and negative charging levels for each particle were drawn. The charging levels have been spread out because of the particle size variation. This is shown in Fig. 1.5. The energy E_C was the total energy required to move an electron from one particle to another and so half of that value was assigned to each particle.

Pike and Seager believed that interparticle barriers contained impurities which offered the barrier conductance. They proposed that at least some of the impurities acted as resonant tunnelling centers, that is, there was an attractive potential within the barrier having a localized energy level at an energy reasonably accesible to electrons. Primarily these centers

enhanced the tunnelling transition especially for the electrons whose energy was near the localized level. For a given type of impurity local environments in the disordered microstructure of the glass would be different and the associated energy levels would spread as shown in Figure 1.5.

The absolute Seebeck coefficients measured on three resistor series were small ($\sim$ 10 μV/k) and very close to the value measured on the extracted metallic material such as lead-bismuth ruthenates. The resistors had thermopower close to that of metallic oxide because the particles were roughly 100 times thicker than the barriers and thus most of thermal gradient was across the metal oxide. The Seebeck coefficients of thick film resistors was an average over the glass and conducting channels, weighted by the conductivity of each,

$$S_{eff} = \frac{S_{gl}\,\sigma_{gl} + S_{ch}\,\sigma_{ch}}{\sigma_{gl} + \sigma_{ch}}$$

The glass conductivity was much lower than the conducting chains and the glass thermopower hardly contributed to S_{eff}.

This tunnel barrier model proposed by Pike and Seager also accounted for other results such as electric-field dependence of conductance, frequency dependence of conductance and Hall effect.

M. P. Ansell[68,69] investigated the structure of three families of thick film resistors by SEM and EPMA and concluded that thick film resistors were principally two phase materials, with a doped lead borosilicate glass surrounding crystalline particles. The phases identified for each resistor series are as follows

Name of the series	Phases identified
DuPont 1100	$Bi_2Ru_2O_7$ crystallites and CdO doped glass.
Alloy B	RuO_2 crystallites and Ru, Ag doped glass.
Electroscience 700	Pd/PdO/Ag crystallites and Pd, Ag doped glass.

He observed that a mixed conduction process which was a combination of the processes occurring in the two phases. Conduction process in thick film resistors would not require strong thermal activation and hence he ruled out processes such as Schottky barrier emission, conduction via field ionisable donor defects, ionic conduction and space charge limited conduction. Processes requiring only a weak thermal activation of less than kT were given by

(1) Narrow band metallic conduction with dense scattering by imperfections rather than phonons, and

(2) Trap tunnelling.

Trap tunnelling in the glass phase has been described by him. In the glass, density of states diagrams have been postulated

to be similar to those of crystalline solids except that the energy band states will be smeared out into regions of localised states as shown in Figure 1.6. If the Fermi level lies between the conduction band and valence band states the conduction cannot be metallic or narrow band metallic and there are two possible mechanisms suggested for conduction via the localised states. They are

(1) Thermal ionization of carriers, e.g. electrons from donor states into the conduction band.
(2) Phonon-assisted quantum, mechanical trap tunnelling or hopping between localised states.

The first process being a highly negative TCR process, it was discounted for thick film resistors. Trap-tunnelling, a weakly activated process with several trap sites below the conduction band was considered (Figure 1.7). Two conduction paths were possible for the transfer of charge from trap A to B. These paths were

(1) Thermal ionization and band conduction.
(2) Phonon-assisted hopping.

Ansel suggested trap-tunnelling conduction between trap sites in glass phase where space and energy limitations allowed the hopping process to be only very weakly activated.

The suggested dual nature of conduction in thick film resistors was supported by his measurements of energies, E_A.

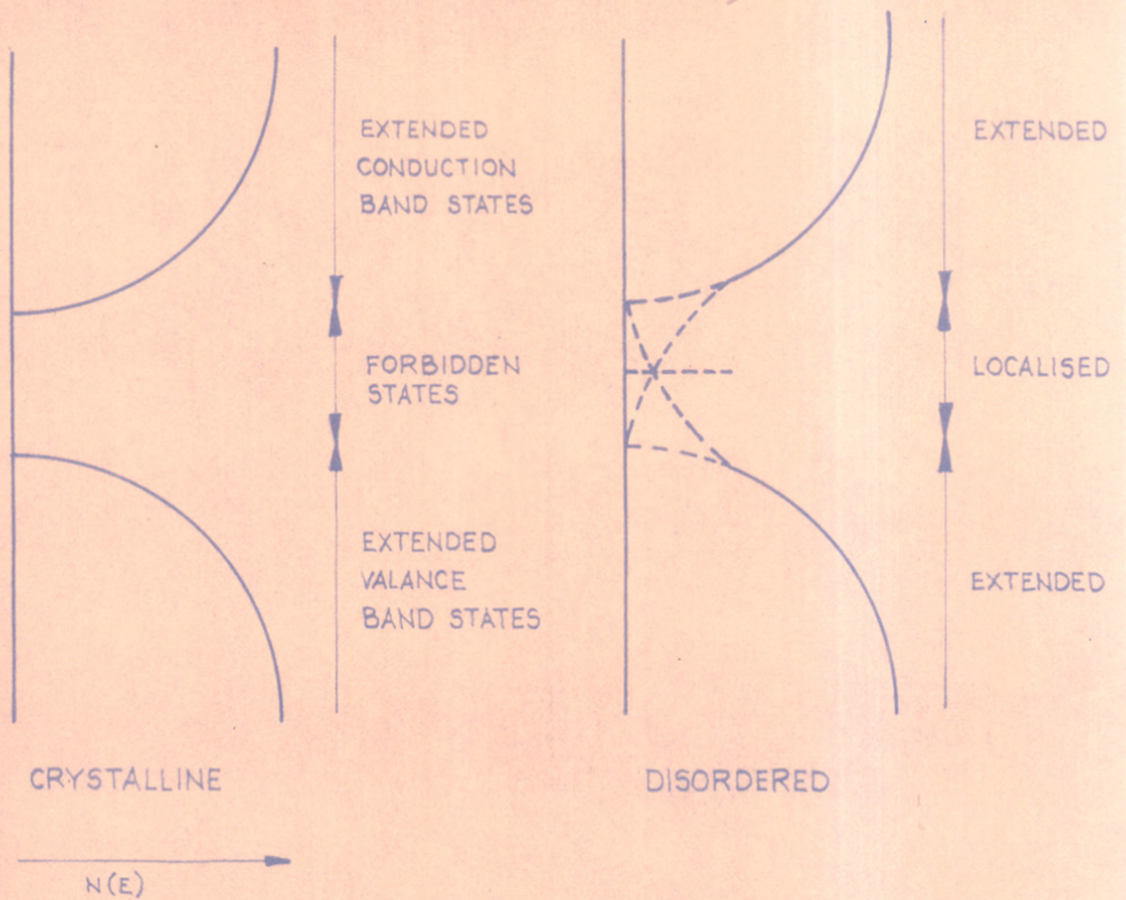

FIGURE 1-6 : THE DISTRIBUTION OF STATES IN CRYSTALLINE AND DISORDERED SOLIDS

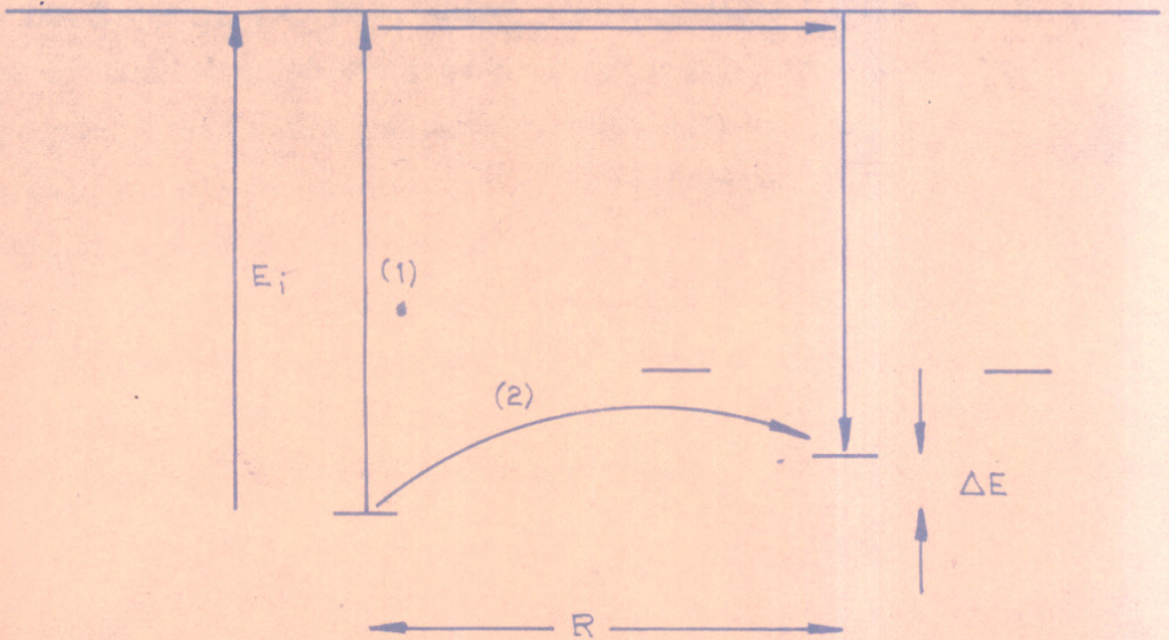

(1) THERMAL IONIZATION AND BAND CONDUCTION

(2) PHONON ASSISTED HOPPING

FIGURE 1-7 : CHARGE TRANSFER VIA TRAPS

for conduction in three series of thick film resistors. Thus he concluded that a mixed conduction process took place which was a combination of the process occurring in the two phases. The crystalline phase conducted metallically and charge flow through the glassy phase occurred by trap-tunnelling with low activation energies between 10^{-5} to 10^{-3} ev. According to Ansel this could only happen in the narrow band of states. This narrow band was suggested to be formed by the doping of the glass by ions either incorporated in the glass structure or diffused in from the crystallite phase.

CHAPTER - 2

E X P E R I M E N T A L

2.1. PREPARATION OF RuO_2-V_2O_5 SYSTEM

Ruthenium dioxide (Fluka, made in Switzerland) and ammonium metavanadate (Reanal, Budapest, Hungary) were used for the preparation of solid solutions of ruthenium dioxide and vanadium pentoxide. Weighed quantity of ammonium metavanadate was taken in an agate mortar and the amount of ruthenium dioxide needed to give the required composition was slowly added to it, and mixed thoroughly in distilled, dry acetone with an agate pestle. The mixture was then transferred to a clean and dry platinum crucible, covered with a platinum lid and heated at 1000°C in an electric furnace for 24 hours, then allowed to cool down to room temperature outside the furnace.

This procedure was followed for all the compositions given in Table 2.1.

TABLE - 2.1

Compositions Prepared

Sr. No.	Weight per cent RuO_2	Weight per cent V_2O_5	Mole per cent RuO_2	Mole per cent V_2O_5	Nomenclature
1	98	2	98.5289	1.4711	A
2	96	4	97.0418	2.9582	B
3	94	6	95.5386	4.4614	C
4	92	8	94.0187	5.9813	D
5	90	10	92.4822	7.5178	E

2.2. X-RAY ANALYSIS

The pure ruthenium dioxide and the prepared compositions of RuO_2-V_2O_5 system were examined by X-ray analysis. These samples were run on a X-ray diffractometer (Philips P W 1730, Holland) at room temperature using CuKα X-ray radiation.

From the diffractometer patterns Bragg angles (2θ) and intensity of the X-ray diffraction peaks were calculated. The d values corresponding to the Bragg angles were taken from the X-ray conversion table. The d values of all the samples thus obtained were compared with the d values of the standard ASTM patterns for RuO_2. This showed that RuO_2 and prepared compositions of RuO_2-V_2O_5 oxide system had the tetragonal rutile structure. Hence the lattice parameters were calculated using the formula

$$\left[\frac{h^2}{a^2} + \frac{k^2}{a^2} + \frac{l^2}{c^2}\right]^{-1/2} = d$$

All these data for RuO_2 and RuO_2-V_2O_5 oxide systems (compositions A, B and C) are listed in Tables 2.2, 2.3, 2.4 and 2.5.

2.3. PREPARATION OF GLASS

A lead borosilicate glass having the composition of 63 % PbO, 10 % B_2O_3, 17 % SiO_2, 3 % Al_2O_3, 2 % ZrO_2 and 2 % ZnO was chosen for this work. To prepare the glass, the ingredient materials were dried in an electric oven at 100°C for two hours and cooled in a desiccator. Weighed quantities of these dried

TABLE 2.2

Structural data for RuO_2

S.No.	Intensity	2 θ	d	hkl	Lattice parameters (Å) a	c
1	100	27.98	3.1861	110	4.5058	
2	52	35.00	2.5615	101		3.1189
3	12.33	40.02	2.2510	200	4.5020	
4	4	40.48	2.2265	111		
5	1	45.00	2.0128	210	4.5008	
6	36	54.22	1.6903	211		3.1318
7	11	57.96	1.5898	220	4.4966	
8	4	59.38	1.5551	002		3.1102
9	6	65.62	1.4215	310	4.4952	
10	7	66.90	1.3974	112		3.1125
11	7	69.54	1.3506			
12	3	74.52	1.2722	202		3.0882
Average values of lattice parameters					4.4897	3.0882 3.10745

TABLE 2.3

Structural data for RuO_2-V_2O_5 system where V_2O_5 is 2%

S. No.	Intensity	2 θ	d	hkl	Lattice parameters (Å) a	c
1	100	27.96	3.1883	110	4.5089	
2	62	35.02	2.5600	101		3.1117
3	16	40.00	2.2521	200	4.5042	
4	4	40.56	2.2222	111		
5	2	45.00	2.0128	210	4.5008	
6	45	54.28	1.6885	211		3.09835
7	10	57.92	1.5908	220	4.4995	
8	4	59.60	1.5499	002		3.0998
9	10	65.50	1.4238	310	4.5024	
10	8	67.08	1.3941	112		3.1012
11	12	69.58	1.3500			
12	4	74.26	1.2760	202		3.0974
Average values of lattice parameters					4.5017	3.0992

TABLE - 2.4

Structural data for RuO_2-V_2O_5 system where V_2O_5 is 4%

S. No.	Intensity	2 θ	d	hkl	Lattice parameters (Å) a	c
1	100	27.82	3.2041	110	4.5313	
2	52	35.08	2.5558	101		3.1009
3	16	39.88	2.2586	200	4.5172	
4	6	40.52	2.0333	111		
5	2	44.80	2.0213	210	4.5198	
6	53	54.16	1.6920	211		3.1031
7	11	57.80	1.5938	220	4.5079	
8	3	59.88	1.5433	002		3.0866
9	9	65.40	1.4257	310	4.5085	
10	7	67.30	1.3900	112		3.0883
11	13	69.46	1.3693			
12	5	74.42	1.2737	202		3.0857
Average values of lattice parameters					4.5134	3.0929

TABLE - 2.5

Structural data for RuO_2-V_2O_5 system where V_2O_5 is 6%

S. No.	Intensity	2 θ	d	hkl	Lattice Parameters (Å) a	c
1	100	27.62	3.2268	110	4.5634	
2	40	35.00	2.5615	101		3.1074
3	13	39.70	2.2634	200	4.5268	
4	4	40.50	2.0342	111		
5	2	47.70	2.0256	210	4.5294	
6	41	54.10	1.6937	211		3.0952
7	13	57.60	1.5988	220	4.5221	
8	3	60.00	1.5405	002		3.0810
9	8	65.20	1.4296	310	4.5208	
10	4	67.44	1.3875	112		3.07965
11	11	69.38	1.3534			
12	3	74.60	1.2711	202		3.0876
Average values of lattice parameters					4.5248	3.0859

ingredient materials, needed to give the required composition were taken in an agate mortar and mixed thoroughly in distilled, dry acetone with an agate pestle. The mixture was then dried and transferred to a clean and dry platinum crucible. The crucible was introduced in an electric muffle furnace at 800°C and heated at this temperature for 20 minutes. The mixture was completely melted. The molten mass was poured into distilled water for fritting the glass. This glass frit was taken in a stainless steel mortar and powdered in distilled water with a stainless steel pestle. The powder was then wetmilled for 24 hours in a porcelain jar using porcelain balls. The wetmilling was done under the medium of distilled water. The milled glass frit powder was examined under optical microscope. The particle size was found to be of the order of 1 to 2 μm.

2.4. FORMULATION OF THE PASTE

Generally the paste consists of four components; electrically active materials (or conductive phase), a low softening glass, organic filler and solvents. Each of the components has a definite role to play. The components which we have used with their specific role are listed in Table 2.6.

The volatility of the solvent system is the important factor for ease of screening. Excessively volatile solvent tends to dry out during use and a solvent of very low volatility

TABLE - 2.6

Components of the paste and their functions

Sr.No.	Components	Materials we used	Function	Total wt.
1	Electrically active material (conductive phase)	RuO_2 and compo-~~nents~~ sitions A,B and C	Conduction	24
2	Glass frit	Lead borosilicate glass	Flux (binder)	56
3	Organic filler	Ethyl cellulose	Filler	1.6
4	Organic solvent	Butyl cellosolve + butyl carbitol acetate + β terpi-neol	Solvent	18.4

does not provide good wetting of the particles. Hence a mixture of three solvents having different volatility is used. β-Terpineol 40%, butyl cellosolve 30% and butyl carbitol acetate 30% are mixed to give a solvent of desired characteristics.

To prepare paste, a weighed quantity of RuO_2 was taken in an agate mortar and the amount of glass frit powder needed to give the required composition was added to it and mixed thoroughly in distilled, dry acetone with an agate pestle. This mixture was then dried at 100°C for one hour in an electric oven. Weighed quantity of ethyl cellulose was taken in another clean and dry agate mortar and the amount of organic solvent needed to give the required composition was added to it and mixed thoroughly with an agate pestle. The above mixture of RuO_2 and glass was then added and mixed thoroughly with an agate pestle to give pastelike structure.

This procedure was repeated using different compositions of RuO_2-V_2O_5 system to give the pastes listed in Table 2.7.

TABLE - 2.7

Composition of the pastes prepared

Sr.No.	Composition of conductive phase wt.% of		Glass frit wt. % of	Organic vehicle wt. % of
	RuO_2	V_2O_5		
1	24	0	56	20
2	23.52	0.48	56	20
3	23.04	0.96	56	20
4	22.56	1.44	56	20

2.5. SCREEN PRINTING[82]

Screen printing is a technique that takes the bulk and puts it on the substrate in the desired geometry[70].

The simplest form of the printer system is a mechanical assembly that maintains the substrate and the screen in their proper relative positions and drives the squeegee.

The squeegee is a device that causes the ink to transfer from the ~~resistor~~ reservoir on the top of the screen onto the substrate beneath the screen.

Figure 2.1 shows the mechanical assembly that maintains the substrate and the screen in their proper relative positions. The screen frame can be fixed to the vertical section with a C-clamp. Together they can be moved up with the help of the ~~things~~ hinges fixed to the main board. This facilitated the changing of the substrates. Arrangement has been provided to hold a 1" x 1" substrate.

Figure 2.2 shows the schematic representation of the screen and the substrate. The screen is tightly fixed to a frame. The screen has all of its mesh blocked with a cellophane tape except the pattern that is to be printed. The squeegee pushes the ink across the open mesh pattern, forcing a portion of the paste onto the substrate placed underneath.

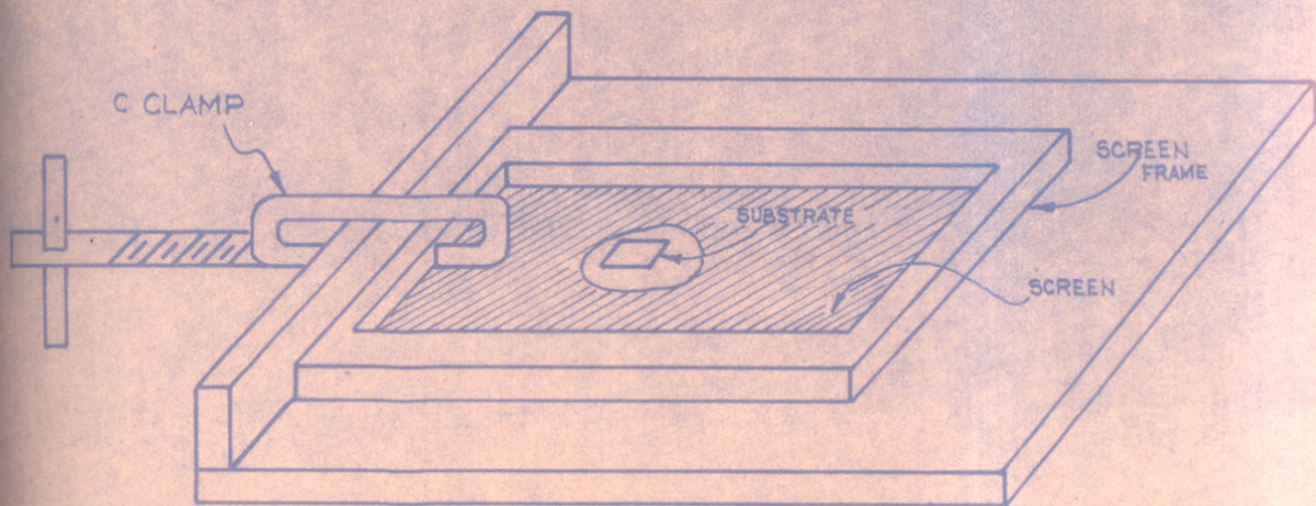

FIGURE 2-1: MECHANICAL ASSEMBLY TO MAINTAIN THE SUBSTRATE AND THE SCREEN IN THEIR PROPER RELATIVE POSITION

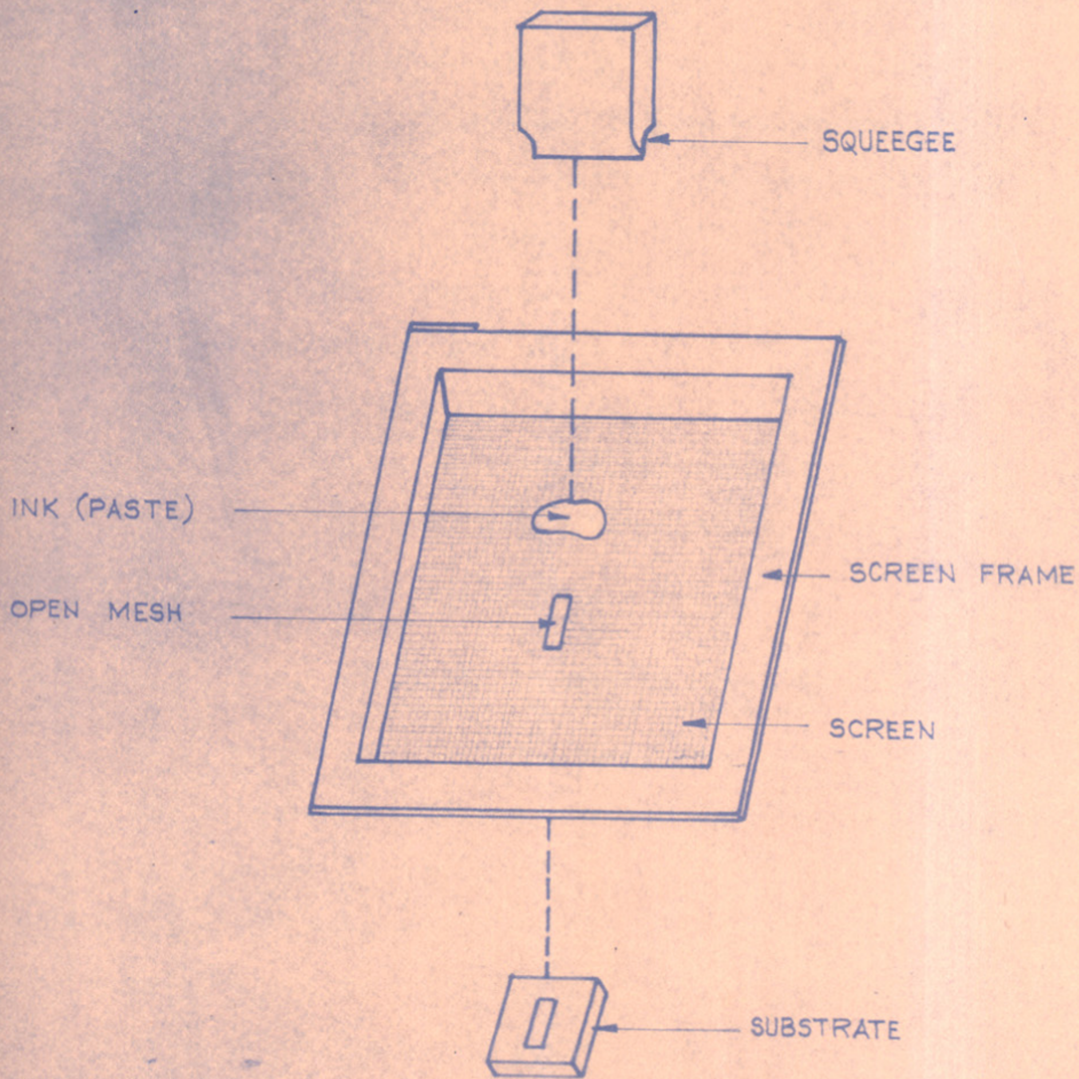

FIGURE 2·2 : SCREEN PRINTING – A SCHEMATIC REPRESENTATION

Figure 2.3 shows a cross-section of the screen printing operation depicted in Figure 2.2. Figure 2.3(a) shows the screen prior to the printing stroke. The screen is held slightly above the substrate. During the stroke there is downward pressure on the substrate. As the squeegee moves over the substrate (Figure 2.3(b)) the paste is forced through the open pattern onto the substrate. As the squeegee moves across, the screen is lifted free behind it, in a peelling action which leaves the deposited paste adherent to the substrate. Normally this peelling action or snap-off is completed before the squeegee finishes its stroke and lifts clear of the screen as shown in Figure 2.3 (c).

2.6. MATERIALS USED FOR SCREEN PRINTING

Substrate : The high firing temperature necessitates the use of ceramic materials for substrate. 96% Alumina has been very widely used in thick film industry. This material has all the required properties. This has coefficient of thermal expansion equal to $6.0 - 8.0 \times 10^{-6}$ in/^{o}C. We also have used 96% alumina substrates (1" x 1" x 0.002) obtained from M/s. Electronic Slicing and Dicing, Inc., U.S.A., having the following specifications:

Material	: 96% Al_2O_3 as fired.
Length and width tol.	: ± NLT ± 0.005 in.
Thickness tol.	: ± 12% NLT ± 0.0015 in.
Camber	: 0.004 in/in.

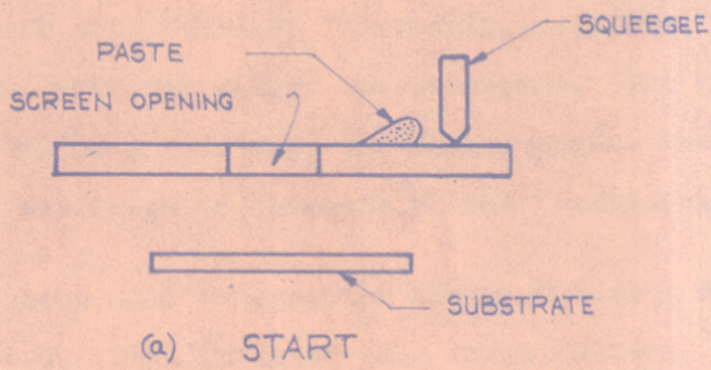

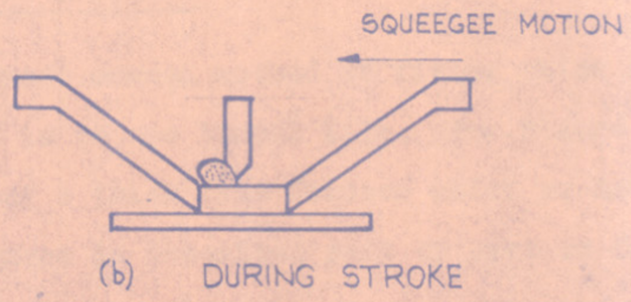

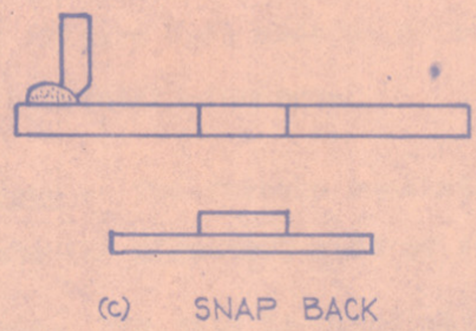

FIGURE 2·3 THE SCREEN PRINTING CYCLE

Squeegee : The squeegee material should be compatible with the solvents used in thick film process. It should not swell, distort or wear off with use. Generally, neoprene, polyurethane or "viton" are used for making the squeegees. The hardness (normally 50-90 on durometer), the attack angle, the pressure we apply and the speed of movement of the squeegee are important.

We have used rectangular piece of 2 cm x 5 cm with a square cut edge. This is fixed in a brass holder.

2.7. FIRING FACILITY

The most common method of firing thick film resistors and conductors is to use tunnel kiln. The Figure 2.4 shows the cross section of a thick film furnace which we have used in this work. The furnace is described part by part as follows:

Silica trolley - The sample to be fired is kept over a silica trolley (Figure 2.5) made up of silica. This silica trolley moves through a tubular furnace.

Furnace - The furnace consists of a five feet long cylindrical tube (2" diameter) made of fused quartz, which is open at both the ends. The tube is wound with 20 s.w.g. Kanthal wire. There are three sections of winding. The central one is controlled independently with its own thermocouple. This furnace is a "three zone" furnace, which has the typical arrangement of one preheating zone and a cooling zone.

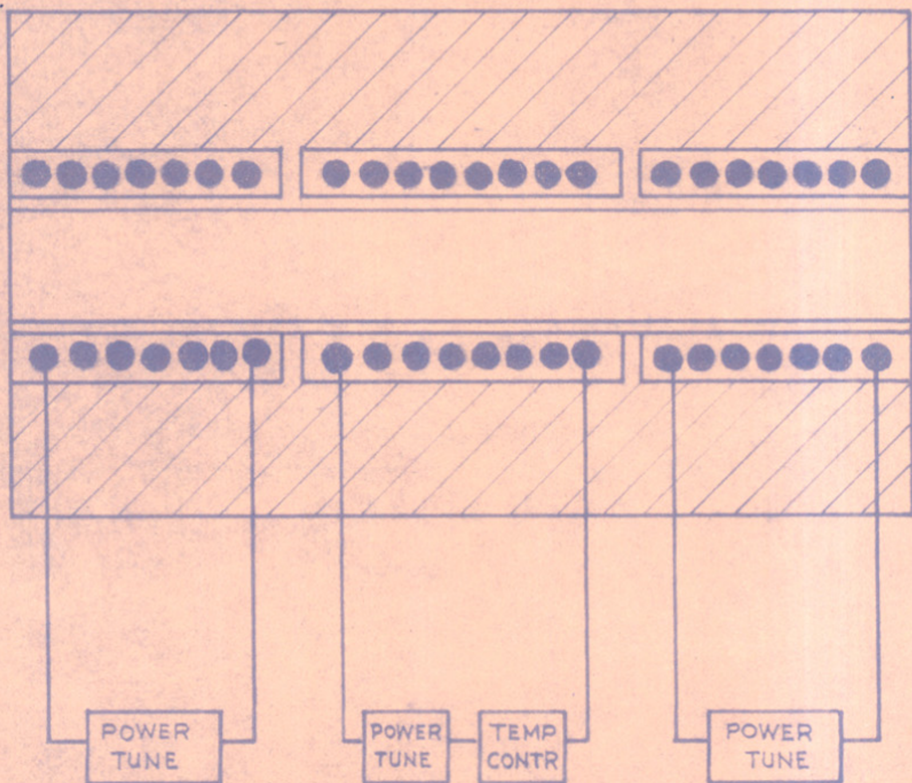

FIGURE 2-4 CROSS SECTION OF THE THICK FILM FURNASE

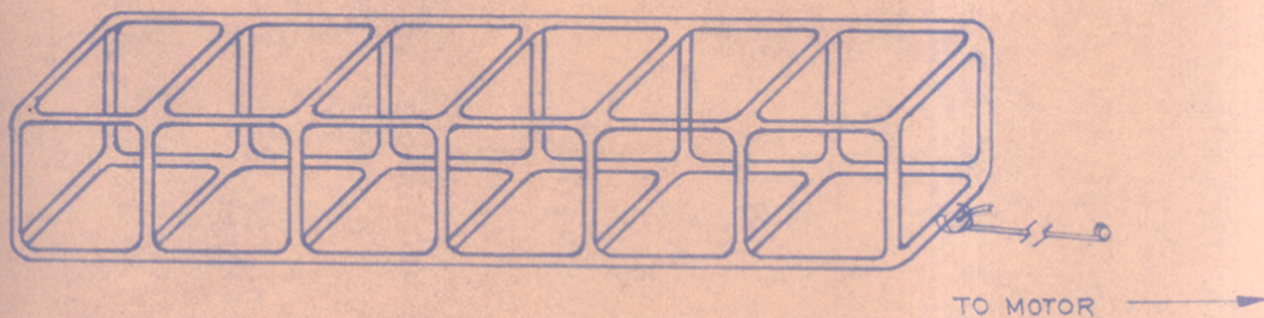

FIGURE 2·5 : SILICA TROLLY

Temperature control - Temperature control is accomplished by placing a thermocouple at the centre of the furnace. The thermocouple is placed close to the heating elements so that the furnace maintains a constant trolley temperature with very little swing.

Silica trolley drive - A specially fabricated silica trolley over which samples to be fired are kept is hooked to a stainless steel rod. The other end of the rod is connected to a rotating wheel through a fine gauge copper wire. The wheel is rotated by a motor through the gear system. The copper wire gets wound over this wheel and pulls the silica trolley through the furnace from one end to the other end.

Temperature profile - A long thermocouple is placed in the furnace such that its tip is at one end of the furnace, then it is pulled inch by inch to the other end. As it moves through the furnace the temperature at the tip of the thermocouple is recorded and converted to a graph form so that the profile can be easily seen (Figure 2.6).

2.8. SCREEN PRINTING AND FIRING OF THE ELECTRODES

Alumina substrate was firmly positioned on the printing board. The screen frame was fixed to the board with the C-clamp such that the pattern to be printed was positioned on the substrate. The silver paste (N.C.L. processed) was deposited on the screen. The squeegee was

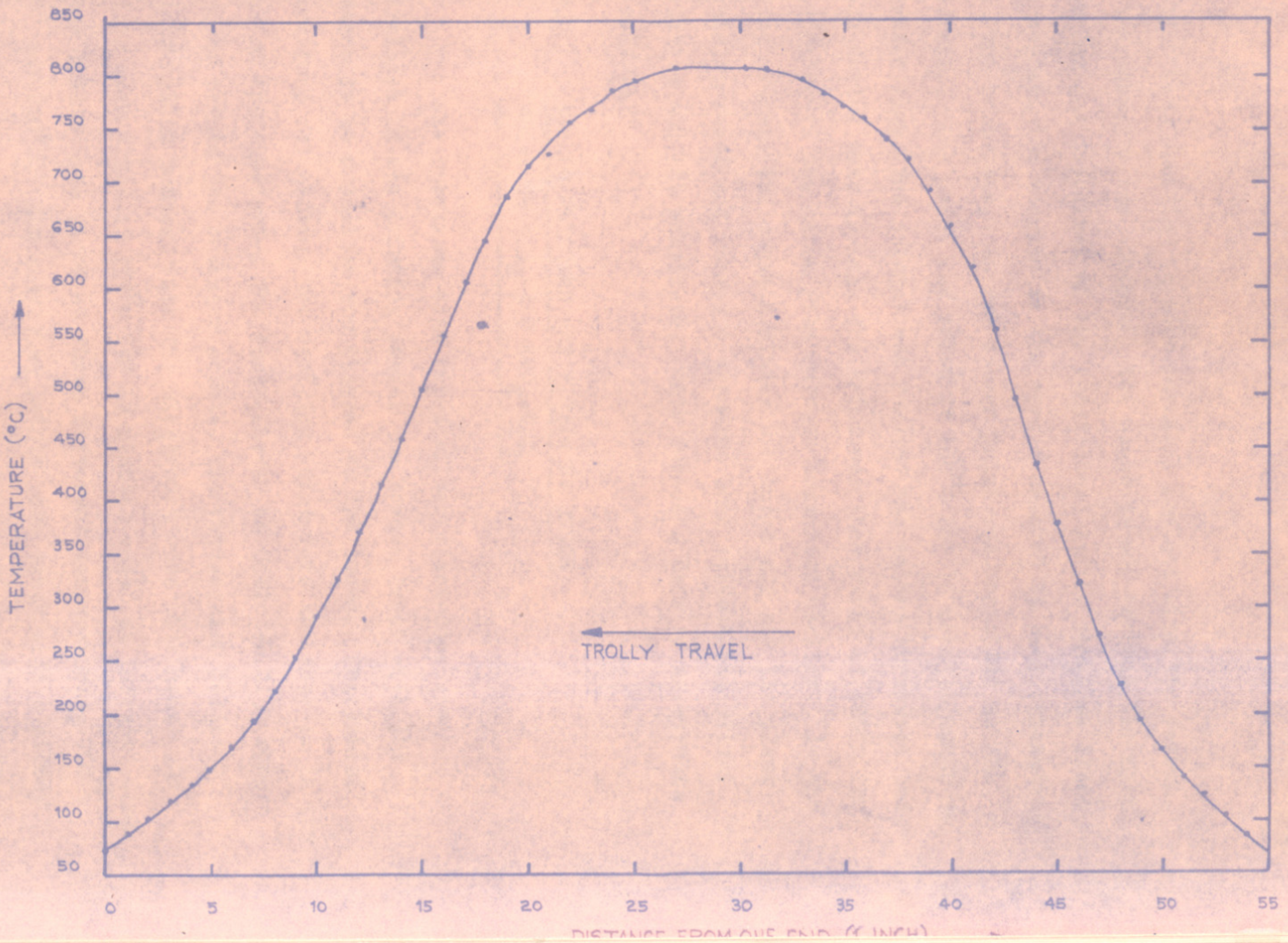

FIGURE 2·6 TEMPERATURE PROFILE OF THE FURNACE

brought into position to have physical contact with the screen. As the squeegee was advanced, the paste passed through the open mesh and got deposited on the substrate. As the squeegee blade was passed, the tension in the screen snapped it back separating from the substrate. An ash colour print was deposited on the substrate. The print was dried at 150°C for 15 minutes under an infrared lamp. The solvent was removed and volume shrinkage took place during this drying. The print was then fired at 800°C for 10 minutes in the thick film furnace described earlier. In the firing process the organic binder was burnt off and the glass particles fused and formed a vitreous bond between the silver particles and the substrate. This formed a pair of electrodes of silver.

2.9. SCREEN PRINTING AND FIRING OF THICK FILMS OF RuO_2 AND RuO_2-V_2O_5

The substrate with fired silver electrodes was positioned on the printing board. The screen frame with the pattern to be deposited was clamped to the board. Sequential operations for getting the resistor print were the same as in the case of the electrode. The paste listed in Table No.2.7 were used to obtain the resistor prints. The rectangular resistor prints making contact with the electrodes were obtained. The prints were dried at 150°C for 15 minutes under an infrared lamp. These prints were fired at three different temperatures, 700°, 800° and 900°C. The resulting prints were black with a glassy smooth surface. The shape and size of the electrodes and the resistive prints are shown in Figure 2.7.

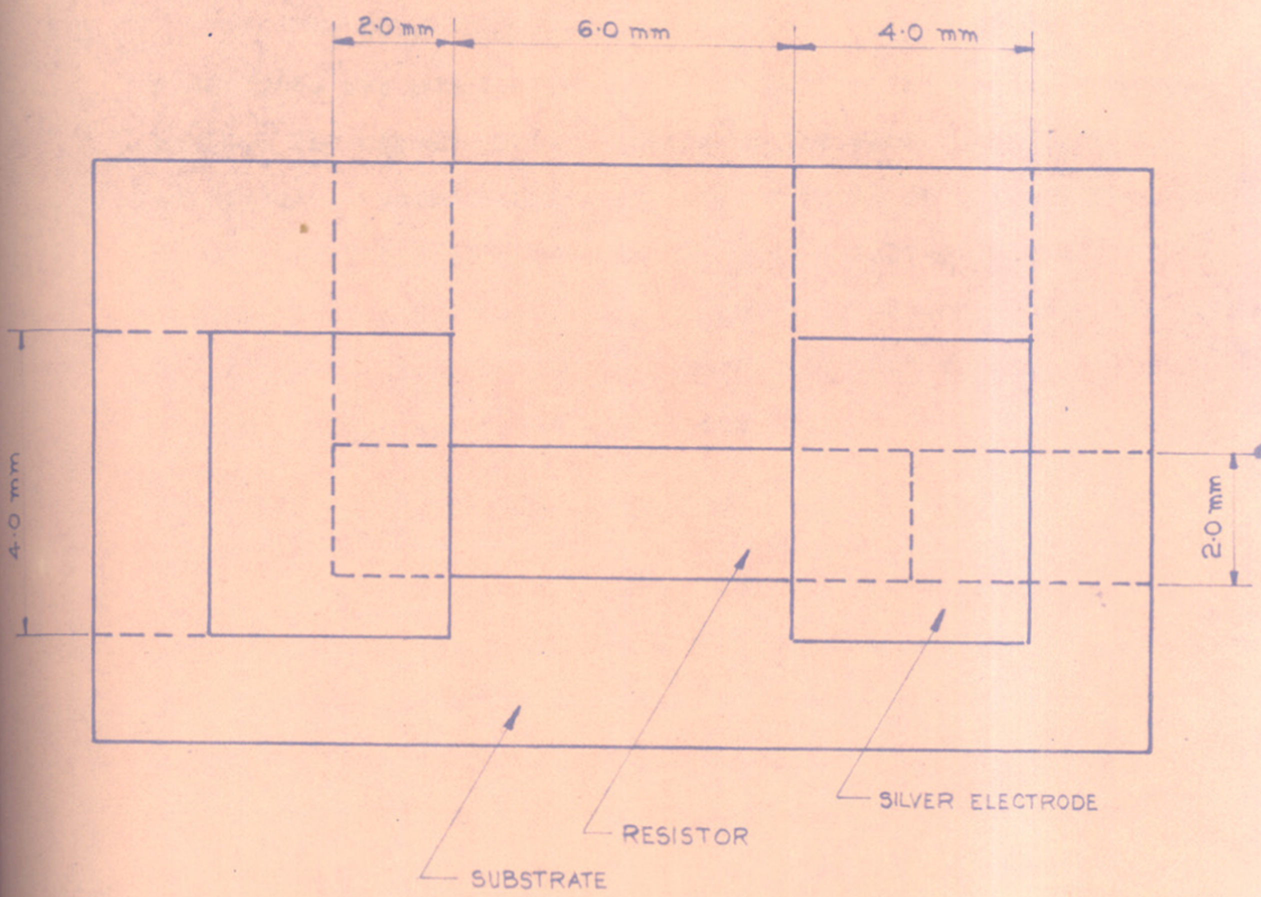

FIGURE. 2-7 SHAPE AND SIZE OF RESISTOR

2.10. THE CURRENT VOLTAGE CHARACTERISTICS

A thick film resistor sample provided with silver electrodes was mounted on a teflon block using phosphor bronze strips. The copper wires soldered to the electrodes were connected to power supply. Regulated variable voltage d.c. power supply (Aplab 0-60V) was used as a voltage source and Yamuna digital multimeter (Model 1010) to measure the current. The circuit used is shown in Figure 2.8. The current voltage characteristic were studied between -50 to + 50 V.

2.11. RESISTIVITY MEASUREMENTS

A resistive film with silver electrodes was screen printed on alumina substrate and fired as described earlier. This alumina substrate was fixed on a teflon block with the help of phosphor bronze strips. To this teflon block two eyelets were fixed. The electrodes were soldered to these eyelets with copper wire. This sample holder is shown in Figure 2.9.

The sample enclosure consists of a corning glass tube closed at one end having a B50 male joint at the other end. B-50 female joint is also made up of Corning glass and has a side tube with B-19 male joint attached to it. Through this B-19 joint, the system can be connected to a vacuum unit. In the walls of B-50 female joint two copper, one chromel and one alumel wires are sealed. The seals are leak-proof at vacuum of the order of 10^{-2} torr. This assembly is shown in Figure 2.9.

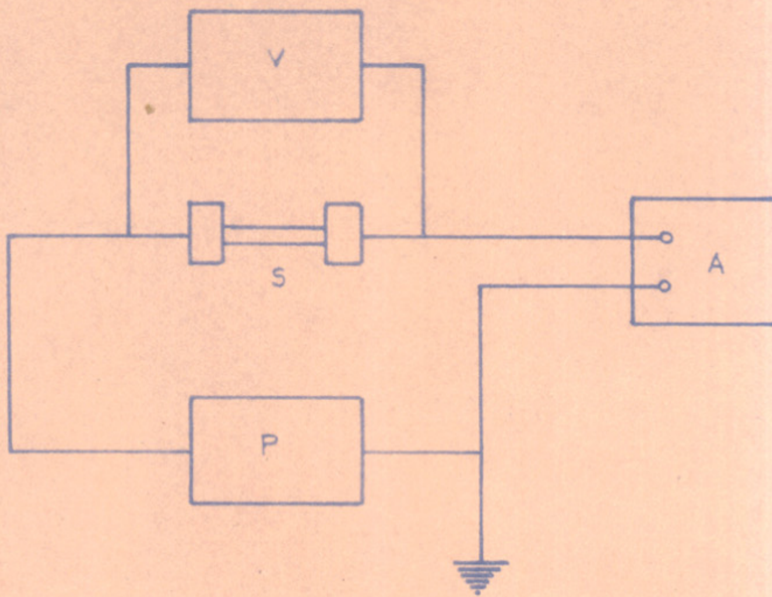

V = VOLTEMETER

S = SAMPLE

A = AMMETER

P = POWER SUPPLY

FIGURE 2·8 CIRCUIT DIAGRAM FOR I-V CHARACTERISTICS

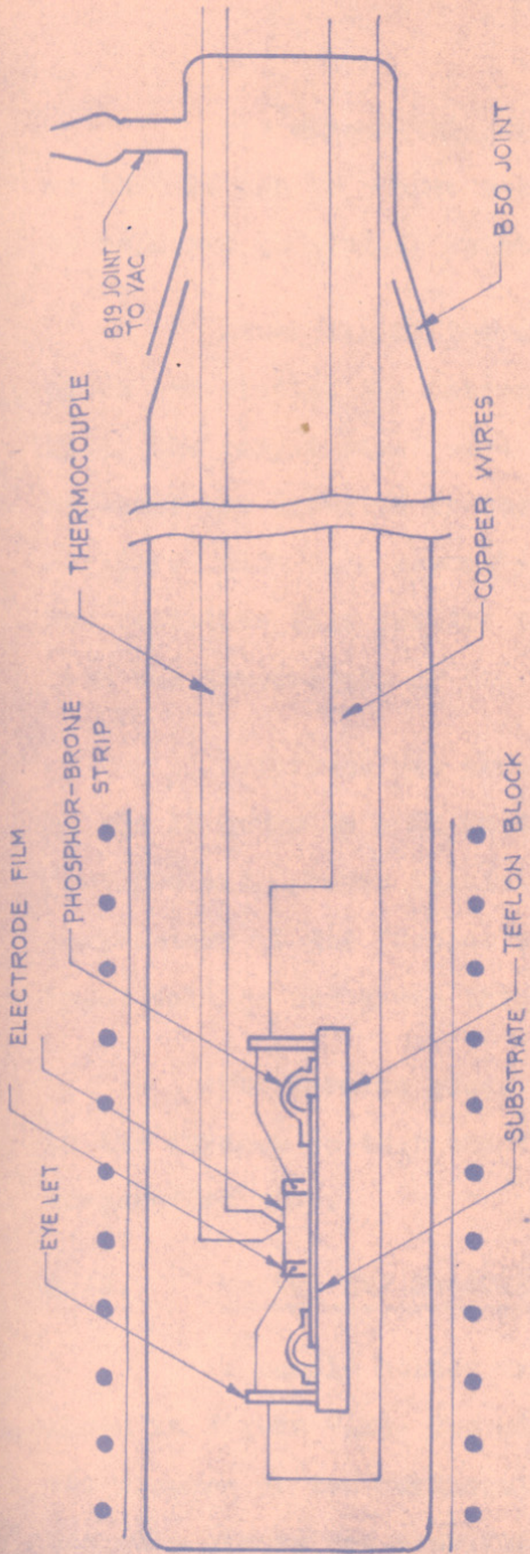

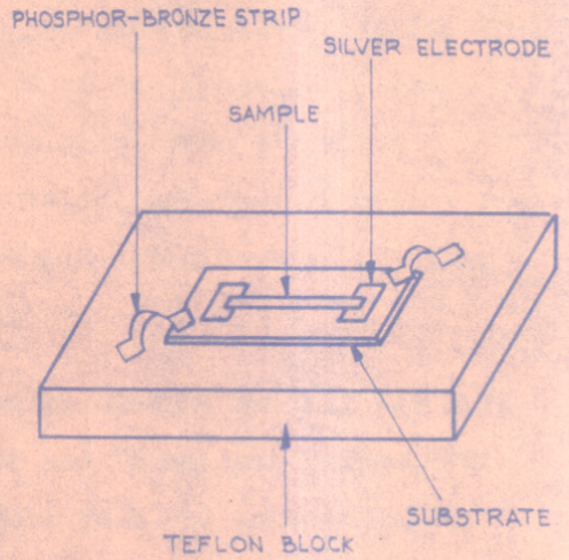

FIGURE 2·9 SAMPLE HOLDER

FIGURE 2·9 ARRANGEMENT FOR SHEET RESISTIVITY MEASUREMENT

The chromel-alumel junction is fixed inside the tube, so that it can be placed near the sample. The copper wires can be soldered to eyelets which are connected to the electrodes.

After fixing the alumina substrate on the teflon block and placing the thermocouple junction on the resistive film, the copper wires were soldered to the eyelets and the assembly was inserted in the Corning glass tube described earlier. With this assembly we could measure the resistance of the resistive film and the thermocouple voltage which in turn gave the temperature of the sample.

A furnace was constructed by winding Kanthal 'A' wire of the 18 gauge on a 50 mm diameter and 25 cm long silica tube provided with proper insulation. To adjust and control the temperature of the furnace to any desired value upto 200°C, the input voltage was given through a temperature controller.

The Corning glass tube with sample holder is inserted in the furnace so that the film was in the adjusted and controlled temperature zone.

2.12. THERMO EMF MEASUREMENTS

A sample holder used for thermo emf measurements is shown in Figure 2.10. Two mica pieces were fixed with screws in the grooves of two rectangular teflon pieces. A 3 mm gap between the mica pieces was provided to avoid the heat transfer by conduction through mica. The substrate on which the sample was printed, wss placed on the mica pieces such that the sample was

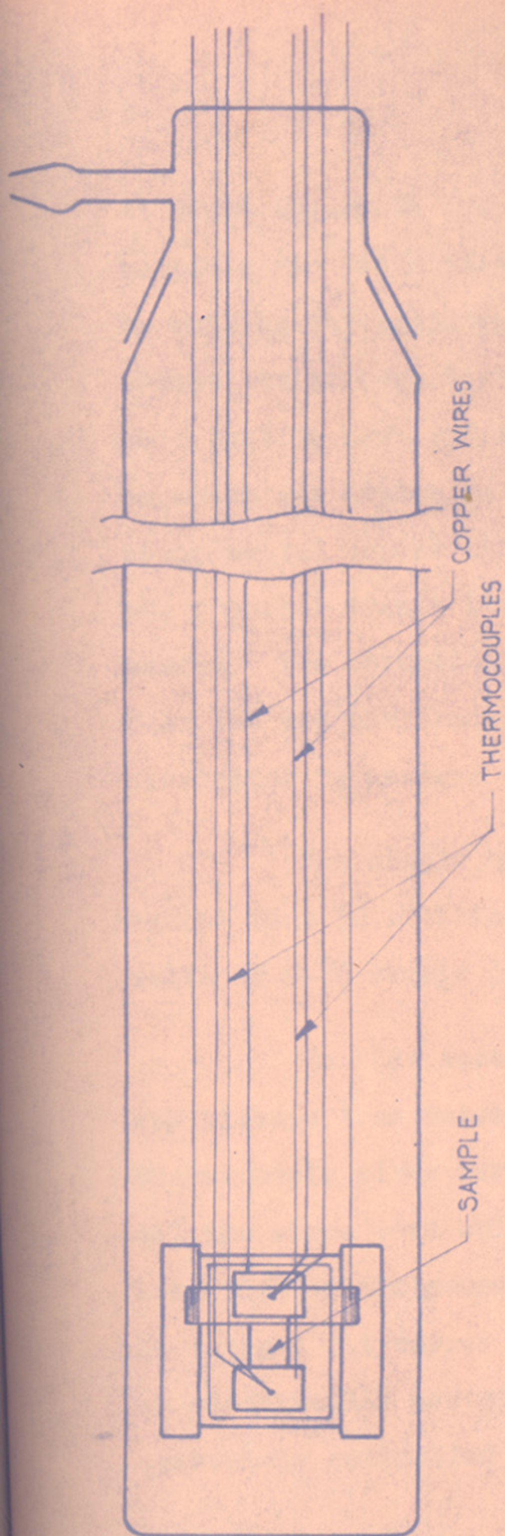

FIGURE 2-10

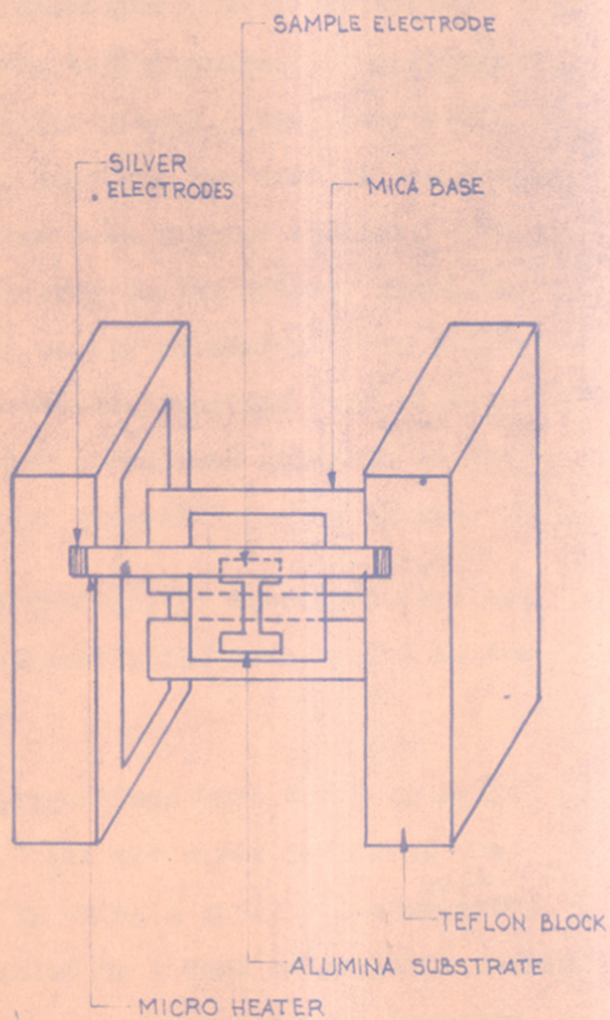

FIGURE 2-10 : SAMPLE HOLDER

at right angles to the gap. On one of the electrodes of the sample a tin oxide coated glass microheater (50 Ω) was seated by cutting out small portions on the teflon pieces. Two phosphor bronze strips were fixed to the teflon pieces. The other ends were bent to have spring action to hold the two ends of the heater on which air drying silver paste had been applied earlier. Two resin coated copper wires were soldered to the eyelets fixed to the phosphor bronze strips for the supply of current from a d.c. source. Two chromel-alumel thermocouple junctions were placed near the two electrodes. Two copper wires were soldered to the electrodes to measure the thermo emf generated in the sample.

The sample enclosure is similar, as described earlier, except that in addition, chromel-alumel wires were sealed in the walls of B-60 female joint.

In this assembly, due precautions were taken to avoid any pickups from outside signals. All the wires including the thermocouple wires were shielded by using a small diameter copper tube. All the wires were suitably insulated by a coat of araldite before inserting in the copper tubes. The glass envelope was inserted in a tight fit copper cap. The whole assembly was introduced in an electrically heated wire wound furnace. The temperature was accurately controlled by using a temperature controller.

2.13. SEM AND EPMA

The thick films of RuO_2 and RuO_2-V_2O_5 system were evaluated by using scanning electron microscope (SEM) with an electron-probe microanalyser (EPMA).

The thick film surfaces were successively polished, washed with distilled acetone and dried. After each polish the scanning electron micrographs were taken and the surfaces were examined with the electron microprobe.

The glass, which is used in thick film compositions is formulated into paste, screen printed and fired at 650°C. This film was also evaluated with EPMA. The ratio of Pb counts to Si counts was 3.4. This ratio was calculated to be 3.7 using the wt. % of PbO and SiO_2 which we had taken to prepare the glass.

CHAPTER - III

R E S U L T S

3.1. X-RAY STUDY

The main observations of X-ray analysis are as follows:

(1) All the diffraction peaks of RuO_2-V_2O_5 system for compositions A, B and C match with the diffraction peaks of RuO_2 (Figs. 3.12, 3.13, 3.14 and 3.15).

(2) In compositions D and E shoulders to the diffraction peaks are observed at Braggs angle 35° and 35.2° respectively.

(3) The d values for RuO_2 and RuO_2-V_2O_5 system were calculated and compared with the d values of the standard ASTM patterns for RuO_2. These results are given in Table 3.1.

TABLE - 3.1

Comparison of d values (calculated) with d values from ASTM cards

Sr. No.	d values calculated for diff.compns.				d values for RuO_2 from ASTM cards
	RuO_2	Compn. A	Compn. B	Compn. C	
1	3.1861	3.1880	3.2041	3.2268	3.13
2	2.5615	2.5600	2.5558	2.5615	2.62
3	2.2510	2.2521	2.2586	2.2634	2.22
4	2.2265	2.2222	2.0333	2.0342	2.03
5	2.0128	2.0128	2.0213	2.0256	1.90
6	1.6903	1.6885	1.6920	1.6937	1.65
7	1.5998	1.5908	1.5938	1.5988	1.58
8	1.5551	1.5499	1.5433	1.5405	1.54
9	1.4215	1.4238	1.4257	1.4296	1.41
10	1.3974	1.3941	1.3900	1.3875	1.39
11	1.3506	1.3500	1.3963	1.3535	1.34
12	1.2722	1.2760	1.2737	1.2711	1.27

(4) The lattice parameters a and c were calculated and tabulated as shown in Table 3.2.

TABLE - 3.2

Variation of lattice parameters with mole % of V_2O_5

Sr. No.	Mole % of RuO_2	V_2O_5	Lattice parameters (Å) a	c
1	100	-	4.4897	3.1074
2	98.5289	1.4711	4.5017	3.0992
3	97.0418	2.9582	4.5134	3.0930
4	95.5389	4.4614	4.5248	3.0859

(5) The variation of lattice parameter of host oxide, RuO_2 with mole per cent of V_2O_5 added is plotted (Figure 3.1). It is observed from the figure that the variation of lattice parameter of RuO_2 with mole per cent of V_2O_5 added is linear, that is, the resultant RuO_2-V_2O_5 oxide system obey Vegard's Law, which states that the extent of change in lattice parameter of host oxide (RuO_2) is proportional to the molecular per centage of added dopant (V_2O_5). The Figure 3.1 also shows that the lattice parameter 'a' increases and 'c' decreases as the concentration of V_2O_5 increases.

Scanning electron micrograph and Electron microprobe analysis

The main observation of SEM and EMPA are as follows:

(1) The top surface of our thick films is one uniform phase (Figure).

(2) The surfaces of each of the film after each successive polishing shows the presence of two phases (Figure 3.16).

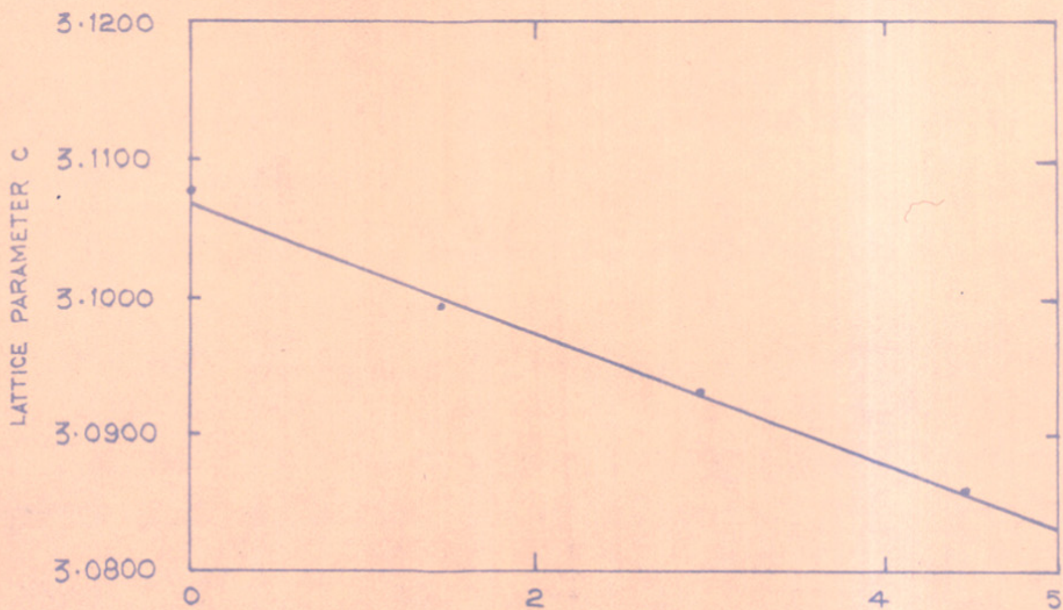

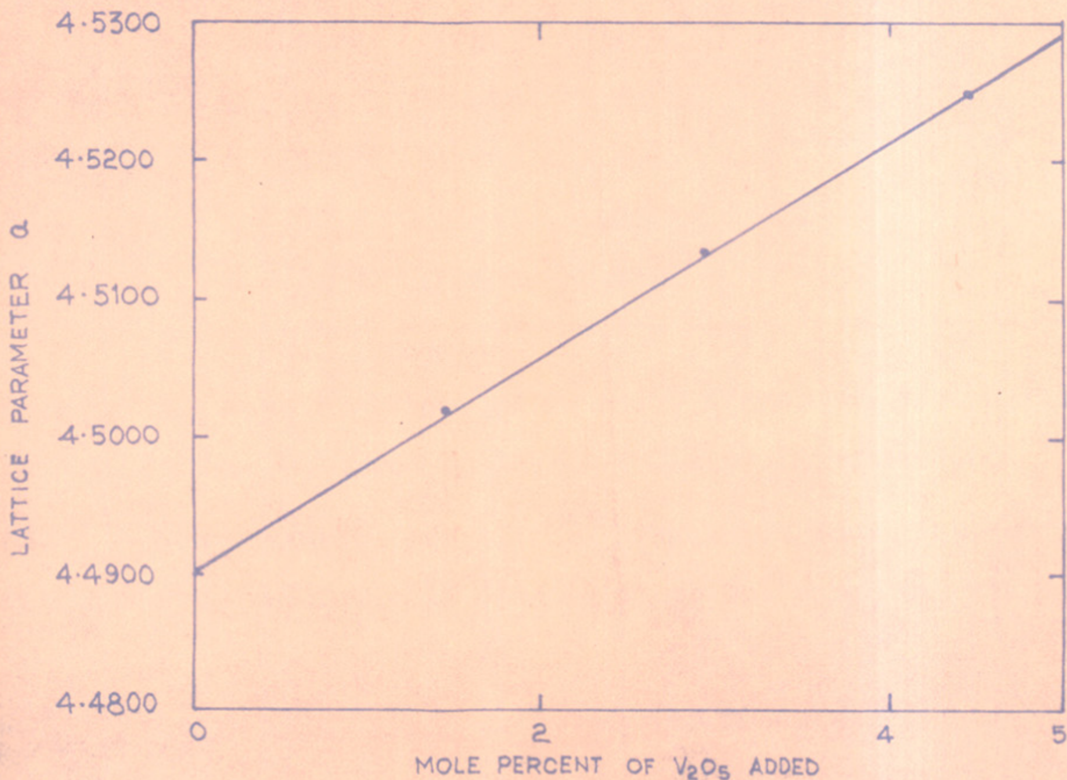

FIGURE 3-1: EFFECT OF ADDITION OF V_2O_5 ON THE LATTICE PARAMETERS OF RuO_2

The crystallite phase is not clear in Figure 3.16, because of two reasons

(i) the glass surrounding the crystallite phase is not etched, and

(ii) the magnification is low.

(3) The results of electron microprobe analysis of glass film is given in the following Table 3.4.

TABLE - 3.4

EMPA of glass

Sr.No.	Counts/second Si	Pb	Pb/Si	Av. Pb/Si	Theoretical value of Pb/Si
1	8472	28973	3.4156		
2	9587	33453	3.4834		
3	11780	41000	3.4805	3.4	3.7
4	9687	31445	3.2461		
5	8742	29461	3.3701		

(4) The concentrations of Ru and V after each polish and for every films obtained by EMPA are listed in Table 3.5.

(5) The diffusion profiles for ruthenium ions in thick films of RuO_2 and RuO_2-V_2O_5 compositions are shown in Figure 3.11.

TABLE - 3.5

Sr. No.	Sequence of polishing	C/S for Ru in thick films of						
		RuO_2	Compn. A		Compn. B		Compn. C	
		Ru	Ru	V	Ru	V	Ru	V
1	U.P.	1462	-	-	4001	349	-	-
2	1st	19.8	12891	949	2068	17.14	4297	
3	2nd	4337	20800	621	203.4	nil	21282	1424
4	3rd	4846	961	44	4937	249	637	82.4
5	4th	12478	16336	459	4311	470	15350	696
6	5th	10795	19670	371	11102	467	12221	78
7	6th	15273	17034	382	7333	217	14321	1058
8	7th	10300	8156	nil	4885	nil	10422	529
9	8th	-	7833	nil	18313	431	18806	1385
10	9th	-	-	-	28573	646	22892	995

3.2. ELECTRICAL PROPERTIES

3.2.1. Current-voltage characteristic

Screen printed and fired silver electrodes were used as electrical contacts for the resistive thick films of RuO_2 and RuO_2-V_2O_5 systems. The results of I.V. characteristic is shown in Figure 3.2. The I-V characteristic for all thick films of RuO_2 and compositions of RuO_2-V_2O_5 systems are similar. The linearity of these curves show that screen printed and fired silver electrodes provide good ohmic contact for our thick films of RuO_2 and RuO_2-V_2O_5 system.

3.2.2. Resistivity measurements

The resistance of thick films of RuO_2 and RuO_2-V_2O_5 system is measured and sheet resistivity is calculated using the following formula[71]

$$\sigma_s = R.\frac{W}{L}$$

where σ_s is sheet resistivity, Ω/sq.

R is resistance of the film, Ω,

W is width of the film, mm.,

L is the length of the film, mm

and L/W is called aspect ratio of thick films.

The sheet resistivity values obtained are plotted as a function of firing temperature and as a function of dopant concentration. The variation of resistivity of thick films of RuO_2 and RuO_2-V_2O_5 system with temperature is measured and plotted.

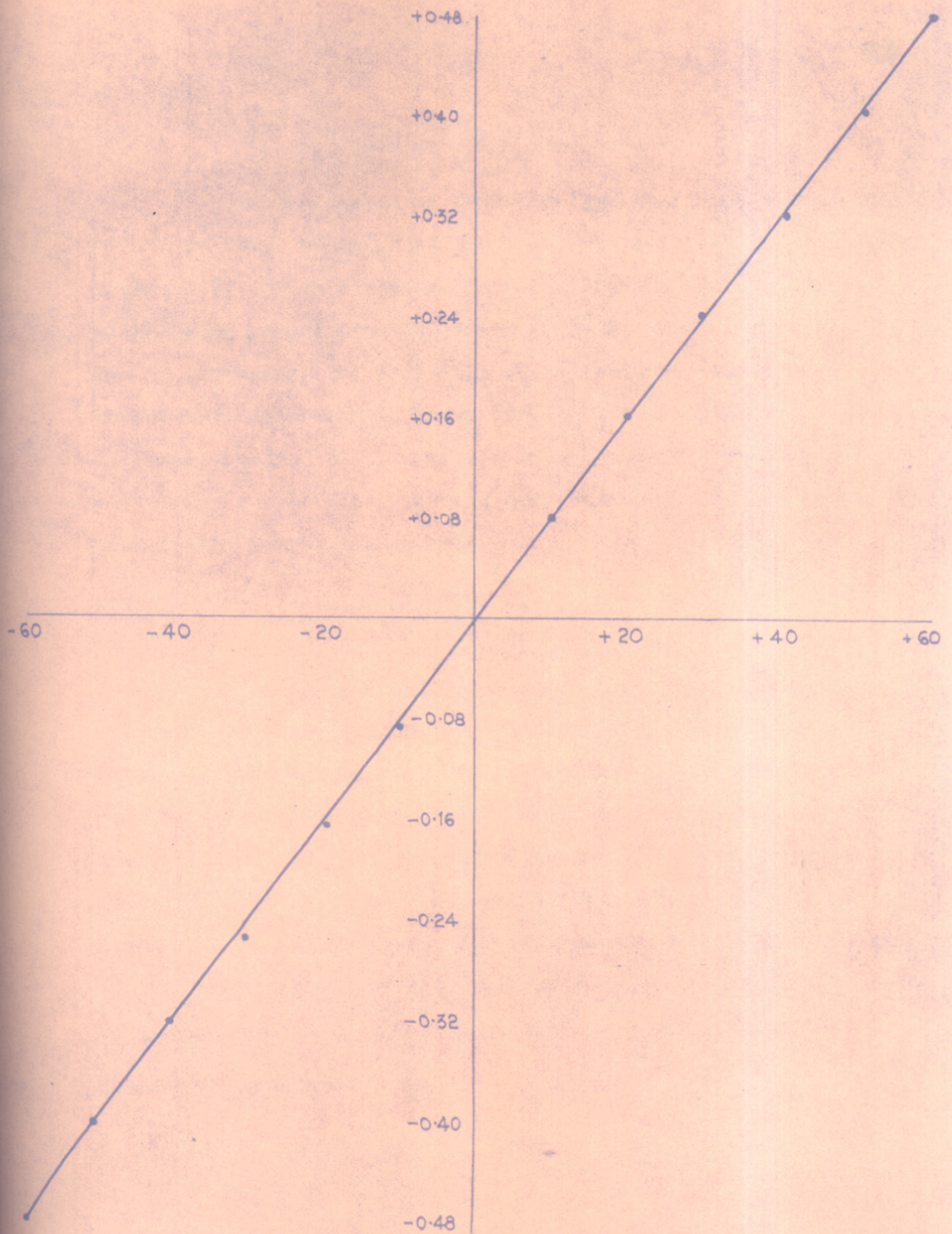

FIGURE 3-2 : CURRENT-VOLTAGE CHARACTERSTIC

3.2.2. (i) Variation of resistivity with firing temperature

The variation of resistivity with firing temperature for thick films of RuO_2 and RuO_2-V_2O_5 compositions is shown in Figure 3.3. Curve I represents the variation of resistivity with firing temperature for thick films of RuO_2. Curve II, III and IV represents the variation of resistivity with firing temperature for thick films of RuO_2-V_2O_5 compositions (A, B and C) respectively. All the curves have the same trend. The resistance of the films for all compositions decreases as the peak firing temperature increases.

3.2.2. (ii) Variation of resistivity with concentration of V_2O_5

The dependence of resistivity of thick films of RuO_2 and RuO_2-V_2O_5 compositions is shown in Figure 3.4. Curve 1, 2 and 3 represent the variation of resistivity with concentration of V_2O_5 for the films fired at 700, 800 and 900°C respectively. All the curves follow the same trend with the only difference that the resistivity values are reduced for the higher firing temperature. The resistance of the films decreases as the concentration of V_2O_5 increases. But the resistance value of the films of RuO_2-V_2O_5 compositions are higher than the resistance values of RuO_2.

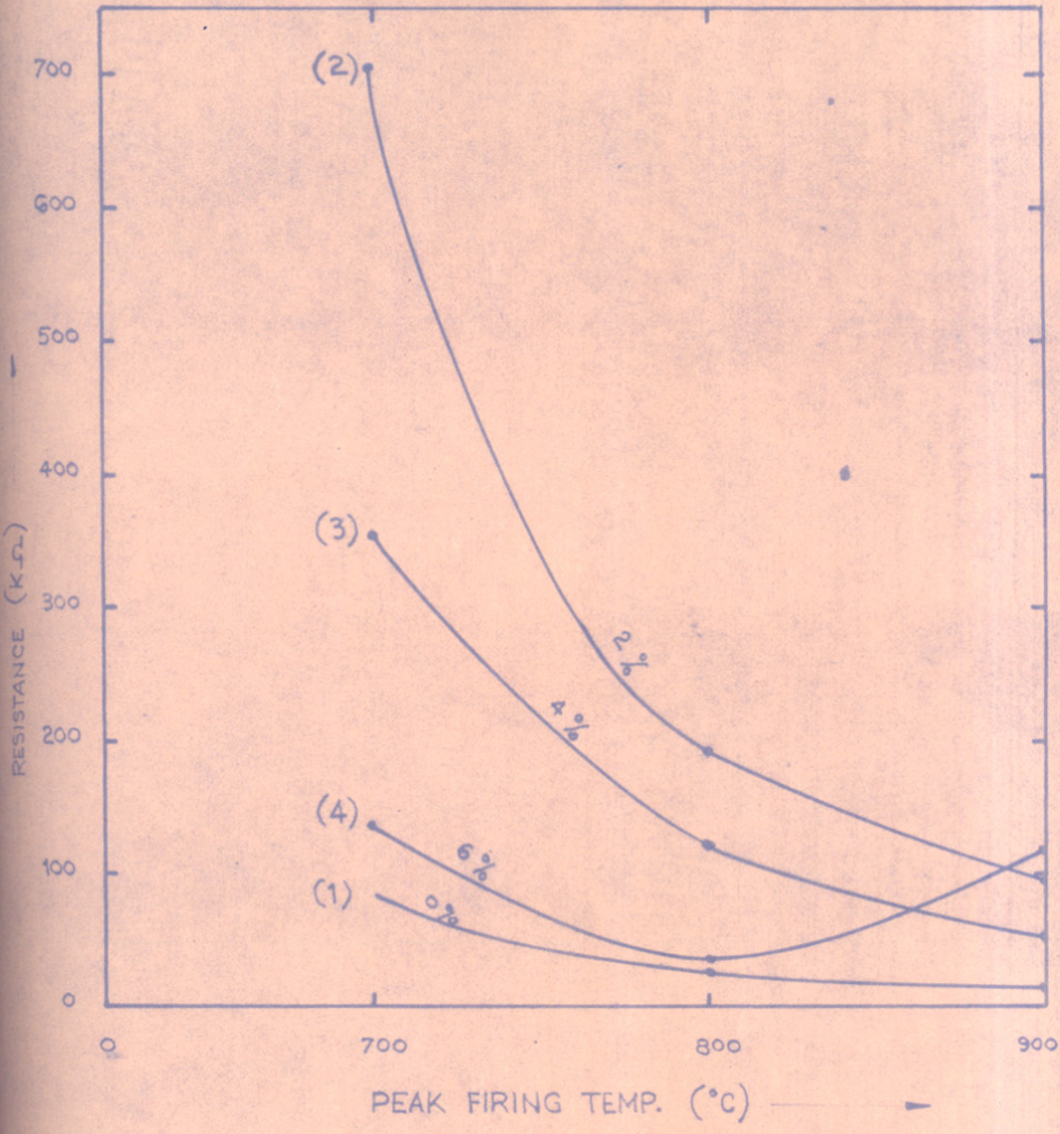

FIGURE 3.3 VARIATION OF RESISTIVITY WITH PEAK FIRING TEMPERATURE

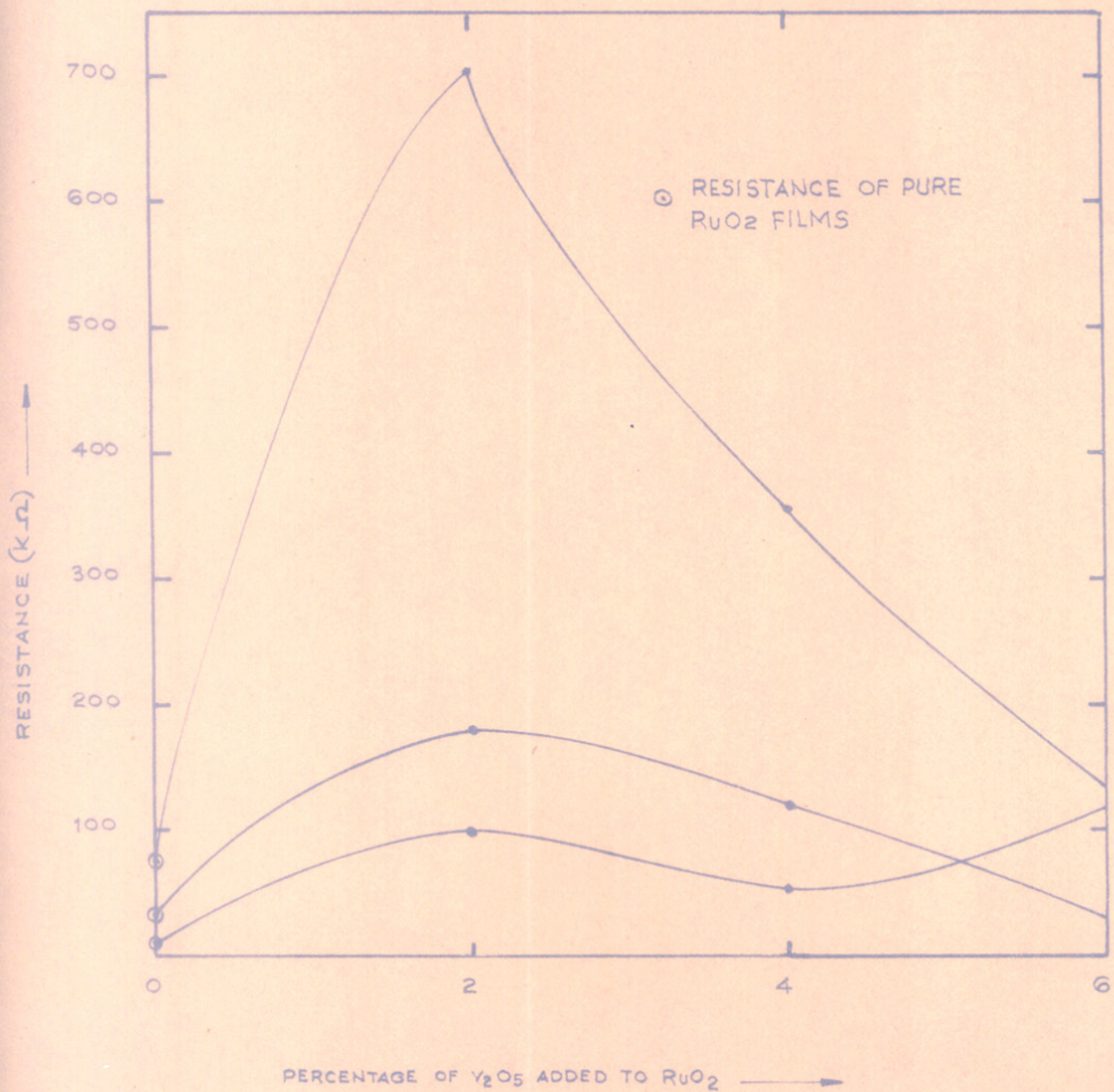

FIGURE 3·4 VARIATION OF RESISTIVITY WITH PERCENTAGE OF V_2O_5 ADDED TO RuO_2

3.2.2. (iii) Variation of resistivity with temperature

Figure 3.5 shows the plot of log R vs 1/T for thick films of RuO_2 fired at 700°C. Figures 3.6, 3.7 and 3.8 show similar graphs for thick films of RuO_2-V_2O_5 compositions fired at 700°C.

All the graphs have straight line nature which shows that $R = R_o \exp{-\Delta E/kT}$. The values of activation energy ΔE are calculated from the formula

$$\Delta E = \frac{k(\log R1 - \log R2)}{[1/T_1 - 1/T_2]}$$

Table 3.6 summarises the calculated activation energies for thick films of RuO_2 and RuO_2-V_2O_5 compositions and the activation energies calculated by J. Robertson.

TABLE - 3.6

Activation energies for Thick Films of RuO_2 and RuO_2-V_2O_5 compositions

Sr.No.	Thick film resistor of	Resistance	Activation energy me V	Ref.
1	RuO_2	10 MΩ/sq.	1.10	J.Robertson, 72.
2	RuO_2	1 MΩ/sq.	0.90	J.Robertson, 72.
3	RuO_2	24.66KΩ/sq.	2.31	Present work
4	RuO_2-V_2O_5	235.33 KΩ/sq.	1.355	Present work
5	RuO_2-V_2O_5	119.00 KΩ/sq.	2.614	Present work
6	RuO_2-V_2O_5	45.00 KΩ/sq.	1.320	Present work

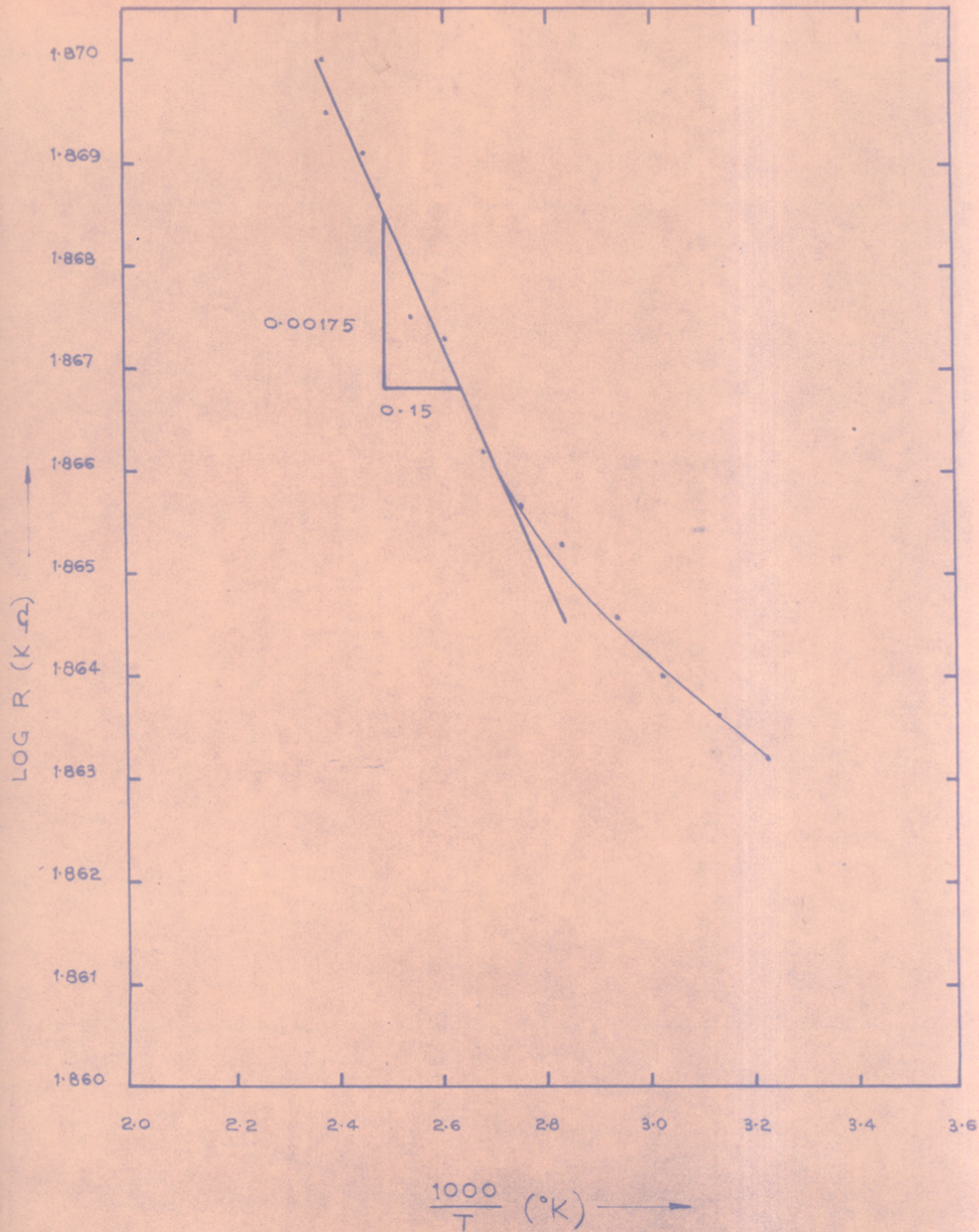

FIGURE 3·5 VARIATION OF RESISTIVITY WITH TEMPERATURE

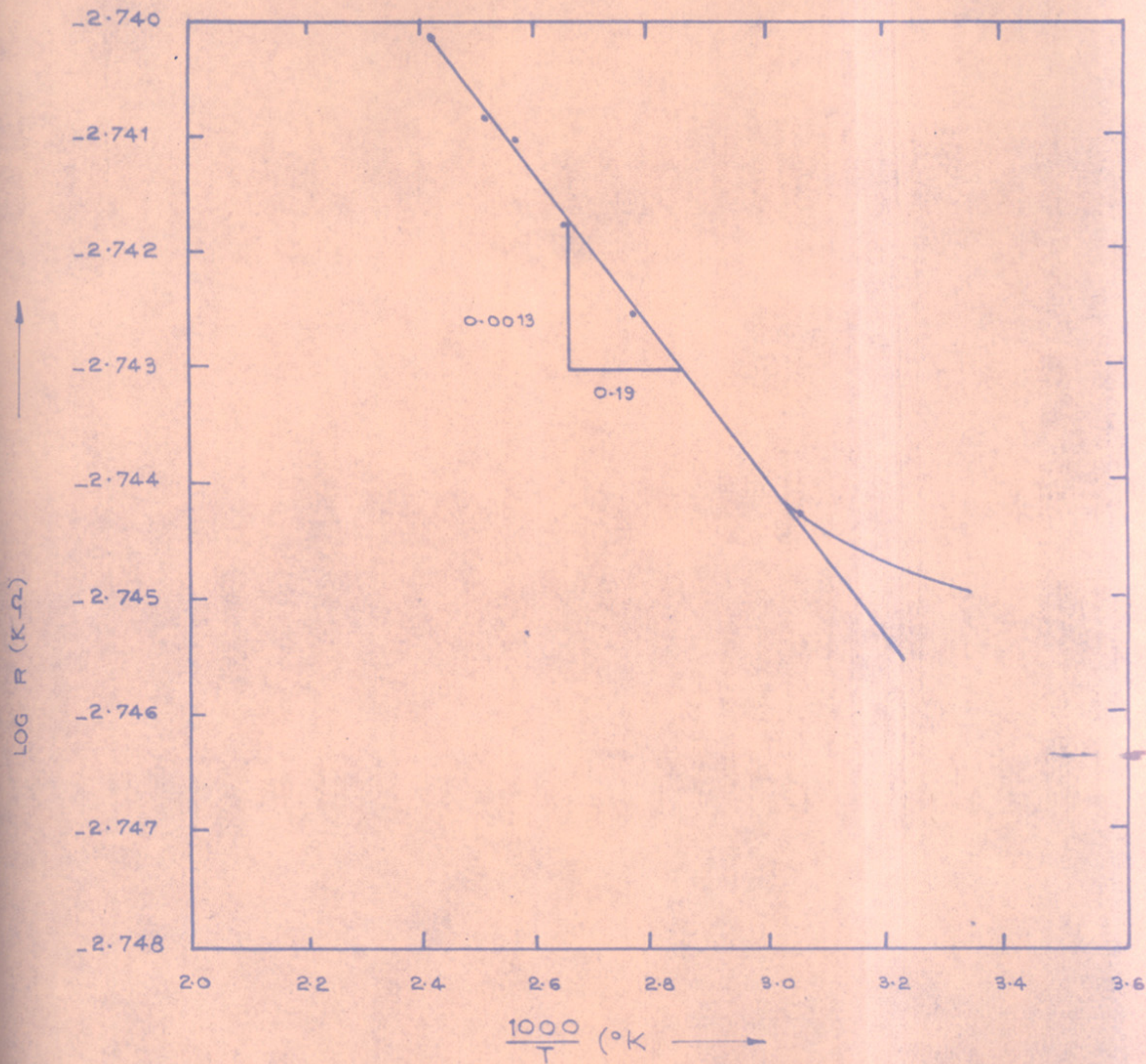

FIGURE 3.6 VARIATION OF RESISTIVITY WITH TEMPERATURE

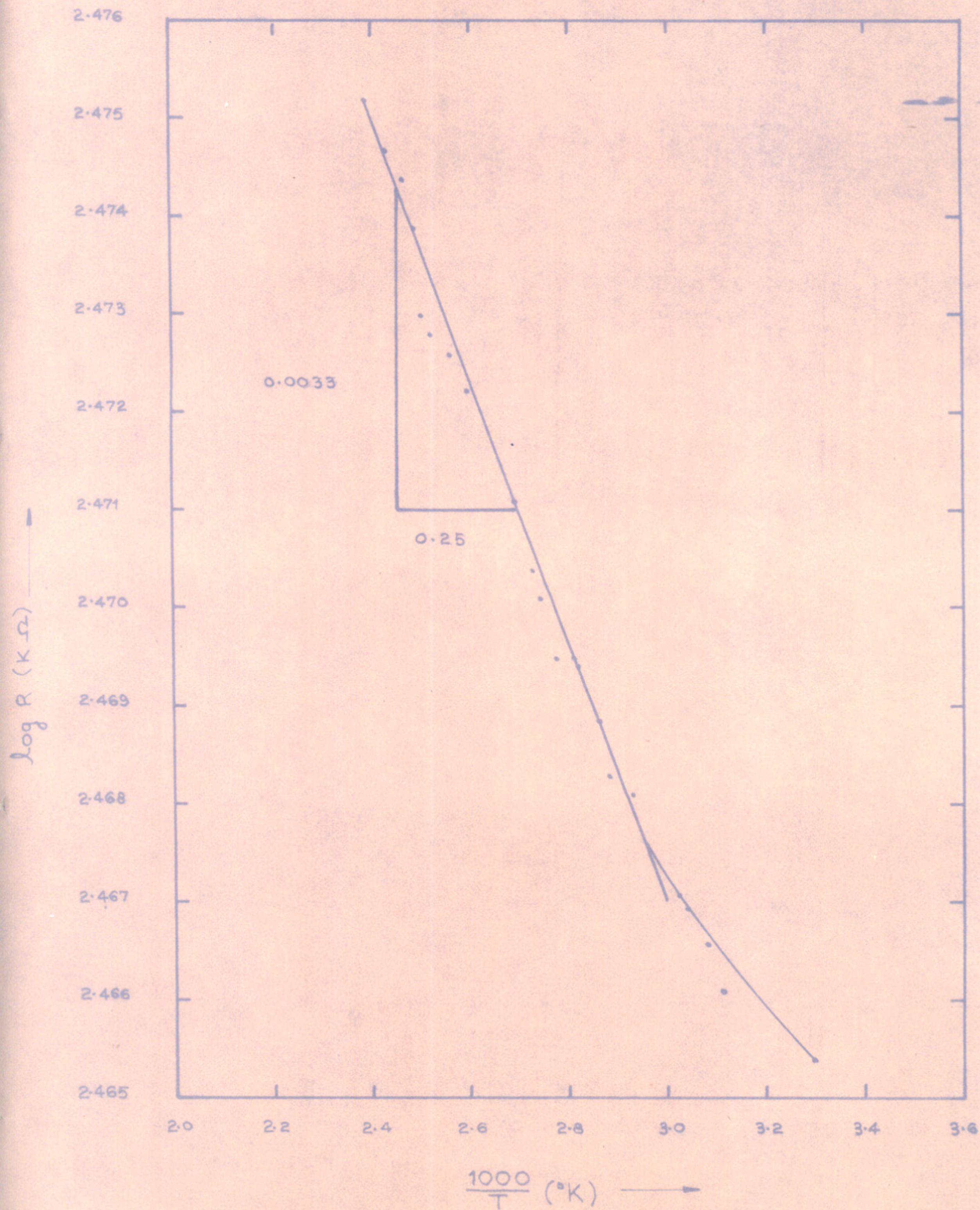

FIGURE 3·7 VARIATION OF RESISTIVITY WITH TEMPERATURE

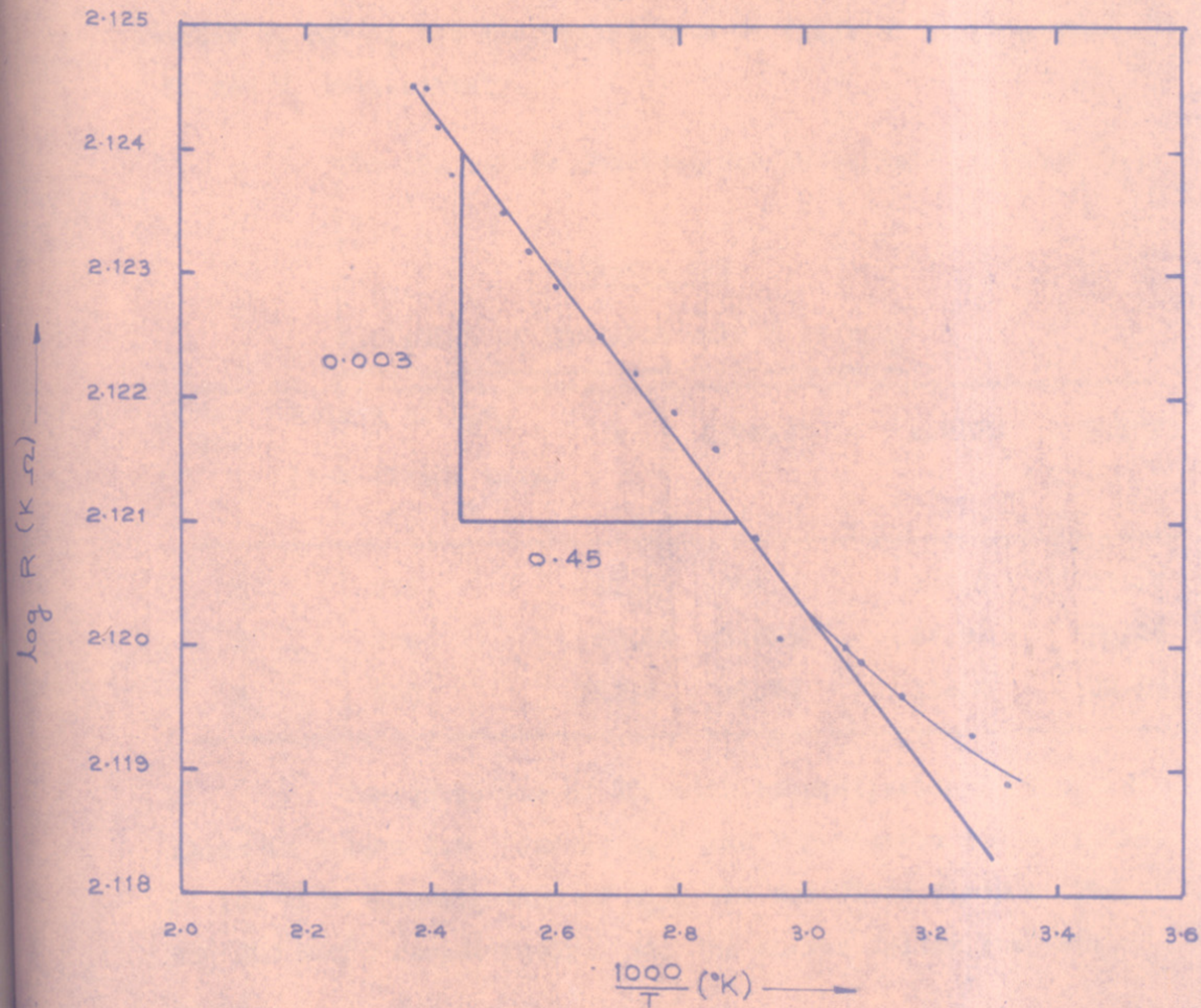

FIGURE 3·8 VARIATION OF RESISTIVITY WITH TEMPERATURE

3.2.2. (iv) Temperature coefficient of resistance (TCR)

Temperature coefficient of resistance (TCR) is calculated using the following formula

$$TCR = \frac{R_2 - R_1}{T_2 - T_1} \times \frac{2}{R_2 + R_1}$$

where R_2 and R_1 are the resistances of films at temperatures T_2 and T_1 respectively.

The TCR values obtained are summarised in Table 3.7.

TABLE - 3.7

Variation of TCR with mole % of V_2O_5

Sr. No.	Mole % of V_2O_5 / Peak firing temp. °C	0	0.96187	1.8973	2.8073
1	700	125.3	-188.7	182.0	114.7
2	800	50.34	-5.024	52.9	36.38
3	900	313.9	25.34	114.6	32.80

The variation of TCR with concentration of V_2O_5 is shown in Figure 3.9. Curves 1, 2 and 3 represent the variation of TCR with concentration of V_2O_5 for the films fired at 700, 800 and 900°C respectively. All the curves follow the same trend.

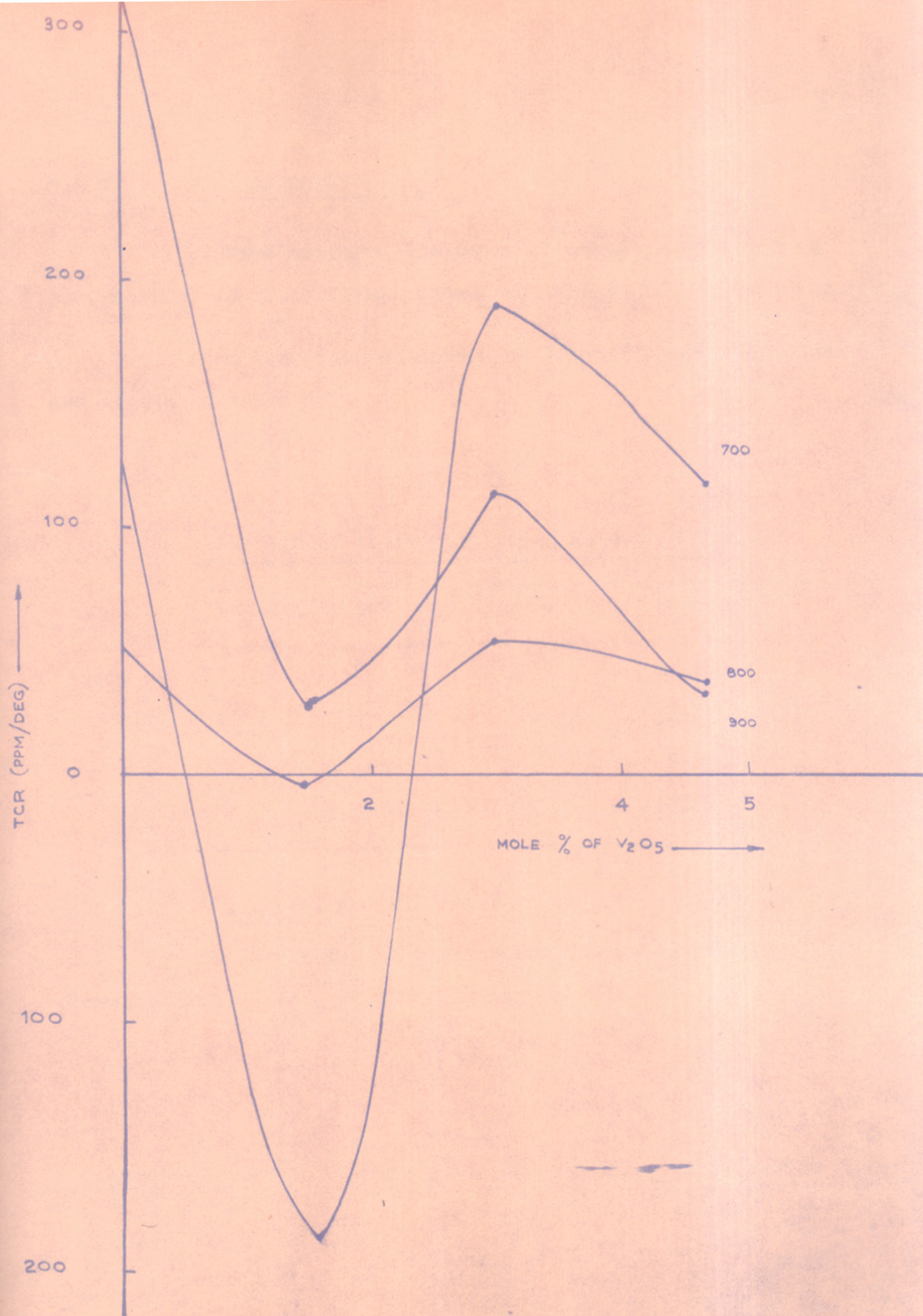

FIGURE 3·9 VARIATION OF TCR WITH MOLE PERCENT OF V_2O_5 ADDED

3.2.3. THERMOELECTRIC POWER

We have measured the thermoelectric power (Seebeck coefficient) of thick films of RuO_2 and RuO_2-V_2O_5 compositions.

Room temperature Seebeck coefficients for the films are listed in Table 3.8.

TABLE - 3.8

Variation of thermopower with mole % of V_2O_5

Sr.No.	Mole per cent of V_2O_5	Thermopower µ V/K
1	0	-0.505
2	0.96187	-0.48
3	1.89730	-0.185
4	2.80730	-0.2175

The values are all negative (n type) and small.

The variation of Seebeck coefficients with concentration of V_2O_5 is shown in Figure 3.10.

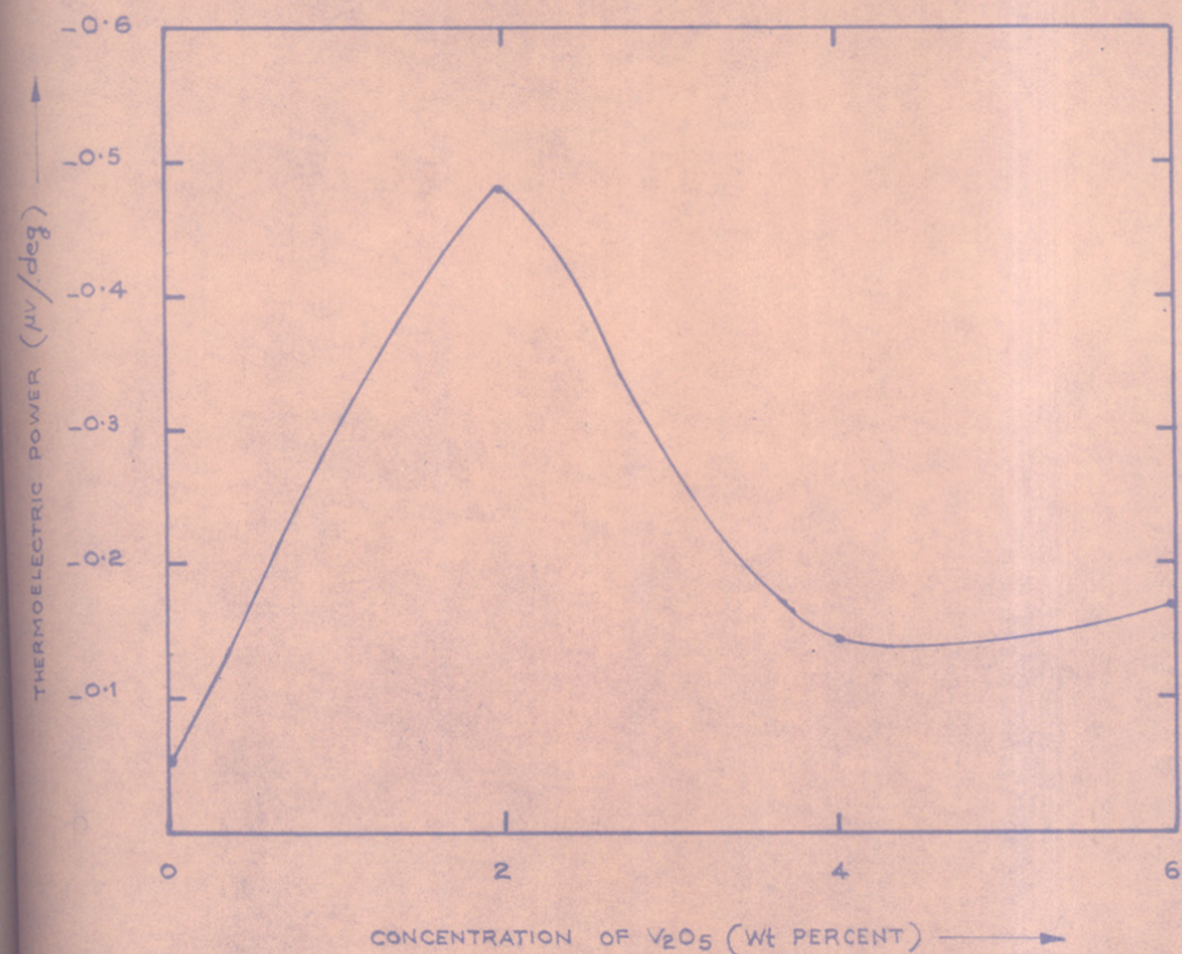

FIGURE 3·10 VARIATION OF THERMOELECTRIC POWER WITH CONCENTRATION OF V_2O_5

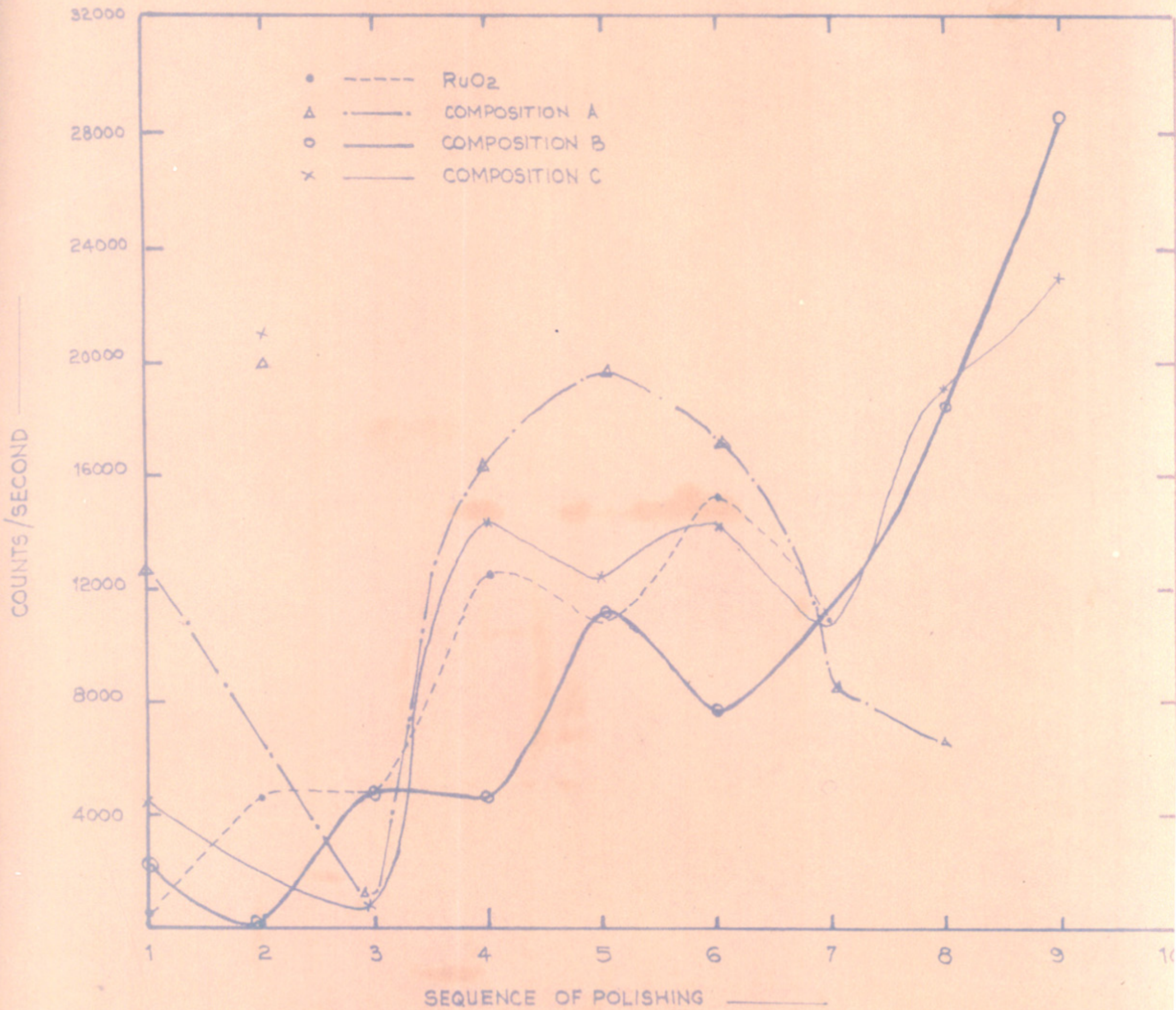

FIGURE 3·11 : THE DIFUSION PROFILES FOR RUTHENIUM IONS IN THICK FILMS OF RuO_2 AND RuO_2-V_2O_5 COMPOSITION

FIGURE 3·12

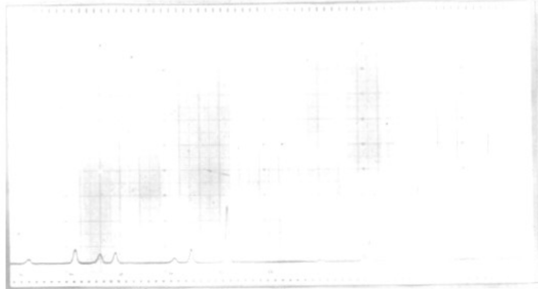

FIGURE 3·13

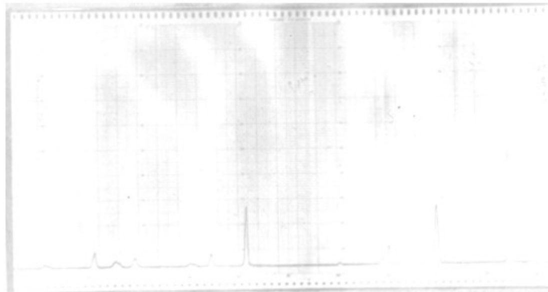

FIGURE 3·14

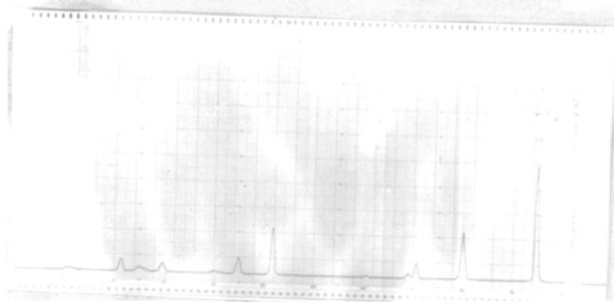

FIGURE 3·15

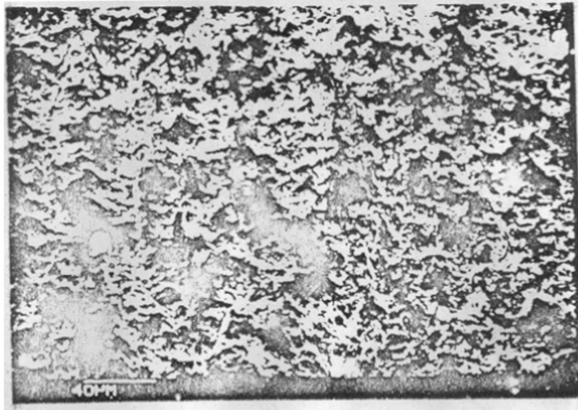

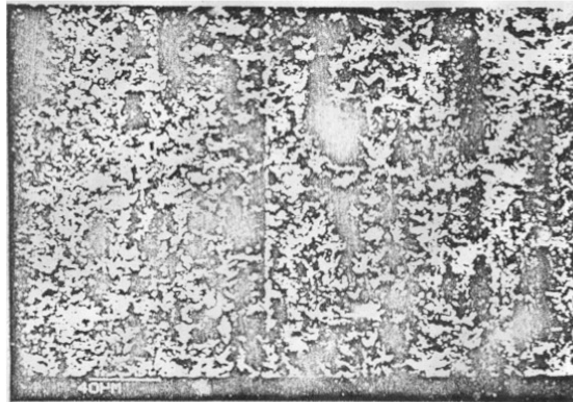

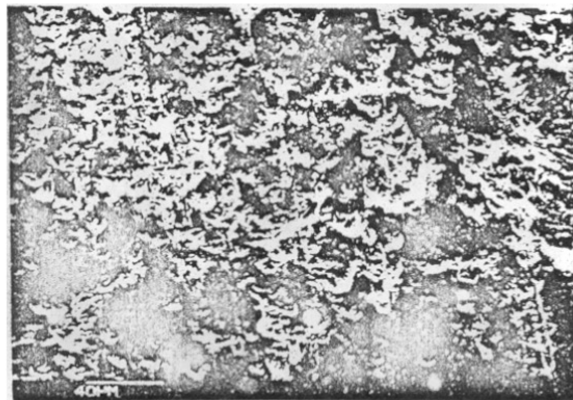

FIGURE 3.16

CHAPTER - 4

D I S C U S S I O N

4.1. THE MIXED VALENCE STATE IN RuO_2

It has been experimentally observed that ruthenium metal oxidises very slowly. R. W. Vest and coworkers[61] have observed that heating ruthenium powder at 1200°C for one hour and at 900°C for 12 hours resulted in 19% oxygen content as compared to 24% required for RuO_2. This might have lead to the conclusion that RuO_2 frequently has oxygen deficiency[6,9]. But Bell and Tagami[80] obtained stoichiometric RuO_2 by heating ruthenium metal for several days at 950°C. However, we[81] observed that when stoichiometric RuO_2 was heated at 600°C for two hours, the loss in weight was 4%. If this loss in weight is due to the loss of oxygen then the oxygen content will be 19.9%. This value is quite comparable with the value obtained by R. W. Vest. Also the derivatograph of RuO_2[81] showed that the total loss in weight is 4.8% at about 1000°C. Thus, the oxygen deficient RuO_2, either obtained by heating stoichiometric RuO_2 or by incomplete oxidation contains 19% of oxygen.

Nonstoichiometric RuO_2 obtained by heating is partially deficient in oxygen, probably with a corresponding amount of Ru^{3+} in place of Ru^{4+} in the crystal lattice[6,9]. In this situation the equivalent number of ruthenium atoms in the crystal lattice which assume a lower valence state release electrons for conduction

$$Ru^{4+}\,O_2^{2-} \longrightarrow Ru^{4+}_{1-2x}Ru^{3+}_{2x}\,O^{2-}_{2-x}$$

This produces what is called as oxygen deficient system.

Alternatively, if we replace some of the quadrivalent ruthenium atoms by atoms of a pentavalent element, which again causes an equivalent number of ruthenium atoms to drop to lower valence state and release electrons into the conduction band

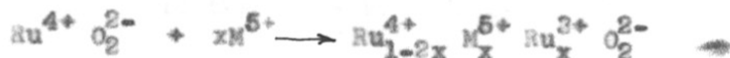

$$Ru^{4+}\,O_2^{2-} + xM^{5+} \longrightarrow Ru^{4+}_{1-2x}\,M^{5+}_x\,Ru^{3+}_x\,O_2^{2-}$$

This is known as controlled valence method. We have successfully introduced various amounts of vanadium into the crystal lattice of RuO_2.

As Honig[28] has represented the incorporation of a trivalent impurity cation (Ga^{3+}) into a divalent host lattice (ZnO) with the quasichemical reaction, the incorporation of a pentavalent impurity cation (V^{5+}) into quadrivalent host lattice (RuO_2) may be illustrated schematically with the quasichemical reaction as follows

$$V_2O_5 \rightleftharpoons 2V^{+}(Ru) + 2\ominus + 2RuO_2(s) + 1/2\ O_2\ (g).$$

Here the sequence of events can be depicted along the following lines : (a) The oxide V_2O_5 comes in intimate contact with the host lattice; eventually (b) the vanadium ions displace two Ru^{4+} ions from their normal positions, giving rise to an excess positive charge at those locations, (c) Four of the five O^{2-} ions originally derived from V_2O_5 and the two displaced Ru^{4+} ions form additional $Ru^{4+}\,O^{2-}_2$ units designated as $RuO_2(s)$. (d) The fifth

O^{2-} ion originally associated with V_2O_5 is ejected into gas phase as 1/2 O_2(g), while (e) two electrons symbolised as - are simultaneously left behind in the crystal. These are carriers responsible for the conductivity of the mixed RuO_2-V_2O_5 oxide. While not shown in equation these electrons may convert two Ru^{4+} ions in the lattice to the Ru^{3+} forms. The mixed oxide could therefore be designated as

which indicate that Ru is encountered in two different valence states.

4.2. X-RAY ANALYSIS

The observation (1) and (2) of X-ray analysis shows that composition A, B and C form complete solid solutions but some unreacted V_2O_5 is present in composition D and E.

RuO_2 and solid solutions of RuO_2-V_2O_5 have rutile structure with tetragonal form (Page).

The variation of lattice parameter of RuO_2 with mole per cent of V_2O_5 added is shown in Figure (3.1). It is observed from the figure that the resultant RuO_2-V_2O_5 oxide system obey the Vegard's Law, which states in effect that the extent of change in lattice parameter of host oxide (RuO_2) is proportional to the molecular percentage of added dopant (V_2O_5).

The Figure 3.1 showes that the lattice parameter 'a' increases and 'c' decreases as the concentration of V_2O_5 increases. The increase in lattice parameter 'a' is due to presence of ions which have got higher ionic radius than Ru^{4+} ions. The incorporation of V^{5+} ions leads to the formation of Ru^{3+} ions. As Ru^{3+} ions increase in amount, the lattice parameter 'a' increases, its ionic radius (0.74Å) is greater than that of V^{5+} (0.59Å) or V^{4+} (0.63Å).

4.3. SEM AND EMPA

The observation 1, 2 and 4 show that the thick films are two phase materials. The phases identified for these films are as follows:

For - Thick films of RuO_2	:	RuO_2 crystallites and a Ru doped glass.
For - Thick films of RuO_2-V_2O_5	:	RuO_2-V_2O_5 crystallites and a Ru, V doped glass.

The observation 3 (page) shows that the value of Pb/Si ratio is smaller than the theoretical value. This could be due to the mutual diffusion between conductive (RuO_2 or RuO_2-V_2O_5) and glass phase[29].

R. W. Vest and coworkers[60] have reported that Ru diffuses in lead borosilicate glass. The observations 5 and 6 confirm (page) the diffusion of Ru in lead borosilicate glass. The diffusion profiles are shown in Fig. 3.11.

4.4. CURRENT-VOLTAGE CHARACTERISTICS

The linearity of the I-V characteristics show that the screen printed and fired silver electrodes provide good ohmic contacts for our thick films of RuO_2 and RuO_2-V_2O_5 compositions.

4.5. RESISTIVITY MEASUREMENTS

4.5.1. Variation of resistivity with firing temperature

The variation of sheet resistivity with firing temperature for thick films of RuO_2 and RuO_2-V_2O_5 compositions (A, B and C) is shown in Figure (3.2). The general trend is same for RuO_2 and all RuO_2-V_2O_5 compositions. The resistivity of thick films of RuO_2 and other compositions (A, B and C) decreases as peak firing temperature increases except for the film of composition C fired and 900°C.

R. W. Vest[61] studied the behaviour of single crystal of RuO_2 (diameter 1.98 μm , 1.79 μm and 2.10 μm) in glass and obtained a relationship between resistance and firing temperature (Figure 4.1). The data of this work obtained at temperatures above softening point of glass will be useful in studying the behaviour of thick films of RuO_2, because the thick films are fired at temperatures above the softening point of glass. The resistance of the single crystals of RuO_2 encapsulated in glass was decreasing with firing temperature at higher temperatures i.e. temperatures above the softening point of glass (latter part of Figure 4.1). R. W. Vest has related this phenomenon to

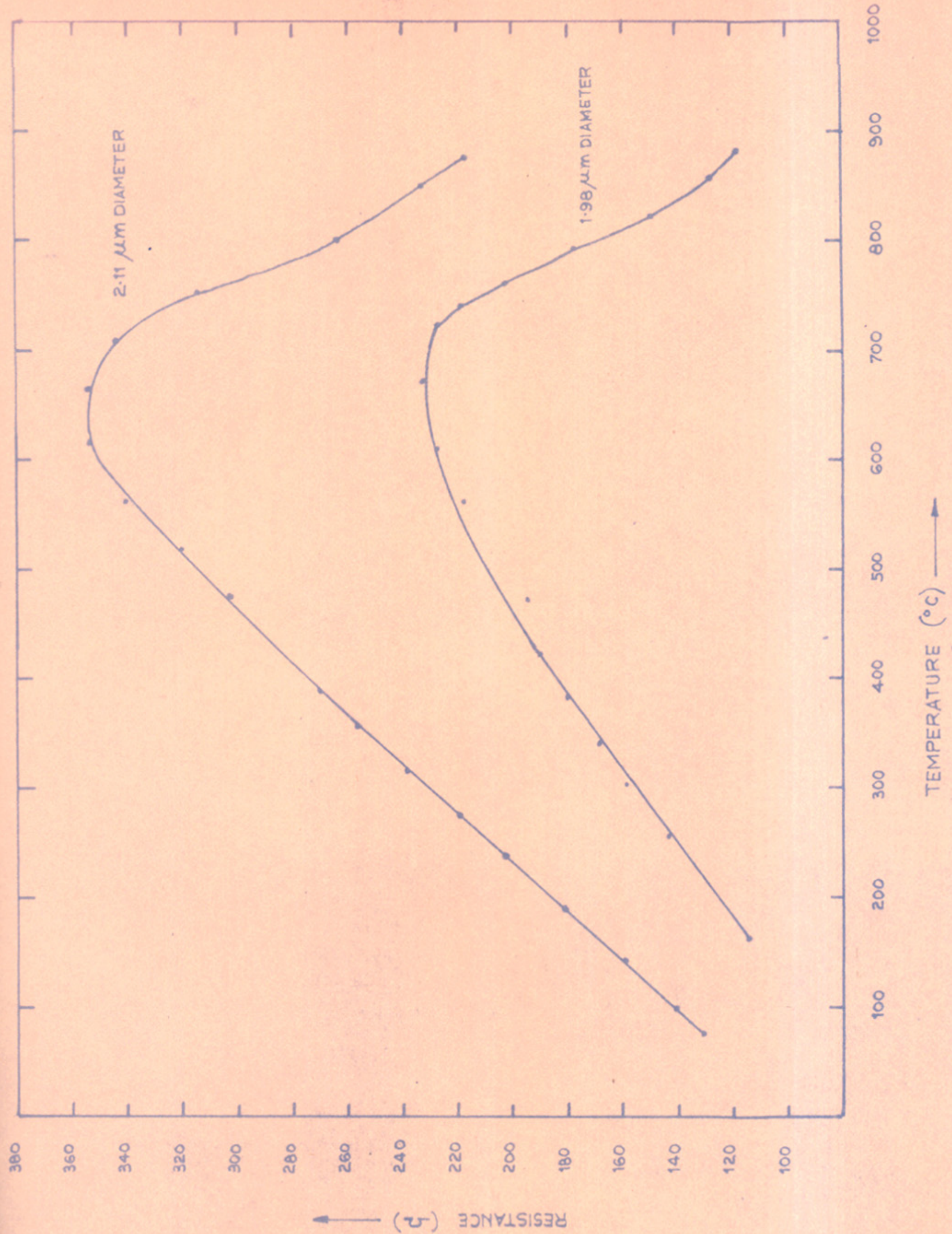

FIGURE 4·1 : BEHAVIOR OF SINGLE CRYSTAL OF RuO_2 IN GLASS

the conductance of glass but he has not given any reason for this phenomenon. He has concluded that the behaviour of the RuO_2-based thick film resistor above the softening point of glass is very similar to the behaviour of the small RuO_2 single crystals in glass. This statement is true for our thick films of RuO_2, because the latter part of the curve obtained by R.W. Vest for single crystals of RuO_2 in glass matches with our curve obtained for thick films of RuO_2 as shown in Figure 4.2.

The influence of firing temperature on our thick films can be explained by using the model for conduction mechanism of RuO_2-based thick film resistors proposed by M. P. Ansell[68,69]. He investigated the structure of thick film resistors and concluded that thick film resistors are principally two phase materials with a doped lead borosilicate glass surrounding crystalline particles. The phases identified for RuO_2-based thick film resistor of Allow B series were RuO_2 crystallites and Ru, Ag doped glass.

Ansell[68,69] suggested that a mixed conduction process takes place which is a combination of the processes occurring in the two phases. The crystallite phase conducts metallically and the charge flow through the glassy phase occurs by trap tunnelling with low activation energies between 10^{-5} to 10^{-3} eV. This can only happen in a narrow band of states. This narrow band is formed by the doping of glass by ions either incorporated or diffused in the crystalline phase.

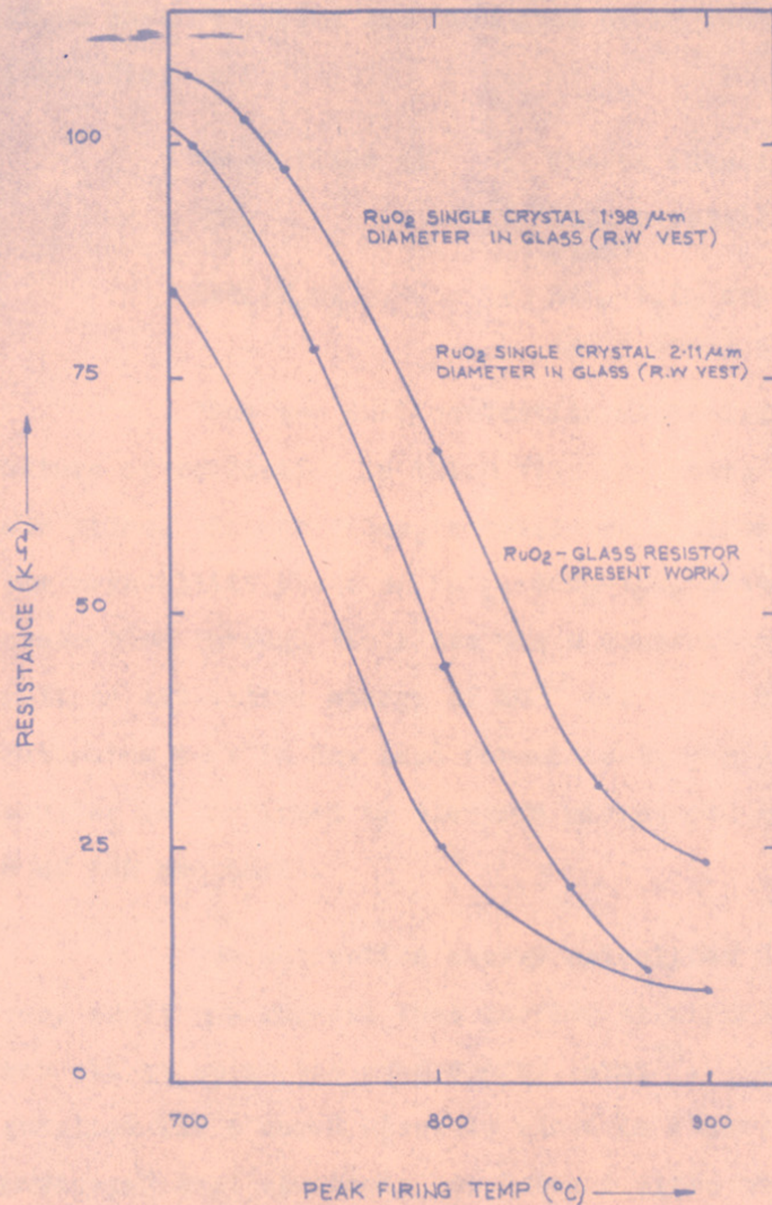

FIGURE 4·2 VARIATION OF RESISTIVITY WITH FIRING TEMPERATURE FOR —
1) THICK FILMS OF RuO_2 — CURVES (1) [PRESENT WORK]
2) SINGLE CRYSTAL OF RuO_2 ENCAPSULATED IN GLASS — CURVE (2) [R.W VEST'S WORK]

Our observation 2 and 4 of SEM and EPMA (Page) shows that our films are also made up of two phases which are identified as

Thick films of	:	Phases identified.
RuO_2	:	RuO_2 crystallite and Ru doped glass.
RuO_2-V_2O_5	:	RuO_2-V_2O_5 crystallite and Ru and V doped glass.

Thus the dual conduction mechanism based on dual nature of conduction in thick film resistors can be applied to our films. In our films, metallic conduction was obtained in the crystallite phase of RuO_2, RuO_2-V_2O_5 systems, whereas conduction through the glass phase occurred by trap tunnelling with an activation energy of 10^{-3} eV. The diffusion of ruthenium ions in the lead borosilicate glass phase reported earlier is confirmed by electron microprobe analysis (observation 5 of SEM and EMPA).

The activation energy calculated for our films is very small and suggest that carrier transport is via states which are all at about the same energy level[72]. The energy band configuration for a doped glass is shown in Figure 4.3 and it is envisaged that electrons hop between sites at almost constant energy (Process 1). The thermal ionization and band conduction (Process 2) can be ruled out because the energy required for this process is greater than 0.5 eV.

Using the conduction model described above the influence of firing temperature can beexplained. With increased firing

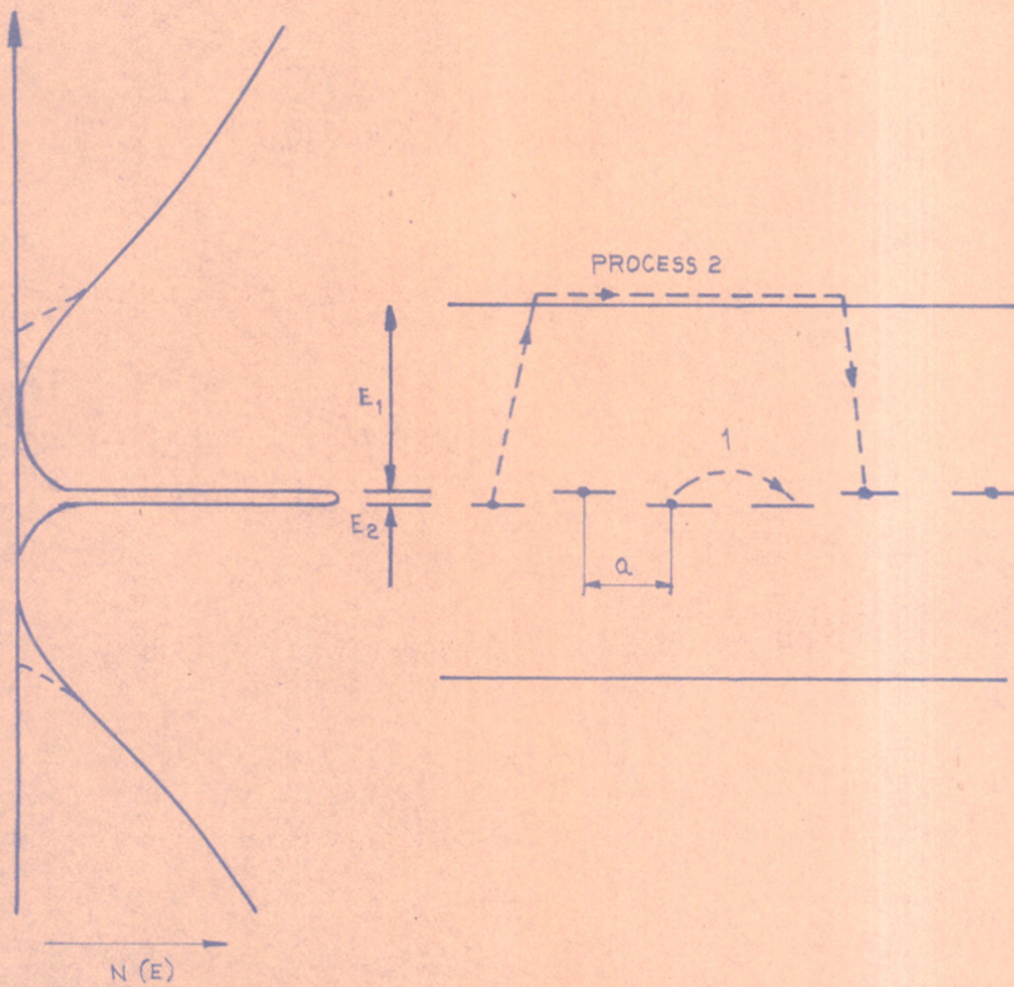

FIGURE 4·3: ENERGY BAND DIAGRAM SHOWING POSSIBLE CONDUCTION PROCESS IN A DOPPED GLASS

temperature the films show a decrease in resistivity. This may be due to the diffusion of more ruthenium ions into the glass phase at higher temperature. Thus average impurity concentration is increased and the jump distance, 'a', (Figure 4.3) is decreased. The decrease in 'a' will increase charge flow and in turn will decrease the resistivity. Almost the same mechanism has been proposed to explain the influence of firing time on resistor properties[72]. With increased time at peak temperatures, high value resistors show some increase in conductivity. This may be due to the diffusion of more ruthenium ions into the glass phase. Thus average impurity concentration is increased and the carrier jump distance 'a' is decreased.

4.5.2. Temperature Coefficient of Resistance

The temperature coefficient of resistance (TCR) values calculated for all the films are summarised in Table 3.7 and the variation of TCR with concentration of V_2O_5 is shown in Figure 3.9.

The TCR of ruthenium dioxide is metallic in nature and strongly positive. Introduction of a compensating oxide might be expected to exert negative influence on it[9]. G. S. Iles[9] confirmed this assumption by experimental evidence using niobium pentoxide as the compensating oxide. The present TCR values, obtained by using vanadium pentoxide as the compensating oxide, also support this assumption. The addition of V_2O_5 to RuO_2 reduces the TCR. For example the RuO_2 glaze film fired at 900°C was found

to have TCR in excess of 300 x $10^{-6}/^{o}C$. As 2 wt. % of V_2O_5 was added, the TCR decreased to 25 x $10^{-6}/^{o}C$. Thus TCR of thick films of RuO_2 can be controlled by adding V_2O_5 to RuO_2 before incorporating it in thick film preparation. The TCR is governed by the type of glass, ratio of doped RuO_2 to glass and the atomic percentage of vanadium contained in RuO_2 (Figure 3.9).

M. F. Ansell[68,69], using Hill's model for the passage of charge carriers via a random array of trap sites for resistive and conducting materials, calculated the TCR values for thick films of RuO_2. He first derived an expression for TCR as follows. For semiconducting behaviour,

$$R = R_o \exp \frac{E}{kT}$$

where E is the activation energy for conduction and k is the Boltzmann's constant. Differentiating with respect to T,

$$\frac{dR}{dT} = -R_o \exp\left(\frac{E}{kT}\right)\left(\frac{E}{kT^2}\right) = -\frac{RE}{kT^2}$$

By a definition of TCR,

$$TCR = \frac{1}{R}\ \frac{dR}{dT} = -\frac{E}{kT^2}\ K^{-1}$$

Hill[73] considered the passage of charge carriers via a random array of trap sites. Assuming that the hopping sites are confined within an energy band $Em < kT$, Hill derived expressions for conductivity and activation energy for resistive and conducting materials. If the width of the band is less than kT the temperature dependence becomes very weak.

At room temperature $Em/kT = 10^{-1}$.

Ansell[68,69] found the $TCR = \frac{E}{kT^2} = -300 \times 10^{-6}\ k^{-1}$.

The calculated TCR values listed in Table are all less than $300 \times 10^{-6}\ k^{-1}$.

Ansel[68,69] further showed that at $300^{\circ}K$ a negative TCR of $< 100 \times 10^{-6}\ k^{-1}$ is equivalent to $E < 800$ µeV. Thus material which conducts with this value of TCR requires $E < 1$ meV. For our thick films $TCR < 300 \times 10^{-6}\ k^{-1}$. Thus our films which possess this value of TCR requires $E < 3$ meV. The activation energies calculated for our films also show $E < 3$ meV.

4.5.3. Variation of resistivity with temperature

Figure 3.5 shows the plot of log R vs 1/T for thick film of RuO_2 fired at $700^{\circ}C$. Figure 3.6, 3.7 and 3.8 show similar graphs for thick films of RuO_2-V_2O_5 compositions (A, B and C respectively) heated at $700^{\circ}C$.

All the graphs have straight line nature which shows that $R = R_o \exp -\Delta E/kT$. The activation energy values ΔE are calculated and listed in Table 3.6. The activation energy values calculated by J. Robertson for thick films of RuO_2 are also listed in the same Table 3.6 for comparison.

J. Robertson[72] states that this small magnitude of activation energy suggests that carrier transport is via states which are all at about same energy level (Figure, 4.3, Process 1).

4.4.6. Effect of dopant concentration on electrical properties

The solid solutions in which the dopant atoms or foreign atoms have a valence different from that of the atom which they replace may belong to one of the following three categories.

(1) The incorporation of foreign atom may form atomic imperfections of well defined concentration. For example incorporation of $CaCl_2$ in NaCl may form vacancies of Na or interstitial chlorine. In either case the concentration of atomic imperfections formed is well defined viz. one per Ca_{Na} atom. It is termed as 'controlled atomic imperfections'[76]. Koch and Wagner[76] first studied the properties related to these.

(2) Atoms of the base crystal may change their valence as a consequence of the incorporation of foreign atom. For example when Li is incorporated in NiO, equivalent amount of Ni atoms changes its valence from 2 to 3 without the formation of atomic imperfections. Verwey and coworkers[8] first reported this and named as 'controlled valence'.

(3) It may occur that foreign atom (pure) when dissolved in case crystal adapt itself and forms a compound similar to the base compound. Thus with manganese in Al_2O_3 and TiO_2, solid solutions Al_2O_3-Mn_2O_3 and TiO_2-MnO_2 are formed[77]. Selwood introduced the term 'induced valence'.

The properties of RuO_2-V_2O_5 solid solution can be explained by means of the controlled valence process. The two methods by which RuO_2 can be obtained as a mixed valence oxide are described earlier.

4.6.1. Effect of dopant concentration on sheet resistivity

The dependence of sheet resistivity of thick films of RuO_2 and RuO_2-V_2O_5 compositions (A, B and C) on concentration of V_2O_5 is shown in Figure 3.4. The curves follow the same trend for all firing temperatures. The sheet resistivity decreases as the concentration of V_2O_5 increases. The sheet resistivities can be calculated by using Honig's formula.

J. M. Honig[28] has concluded that at constant temperature, conductivity of mixed valence oxide can be given by the following equation

$$\sigma \sim S(1-S) \qquad \ldots (1)$$

Here S is the probability that a given cationic site will contain an extra charge carrier.

To develop this dependence further, he considered $M^{(n)}$ and $M^{(n+1)}$ as the number of cations in valence states n and n + 1 respectively and showed that

$$S = \frac{M(n)}{[M^{(n)} + M^{(n+1)}]} \qquad \ldots (2)$$

Using equations (1) and (2) the resistivity of RuO_2-V_2O_5 compositions are calculated. For this the concentration

of V^{5+} ions is taken as concentration of Ru^{3+} ions because of incorporation of V^{5+} ions in RuO_2 forms equivalent amount of Ru^{3+} ions.

To calculate the sheet resistivity of thick films of mixed valence oxide the equation (1) is modified as

$$\sigma = k\,S(1-S)$$

where k is constant which depends on following factors:

(1) Type of glass used.

(2) Ratio of glass to mixed valence oxide.

(3) Firing temperature.

For our thick films the first two factors are constant. The sheet resistivity values measured for the films fired at different firing temperatures and the resistivity values calculated are summarised in Table 4.1. For the calculated resistivity values listed in Table 4.1, k = 1. The comparison shows that when $k = 10^3$ the calculated resistivity values are in good agreement with the measured sheet resistivity values.

Thick films of RuO_2 when heated loses 5% of oxygen forming equivalent amount of Ru^{3+} ions. Taking this concentration of Ru^{3+} ions the resistivity value for thick film of RuO_2 is calculated which is also in good agreement with the measured sheet resistivity values (Table 4.1).

All these resistivity values calculated and measured were plotted as a function of concentration of Ru^{3+} ions for comparison (Figure 4.4, 4.5).

TABLE - 4.1

Observed and calculated sheet resistivity values

Sr. No.	Concentration of V^{5+} ions atomic per cent	Measured sheet resistivity k /sq. for firing temps.			Resistivity calculated
		700°C	800°C	900°C	
1	0.96187	235.37	60.03	33.24	54.6448
2	1.8973	119.15	43.43	17.312	18.4604
3	2.8073	46.05	11.3464	37.566	12.8008
4	0	24.9667	9.5163	3.4593	4.7

4.6.2 Effect of dopant concentration on thermoelectric power

We have measured the thermopower or Seebeck coefficient of thick films of RuO_2 and RuO_2-V_2O_5 compositions.

Room temperature Seebeck coefficients for these films are listed in Table 3.9. The values are negative (n-type) and small.

Ruthenium dioxide is reported to be n-type[19] and we have got n-type of conductivity for thick films of RuO_2 and RuO_2-V_2O_5 compositions. Hence no chemical alteration of metal oxide has occurred during firing as Pike and Seager have observed.

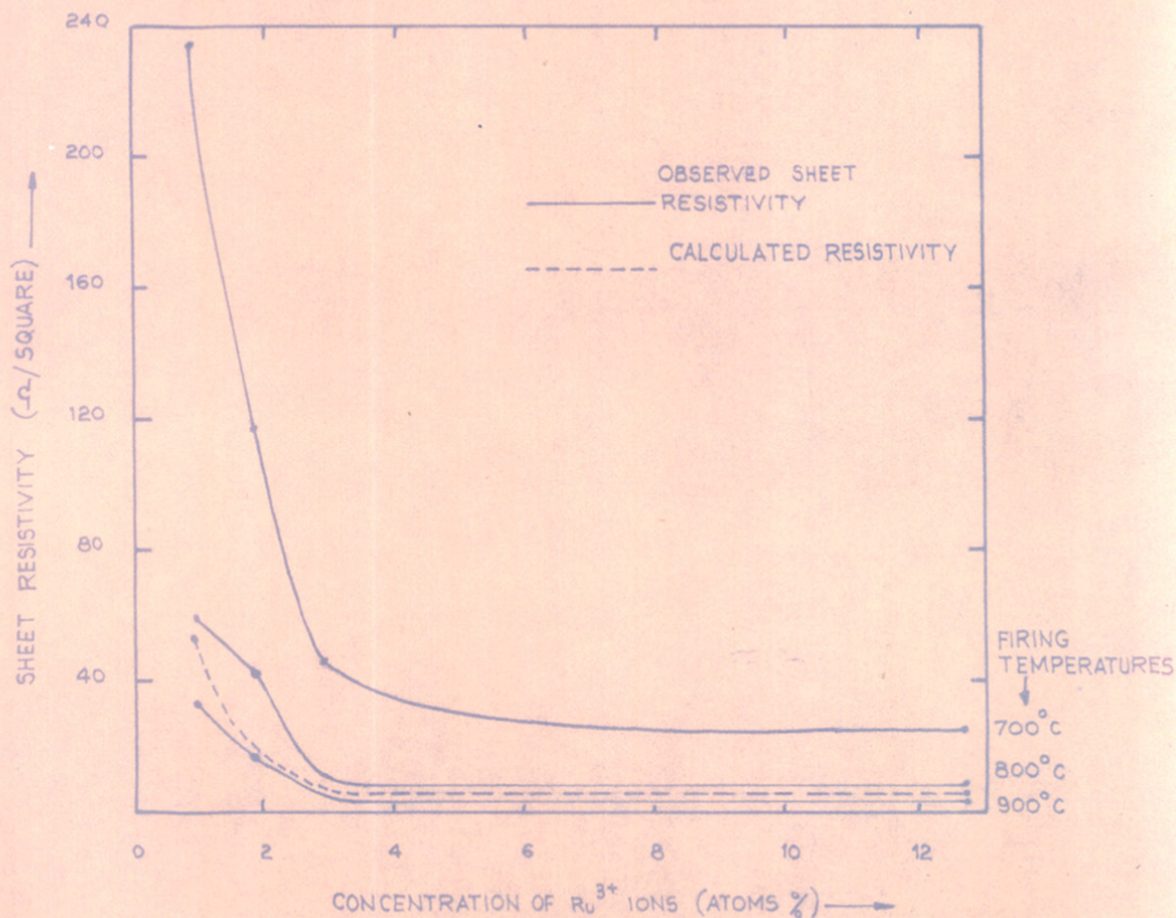

FIGURE 4.4 VARIATION OF RESISTIVITY WITH CONCENTRATION OF Ru^{3+} IONS

EXPERIMENTALLY OBSERVED

CALCULATED BY HONING's FORMULA

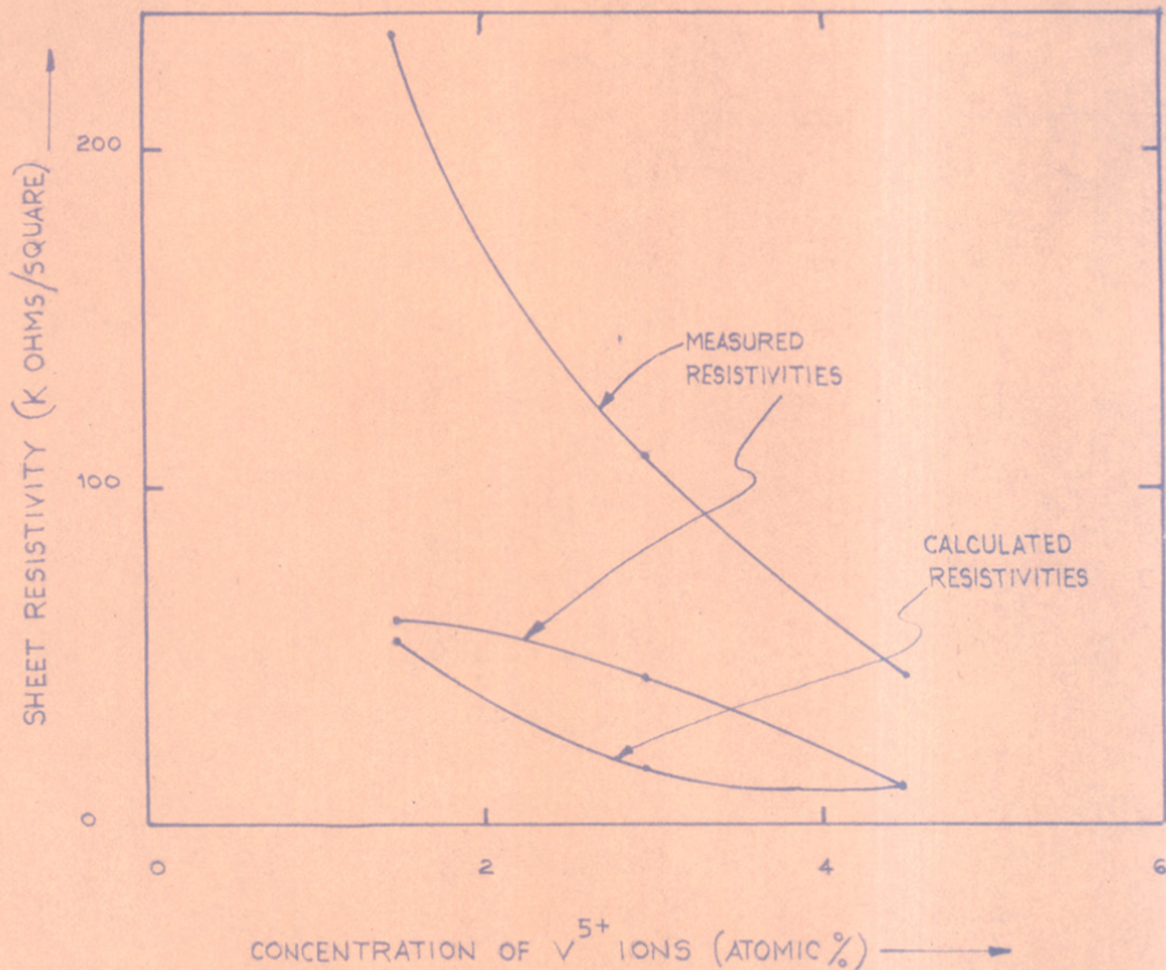

FIGURE 4·5 : VARIATION OF SHEET RESISTIVITY WITH CONCENTRATION OF V^{5+}

Pike and Seager[62] measured the thermopower of thick films of bismuth ruthenate. The values were all positive. For comparison they also measured thermopower of polycrystalline bismuth ruthenate. The value was -8.9 μV/k. Hence they concluded that a chemical alteration of metal oxide had occurred during the firing.

The variation of thermopower with concentration of V_2O_5 added is shown in Figure . The thermopower for RuO_2-V_2O_5 compositions is calculated by using Honig's formula.

Honig[28] has obtained an expression for Seebeck coefficient (α) for mixed valency oxide as

$$\alpha \sim \ln (1-S)/S \qquad \ldots (3)$$

where S is given by

$$S = \frac{M^{(n)}}{[M^{(n)} + M^{(n+1)}]}$$

Here $M^{(n)}$ and $M^{(n+1)}$ represent the number of cations in valence states n and n + 1 respectively.

Using the above equations and taking the concentration of V^{5+} ions as the concentration of Ru^{3+} ions, the thermopower is calculated. The calculated values of thermopower and its measured values are plotted as a function of V^{5+} concentration. Considering the thick film parameters for the measured thermopower, the agreement with calculated thermopower is good (Fig. 4.7).

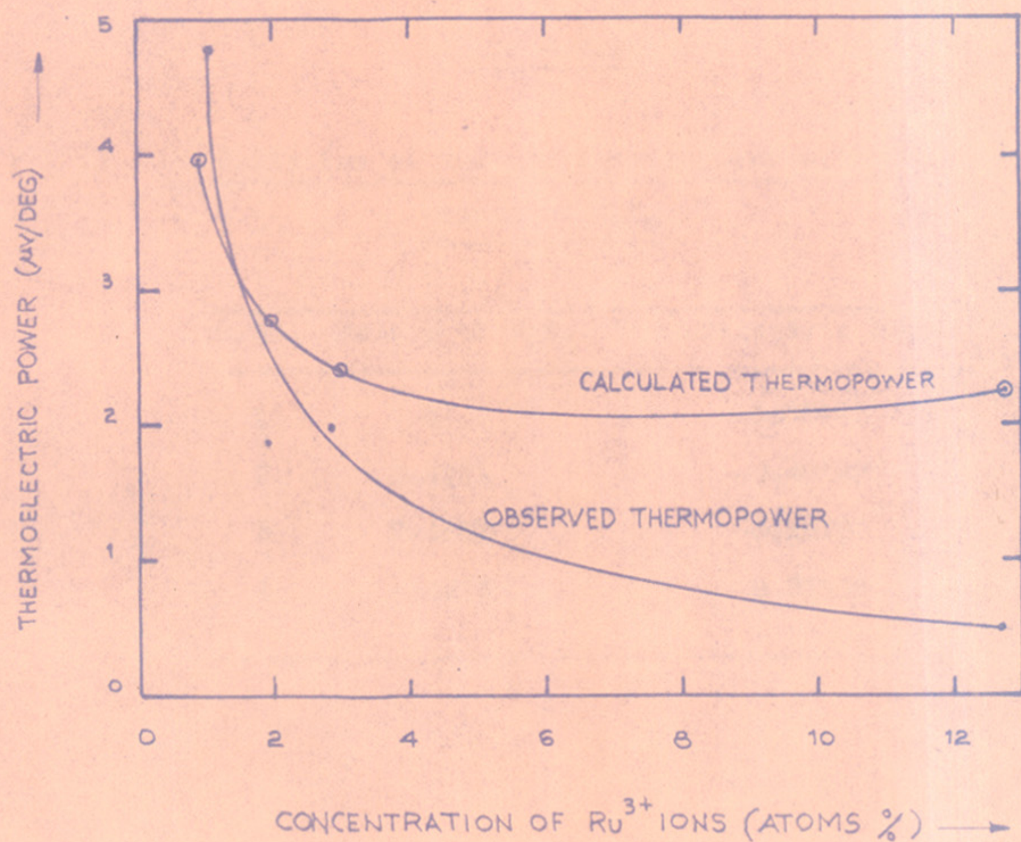

FIGURE 4-6 VARIATION OF THERMOELECTRIC POWER WITH CONCENTRATION OF Ru^{3+} IONS

The thick film of RuO_2 when heated loses oxygen forming equivalent amount of Ru^{3+} ions. Taking this concentration of Ru^{3+} ions the thermopower for thick film of RuO_2 is calculated.

All these values of thermopower or Seebeck coefficient calculated and measured are plotted as a function of Ru^{3+} ions concentration (Fig. 4.6).

TABLE - 4.2

Variation of thermoelectric power with conc. of V_2O_5

S.No.	Mole % of V_2O_5	Thermoelectric power
1	0	-0.05125
2	1.4711	-0.48125
3	2.9582	-0.18750
4	4.4614	-0.21875

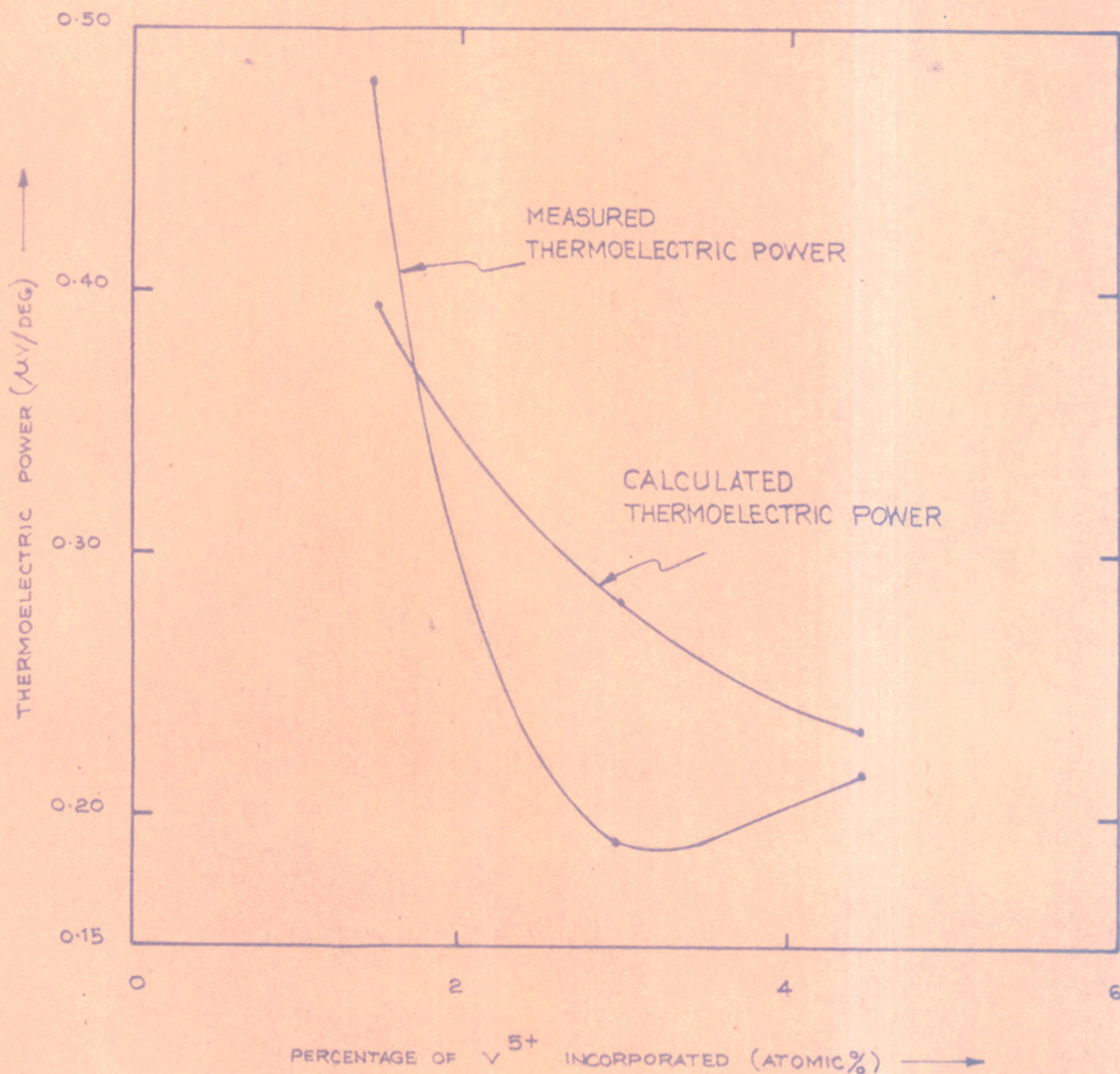

FIGURE 4·7 VARIATION OF THERMOELECTRIC POWER WITH CONCENTRATION OF V^{5+}

R E F E R E N C E S

1. F. A. Cotton and J. T. Mague, Inorg. Chem., 5(2), 1966, 317-318.

2. J. M. Fletcher, W. E. Gardner, B. F. Greenfield, M. J. Holdoway and M. H. Rand, J. Chem. Soc. A(3), 1968, 653-657.

3. D. B. Roger, R. D. Shannon, A. W. Sleight and J. L. Gillson, Inorg. Chem., 8(4), 1969, 841-849.

4. K. V. Krishna Rao, Leela Iyengar, Acta. Crystallogr, Sect.A 25 1969, 302-303.

5. C. E. Bowman, Acta Chem. Scand. 24(1), 1970, 116-22.

6. F. A. Cotton and G. Wilkison,"Advanced Inorganic Chemistry" (II edition), p. 984.

7. W. E. Bell and M. Tagami, J. Phys. Chem., 67(11), 1963, 2432-2436.

8. E. J. W. Verwey, P. W. Haaijman, F. C. Romeijn and G. W. van Oosterhout, Philips Res. Rep., 5, 1950, 173-187.

9. G. S. Iles, Proc. Jt. Conf. Thick Film Technol., 1968, 29-41.

10. G. S. Iles, M. E.A. Casale, Platinum Metals Rev., 11-(4), 1967, 126-129.

11. T. H. Lemon, Platinum Metals Rev., 17-(1), 1973, 14-20.

12. C. L. McDaniel and S. J. Sehneider, J. Reserch. Nat. Stand. Sect. A, 73(2), 1969, 213-219.

13. K. Wazo, M. Yusuke and K. Hedejiro Yogyo Kyokai Shi, 80(9), 1972, 354-357.

14. V. K. Tarigrov, D. M. Chizlikov, E. K. Kazenas and L. K. Strubochkin, Zh. Neorg. Khim. 20(8), 1975, 2035-2037.

15. H. Shafer, W. Gerhardt and A. Tebben, Angew Chem., 73, 1961, 27.

16. G. Bayer and H. G. Wiedemann, Thermochim. Acta, 11(1), 1975, 79-88.

17. G. Bayer and H. G. Wiedemann, Therm. Anal, Proc. Int. Conf. 4th, 1974, 1, 763-776.

18. G. Bayer and H. G. Wiedemann, Arch. Huln, 22(1), 1977, 3-13.

19. W. D. Ryden, A. W. Lawson and C. C. Sartain, Phys. Rev. B [3] 1(4), 1970, 1494-1500.

20. W. D. Ryden, A. W. Lawson and C. C. Sartain, Phys. Lett. A, 26(5), 1968, 209-210.

21. H. Shafer, G. Schneidereit and W. Gerhardt, Zn. Anorg. Allgen. Chem., 319, 1963, 327.

22. S. M. Marcus and S. R. Butler, Phys. Lett. 26(a), 1968, 518-519

23. C. Z. Wagner, Z. Physik Chem. (B) 22,

24. H. H. Baumback and C. Z. Wagner, Zo Physik Chem. (B) 22, 1933, 199.

25. H. H. Baumback and C. Z. Wagner, Zo Physik Chem. (B) 24, 1934, 59.

26. C. Z. Wagner and E. Koch, Z. Physik Chem.(B) 32, 1936, 439.

27. W. D. Johnston, J. of Chem. Education, 36(12), 1959, 605.

28. J. M. Honig, J. Chem. Education, 43, 1966, 76-82.

29. Y. Taketa, N. Masayoshi, S. Kanefusa and M. Hasadome, Nippon Daigaku Seisan Kogakubu Hokoku, 8(1) 1975, 25-29. (C.A. 85: 115198, 1976).

30. Y. Taketa and M. Haradome, IEEE Trans Part Hybride Packag, 10(1), 1974, 74-81.

31. Y. Taketa, N. Masayoshi, E. Kazuko, M. Haradome, Nippon Daigaku Seisan Kogakubu Hokoku, 8(1), 1975, 17-24.

32. Y. Taketa, N. Masayoshi, E. Kazuko and M. Haradome, Nippon Daigaku Seisan Kogakubu Hokuku, 7(2), 1974, 109-116.

33. L. J. Braddy, IEEE Trans. Parts. Mater. Packag., 6(4), 1971, 144-6.

34. S. Hirokatsu, T. Chiaki, K. Kuniaki, Gummaken Kozyo Shikenjo Nempo, 1976, 125 (C.A. 89; 138852y, 1978).

35. Y. Taketa, Nippon Daigaku Seisan Kogakubu Hokoku, 8(2), 167-180.

36. W. M. William, L. H. Curtis, L. F. Gaylord, F.B. Boykin, (C.A. ~~91: 67362s, 1977~~.
89: 138852d, 1978).

37. E. Asada, K. Kaneko, C. A. 87: 119431c, 1977.

38. N. Kazuo, K. Kyoko, C. A. 91: 67362s, 1977.

39. N. Kazuo, K. Kyoko, C.A. 90: 32835a, 1979.

40. A. H. Hendrik, M. C. Adrianus, A. Henricus, C. A. 91: 48314m, 1979.

41. Y. Yoshino, N. Sugishita, C.A. 86: 181611u, 1977.

42. Y. Yoshino, N. Sugishita, C.A. 87: 61559g.

43. C. Robert, M. Abrash, C.A. 85: 67233b, 1976.

44. K. Fujimura, P. No. 78100496, C.A. 90: 15366f, 1979.

45. C. J. Pukaite, C.A. 82: 67248y, 1975.

46. C. J. Pukaite, C.A. 86: 114449j, 1977.

47. T. M. Kudza, R. E. Schwyn, M. Berg., C.A. 84: 83251r, 1976.

48. E. Asada, K. Kaneko, C. A. 86: 157220v, 1977.

49. A. Ikegami, C.A. 86: 64465p, 1977.

50. J. R. Lorry, Ger. Often 2812912 (C.A.: 89: 207993j, 1978).

51. T. Kasanami, O. Kano, C. A. 82: 92233x, 1975.

52. T. Kasanami, O. Kano, C.A. 82 : 92232w, 1975.

53. A. W. Steight, Ger. Often 1932720, C.A. 73: 40032a, 1970.

54. R. J. Bouchar, Ger. Offen. 2058253, C.A. 76: 160037q, 1972.

55. F. Kumar, Ger. Offen. 2115814, C.A. 79: 1125r, 1973.

56. D. H. Scheiber, Ger. Offen. 2403628, C.A. 81: 161198h, 1974.

57. J. Mukherji, Proc. Chem. Symp. 2nd (1) 1970, 256-267.

58. J. Mukherji, Ind. Eng. Chem. Prod. Res. Develop. 11(2), 1972, 178-183.

59. J. Mukherji, Glass Technol. 13 (5), 1972, 135-137.

60. A. Prabhu, G. L. Fuller and R. W. Vest, J. Amer. Ceram. Soc. 67(9), 1974, 408-409.

61. R. W. Vest, Final Tech. Rep., 1975, Purdue Res. Found.

62. G. E. Pike and C. H. Seager, J. Appl. Phys. 48(12), 1972, 5152-69.

63. C. C. Sartain, W. D. Ryden, A. W. Lawson, J. Non-Cryst. Solids, 5, 1970, 55.

64. C. C. Sartain, J. Non-Cryst. Solids, 6, 1971, 173.

65. L. J. Brady, Proc. of the 1967 Electronic Comp. Conf. p. 238.

66. W. R. Smith,"Static and Dynamic Electricity" (McGraw-Hill New York 1968).

67. American Institute of Physics Handbook, 3rd edn., edited by D. E. Gray (McGraw-Hill New York 1972) Chap. 5, p. 12.

68. M. P. Ansell, Electrocomp. Science and Technology, 3, 1976, 131-140.

69. M. P. Ansell, Electrocomp.Science and Technology, 3, 1976, 141-151.

70. The Thick Film Microcircuitry Handbook, Vol. I, edited by Du Pont 1968.

71. Handbook of Thick Film Hybrid Microelectronics, edited by C. A. Harper (McGraw-Hill New York 1974).

72. J. Robertson, Electrocomp. Science and Technology, 4, 1977, 105-109.

73. D. A. Cash, M. P. Ansell, R. M. Hill, 1974, Final Report M D contract No. Ru 7-41.

74. F. A. Kröger, "The Chemistry of Imperfect Crystals" 2nd edn. (North Holland 1974), p. 478, p. 499.

75. W. Koch and C. Wagner, Z. Phys. Chem. B38, 1957, 295.

76. F. A. Kröger and H. J. Vink, Solid State Phys. Eds F. Seitz and D. Turnbull, 3 (1956), 307.

77. P. W. Selwood, T. E. Moore, M. Ellis and W. Wethington, J. Am. Chem. Soc., 71, 1949, 693.

78. Y. Taketa and M. Haradome, "Microelectronics and Reliability 13, 1974, 281-289.

79. B. M. Cohen, D. R. Uhlmann and R. M. Shaw, J. Non-Cryst. Solids, 12, 1973, 177.

80. W. E. Bell and M. Tagami, J. Phys. Chem., 67, 1963, 2432.

81. R. F. Shinde, M. S. Setty (unpublished).

82. M. S. Setty, M.Sc. Thesis.